

ATRAP Buffer-Gas Positron Accumulator

Daniel Comeau

A DISSERTATION SUBMITTED TO
THE FACULTY OF GRADUATE STUDIES
IN PARTIAL FULFILLMENT OF THE REQUIREMENTS
FOR THE DEGREE OF
DOCTOR OF PHILOSOPHY

GRADUATE PROGRAM IN PHYSICS AND ASTRONOMY
YORK UNIVERSITY
TORONTO, ONTARIO

June 2014

©Daniel Comeau, 2014

Abstract

The ATRAP collaboration has been creating antihydrogen, the simplest antimatter atom, since 2002 and has a long-term goal of performing precision laser spectroscopy on these antihydrogen atoms. ATRAP has produced antihydrogen by positron cooling of antiprotons and by a laser-controlled charge-exchange process. Both methods require large numbers of antiprotons and positrons (the constituent particles of antihydrogen). This dissertation describes the methods developed to increase the number of positrons available for the ATRAP experiments by a factor of 200. The development of the new positron loading scheme has enabled the ATRAP collaboration to greatly increase the daily rate of antihydrogen production.

Positrons originating from a radioactive source travel through a moderating material and are accumulated in a differentially pumped vacuum chamber. When required, the positrons are sent through a complex magnetically-guided beamline to the location where antihydrogen is produced. The system built allows for a reliable, highly-efficient method of providing positrons to the ATRAP experiment.

Acknowledgements

I am grateful to have had the opportunity to work with a world-class group of researchers at a world-class research facility. I would especially like to thank my advisor, Dr. Eric Hessels for his support, patience and guidance. I would also like to thank every member of the ATRAP collaboration who helped to motivate and create such an environment of excellence. Five years at CERN would have been unbearable without the help and dedication of each member.

I would also sincerely like to thank my wife, Jennifer, for understanding the phrase ‘It can’t NOT be done.’ when explaining my 100 hour weeks at the lab. Also, for her patience when a trip to Switzerland with her husband turned into a trip to Switzerland by herself. Her constant reassurance and encouragement was, at many times, my sole reason to keep going.

Table of Contents

Abstract	ii
Acknowledgements	iii
Table of Contents	iv
List of Tables	viii
List of Figures	ix
1 Introduction	1
1.1 Antihydrogen	1
1.1.1 Antihydrogen Constituents: e^+ and \bar{p}	2
1.2 Motivation for the Buffer-Gas Accumulator	3
1.3 ATRAP Collaboration	3
1.4 CERN and the Antiproton Decelerator	4
1.5 Penning Trap	4
1.5.1 Theory	4
1.5.2 Electrode Stack: Implementation of a Penning Trap	7
1.6 Antihydrogen Production	8

1.7	New ATRAP Apparatus	9
1.7.1	ATRAP Electrode Stack	9
1.8	Previous ATRAP Method of Positron Loading	12
1.9	Overview	14
2	Buffer-Gas Accumulator	16
2.1	^{22}Na Source	16
2.2	Neon Moderator	19
2.2.1	Moderator Theory	21
2.2.2	Moderator Design	21
2.3	Jog Section and Drift Tube	23
2.4	Scintillation Detection for Particle Counting	25
2.5	Moderator Growth	27
2.6	Moderator Efficiency	29
2.7	Energy Spread of Moderated Positrons	31
2.8	The Accumulator Penning Trap	31
2.9	Buffer-Gas Accumulation	33
2.9.1	Magnetic Field	33
2.9.2	Positron Interactions with Nitrogen Molecules	34
2.9.3	Pressures in the Accumulator	36
2.9.4	Electrostatic Potentials in the Accumulator	38
2.10	Rotating Wall	39
2.10.1	Rotating Wall Theory	39
2.10.2	Rotating Wall Implementation	41
2.11	Plasma Compression with Rotating Wall	42

2.11.1	Plasma Radius Measurement	42
2.11.2	Number of Accumulated Positrons Versus Accumulation Time . . .	45
2.11.3	Rotating Wall Amplitude and Frequency	49
3	Transferring Positrons	52
3.1	Pulsing Positrons Out of the Accumulator	52
3.1.1	Timing Sequence	54
3.2	Counting Accumulated Positrons	56
3.2.1	Charge Measurement	57
3.2.2	Calibrating the Charge Amplifiers	57
3.2.3	NaI Integral Counting	59
4	Bridging the Gap: The Positron Guide	62
4.1	Magnetic Field of the Superconducting Solenoid	62
4.2	Location of the Positron Accumulator	64
4.3	Vacuum Considerations	67
4.4	Motion of a Positron in a Magnetic Field	69
4.4.1	Homogeneous Magnetic Field	69
4.4.2	Non-Homogeneous Magnetic Field	72
4.5	Additional Design Considerations	75
4.6	Modelling	77
4.6.1	Magnetic Field Modelling	77
4.6.2	Trajectory Modelling	78
4.7	Overview of Positron Guide	82
4.8	Control of Current to the Magnets	92

4.9	Optimization Tools	94
4.9.1	Faraday Cup Detection	100
4.9.2	Timing Signals	107
5	Catching Positrons in the ATRAP Penning Trap	112
5.1	Cloud Characteristics	112
5.1.1	Energy Distribution	114
5.1.2	Temporal Distribution	117
5.1.3	Cloud Shape	121
5.2	Catching Positrons in the ATRAP Electrode Stack	124
5.3	Counting Positrons in the ATRAP Penning Trap	126
5.4	Electron Cooling of Positrons	128
5.4.1	Electron Loading	132
5.4.2	Enhancement Using Electron Cooling	135
5.5	Stacking Positrons	136
6	Summary of Results	140
	Bibliography	142

List of Tables

2.1	Source strength and positron yield	20
2.2	Electrode stack dimensions and pressures within each stage	38
4.1	Cyclotron frequencies, cyclotron radius and magnetic fields at different positions	71
4.2	Initial bending coils	95
4.3	Axial coils along the positron guide	96
4.4	Rectangular vertical coils	97
4.5	Rectangular horizontal coils	98
4.6	Control of all of the Final steering coils	99
4.7	Positron annihilation time delays along the transfer system	108
6.1	Efficiencies of transferring positrons along transfer system	141

List of Figures

1.1	The three motions of a charged particle in a Penning trap	6
1.2	Three cylindrical electrodes	7
1.3	The new ATRAP apparatus	10
1.4	Cut away showing the interior of the ATRAP electrode stack	11
1.5	Schematic of entire apparatus	15
2.1	Schematic of accumulator	17
2.2	Source capsule for ^{22}Na	18
2.3	Decay scheme for ^{22}Na	19
2.4	Schematic of the source chamber	22
2.5	Schematic of the source and solid-neon moderator mount	24
2.6	Source and jog section to filter out the unmoderated fast positrons	25
2.7	Positron annihilation signal on NaI detector and photomultiplier	26
2.8	Signal from the ratemeter during moderator growth	28
2.9	Schematic of the assumed geometry used for the GEANT4 simulation to calculate NaI detection efficiency	30
2.10	Energy distribution of the moderated positrons	32
2.11	Schematic of the accumulator	34

2.12	Magnetic field, stack and potentials	35
2.13	Positron range of motion during each step of accumulation	37
2.14	Segmented electrode in Stage 3 used to produce rotating wall	43
2.15	Picture of skimmer used to make plasma radius measurements	44
2.16	Cloud size measurement with rotating wall applied	46
2.17	Load time results	48
2.18	Electric potential applied to produce rotating wall	49
2.19	Scanning rotating wall amplitude	50
2.20	Scanning rotating wall frequency	51
3.1	Pulsing steps	53
3.2	On-axis potentials to prepare the accumulated positrons to be pulsed . . .	55
3.3	Avtec saturated switch signal	56
3.4	Physical setup to calibrate the charge amplifiers	58
3.5	Positron signal on charge preamplifier	59
3.6	Signal of 28 million positrons annihilating on the output valve	60
3.7	Calibration of NaI detector when annihilating at the output of the accu- mulator	61
4.1	Positron guide	63
4.2	Superconducting solenoid fringing field contour plot	65
4.3	Superconducting solenoid field lines	66
4.4	Schematic of the 1-mm tube	68
4.5	Magnetic gradient along the positron path	73
4.6	Definition of pitch angle	74

4.7	Magnetic field grid produced by Mathematica program to calculate the actual positron trajectory	79
4.8	Axial velocity of transferred positions	80
4.9	Axial velocity of transferred positions with different initial perpendicular velocities	81
4.10	Displacement in the y-direction due to magnetic field gradients	83
4.11	Electromagnets making up the initial bend	85
4.12	Types of coils for producing the axial fields	87
4.13	Geometry of the rectangular coils	88
4.14	Rectangular vertical and horizontal compensation coils	89
4.15	Overlap of rectangular vertical coils	91
4.16	Coils positioned around the cube	93
4.17	Location of the Faraday cups	101
4.18	3 positions of mirror Faraday cup	103
4.19	The 1-mm tube for admitting positrons into the ATRAP Penning trap . . .	104
4.20	Segmented Faraday cup around 1-mm tube in ATRAP	105
4.21	Electron gun used for steering	106
4.22	Annihilation signals at the output valve and the 3-m valve	109
4.23	Scintillation signals at annihilation points along the transfer system	111
5.1	Sections of the ATRAP Penning trap	113
5.2	Potentials applied to measure energy distribution	115
5.3	Energy distribution as measured in ATRAP Penning trap	116
5.4	Potentials applied to measure temporal distribution	118
5.5	Temporal spread of positrons inside ATRAP Penning trap	119

5.6	Analog signal from the fiber detectors around ATRAP	120
5.7	XY stage that enables the 1-mm tube to be moved relative to the electrode stack	122
5.8	Radial profile of positron cloud measured inside ATRAP 1-tesla solenoid	123
5.9	Potentials applied to ATRAP electrode stack to capture positrons	127
5.10	Adiabatic transfer of positrons between three electrodes in the ATRAP Penning trap	129
5.11	On-axis potential applied to pulse positrons onto degrader	130
5.12	Energy distribution of positrons once cooled in single well in ATRAP Penning trap	131
5.13	Potentials applied to ATRAP electrode stack to capture positrons using electron cooling	133
5.14	Potentials applied to ATRAP electrode stack to load photoelectrons off of the degrader	134
5.15	Time required to cool positrons into a single electrode well with and without electrons.	137
5.16	Electron number dependence on the efficiency of positron catching	138
5.17	Stacking positrons into the ATRAP Penning trap	139

Chapter 1

Introduction

1.1 Antihydrogen

Antihydrogen is the simplest neutral antimatter atom. It is a bound state of an antiproton (\bar{p}) and a positron (e^+). The first creation of antihydrogen was accomplished at CERN in 1996 [1]. In this first demonstration, nine antihydrogen atoms were detected, but these atoms were travelling at almost the speed of light. With widespread interest in the creation of antihydrogen, there has been a push to create antihydrogen that could be eventually trapped and studied (and eventually used for precision spectroscopic research). In response, the Antiproton Decelerator (AD) was built at CERN [2] near Geneva, Switzerland. The AD was completed in the year 2000. In 2002, two groups using the AD, ATRAP [3] and ATHENA [4], were successful in creating much slower antihydrogen atoms.

Antihydrogen research is an exciting field of study with many significant implications to the physics community. CPT (charge conjugation, parity, time reversal) invariance implies that the energy levels of hydrogen and antihydrogen would be identical. Any measurement of the energy levels of antihydrogen could (when compared to existing high-

precision spectroscopy in hydrogen) form a test for CPT. Also, since antihydrogen is a neutral form of antimatter, it is ideal for testing gravity acting on a system consisting only of antimatter. Finally, antimatter physics tests are important in that the matter/antimatter balance in the universe (that is, the fact that the universe is dominated by matter) is still not understood.

1.1.1 Antihydrogen Constituents: e^+ and \bar{p}

Paul Dirac first postulated [5] the existence of antimatter particles in 1928. He formulated a theory that describes the behaviour of relativistic electrons and his equation permitted negative energy values, indicating the possibility of antielectrons. Positrons (the antimatter counterparts of electrons) were first observed [6] in a cloud chamber photograph of cosmic rays in 1933 by Carl D. Anderson. That same year, the creation of a positron and electron by pair production was observed [7] by Blackett and Occhialini. The positron has become an important tool in medical diagnostics, material science, and fundamental physics. Positrons can be obtained from β^+ -decay of radioactive isotopes (^{22}Na , ^{64}Cu , ^{58}Co , etc.) or pair production (of e^+ and e^-) from high-energy photons.

The antiproton (the antimatter counterpart of the proton) was discovered [8] by Owen Chamberlain and Emilio Segrè in 1955 at what is now known as the Lawrence Berkeley National Laboratory using the Bevatron accelerator. Antiprotons are now produced in large numbers at accelerator facilities around the world, but CERN is the only facility able to supply large numbers of decelerated antiprotons.

1.2 Motivation for the Buffer-Gas Accumulator

This report details the new positron production and accumulation apparatus used by the ATRAP collaboration for the creation of antihydrogen. Before the construction and implementation of the apparatus detailed here, the loading time of positrons (not antiprotons) was the bottle-neck for antihydrogen production. A new method of loading large numbers of positrons in a short period of time was required to go forward in the pursuit of antihydrogen research. This dissertation describes the buffer-gas positron accumulator that was built and interfaced with the ATRAP apparatus to provide large numbers of positrons for ATRAP experiments.

1.3 ATRAP Collaboration

The ATRAP collaboration is made up of scientists from York University, Harvard University, Forschungszentrum Jülich and Johannes Gutenberg Universität Mainz. In 2002, ATRAP [3] and ATHENA [4] demonstrated the creation of cold antihydrogen in a cryogenic environment. Both groups identified three-body recombination of an antiproton and two positrons as the likely mechanism for antihydrogen production. Two years later, ATRAP demonstrated the first laser-controlled production of antihydrogen [9]. Although many exciting developments have occurred in antihydrogen research since then, these developments are not included in this thesis since they occurred after (November 2007) the completion of the research described in this dissertation.

1.4 CERN and the Antiproton Decelerator

Bunches of low-energy antiprotons are provided by the CERN Antiproton Decelerator (AD). These antiprotons are produced by a beam of 26-GeV/c protons hitting a fixed iridium target. The antiprotons are collected at 3.5 GeV/c and directed into the AD, where they are cooled by stochastic and electron cooling.

Every 100 seconds, a short pulse of cooled antiprotons is ejected from the AD at a momentum of 5 MeV/c. These antiprotons are directed to the ATRAP apparatus, where their energy is further reduced in a Be degrader. The antiprotons are then captured in a Penning trap and further cooled by electrons [10, 11, 12, 13]. The techniques to trap and cool antiprotons were developed by the TRAP collaboration, the predecessor to the ATRAP collaboration.

1.5 Penning Trap

A Penning trap consists of a uniform magnetic field in the z direction that confines charged particles to orbits around the magnetic field lines and electrodes to provide electric fields that confine particles in the z direction. A Penning trap is used to load, store and manipulate charged particles (positrons and antiprotons in the case of antihydrogen experiments).

1.5.1 Theory

A charged particle travelling in a spatially-uniform magnetic field feels a force in the direction transverse to the magnetic field and travels in a circular cyclotron orbit [14, 15].

The cyclotron frequency is magnetic field dependent:

$$\vec{\omega}_c = \frac{q\vec{B}}{m}. \quad (1.1)$$

This circular orbit constrains the motion transverse to the magnetic field direction but does not constrain the motion along the direction of the field. The particle can be bound along the field direction by superimposing an electrostatic potential on the magnetic field. A Penning trap consists of such a superposition of a uniform magnetic field $\vec{B} = B_o\hat{z}$ and a quadrupole electrostatic potential of the form [14]

$$V = V_o \frac{z^2 - \frac{\rho^2}{2}}{2d^2}, \quad (1.2)$$

where d is a distance that characterizes the size of the trap and ρ and z are the radial and axial distances from the centre of the trap.

The motion of a charged particle in a Penning trap is the superposition of three motions: cyclotron motion, axial motion and magnetron motion, as depicted in Figure 1.1.

The axial motion, which is decoupled from the magnetic field, is simple harmonic motion:

$$\ddot{z} + \omega_z^2 z = 0, \quad (1.3)$$

where the axial frequency is given by

$$\omega_z^2 = \frac{qV_o}{md^2}. \quad (1.4)$$

The radial motion is described by

$$m\ddot{\vec{\rho}} = q \left[\vec{\rho} \left(\frac{V_o}{2d^2} \right) + (\dot{\vec{\rho}} \times \vec{B}) \right], \quad (1.5)$$

where $\vec{\rho} = \rho\hat{\rho}$, with $\hat{\rho}$ being a unit vector in the radial direction. Substituting the cyclotron

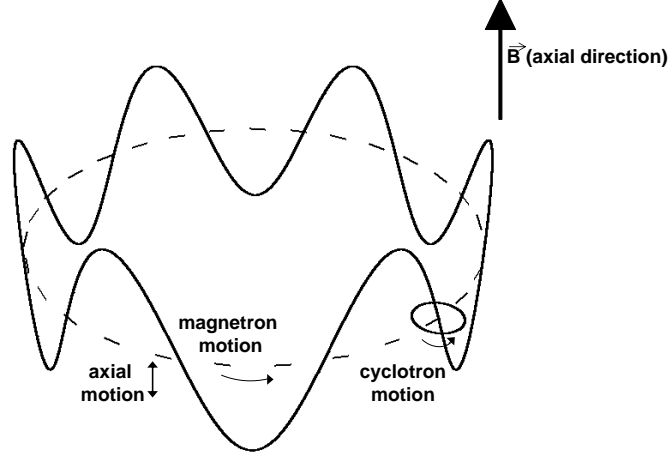


Figure 1.1: The three motions of a charged particle in a Penning trap

frequency ω_c and the axial frequency ω_z into Equation 1.5 gives

$$\ddot{\vec{\rho}} - \vec{\omega}_c \times \dot{\vec{\rho}} - \frac{1}{2}\omega_z^2 \vec{\rho} = 0. \quad (1.6)$$

The term $-\frac{1}{2}\omega_z^2 \vec{\rho}$ comes from the fact that there is a repulsive radial term in the quadrupole potential of Equation 1.2. An implication of this term is that the cyclotron motion is superimposed upon a magnetron orbit with a much lower frequency ω_m . The magnetron motion is an $\vec{E} \times \vec{B}$ drift due to the perpendicular \vec{E} and \vec{B} fields. Figure 1.1 shows the superposition of the cyclotron and magnetron motions in the plane normal to \vec{B} , along with the harmonic axial motion. For typical values of \vec{B} , V_o and d , the frequencies of the three motions are related by

$$\omega_c \gg \omega_z \gg \omega_m. \quad (1.7)$$

1.5.2 Electrode Stack: Implementation of a Penning Trap

To produce the quadratic potential of Equation 1.2, axially-symmetric hyperbolic electrodes could be used [14]. However, hyperbolic electrodes are difficult to construct and they would not allow for easy access for particle loading. A geometry based on hollow cylindrical electrodes can be used to give an approximately quadratic potential [16], while still allowing for open access to the centre of the electrode, as shown in Figure 1.2. Such access is required to allow the charged particles to travel into and out of the Penning trap. Cylindrical electrodes can be easily machined to much greater accuracy in a much shorter time than hyperbolic electrodes could be. All Penning traps used by ATRAP use the cylindrical geometry, with different sizes (length and diameter) used for different traps.

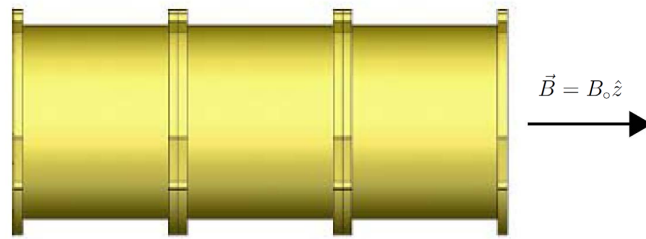


Figure 1.2: Three cylindrical electrodes. Each electrode is a hollow cylinder and is electrically isolated from the adjacent electrodes. Positive potential applied to the two end electrodes cause axial confinement of positrons to the central, grounded electrode. The open ends of the cylinder allow for easy access to the trap centre.

1.6 Antihydrogen Production

Antihydrogen in a Penning trap was first produced with positron-cooled antiprotons [17] via three-body recombination [18],



The three-body recombination is largely due to a positron captured in a high-n state and a second positron efficiently carrying off the excess energy that results from weak binding of the first positron to the antiproton.

A second demonstrated method [9] of creating antihydrogen uses lasers to excite cesium atoms to weakly-bound Rydberg states (Cs^*). Antihydrogen is produced via two resonant charge exchange collisions [19]:



and



Cesium atoms from a thermal oven are excited by two lasers (852.2-nm light from a diode laser and 510.7-nm light from a copper-vapour laser). A transition between cesium $6S_{1/2}$ ($m_J = +1/2$, $m_I = -5/2$) and $6P_{3/2}$ ($m_{J'} = +3/2$, $m_{I'} = -5/2$) is excited with the diode-laser light. Subsequently, the copper-vapour-laser light excites the cesium from $6P_{3/2}$ to a Rydberg state which is a mixture of many states due to the presence of the large Penning-trap magnetic field, with the mixture including some $37D$ character. The excited cesium (Cs^*) travels through a cloud of trapped positrons and, via a resonant charge exchange, the Rydberg electron is captured by the trapped positron to create a Rydberg positronium atom (Ps^*). Since positronium is neutral, it is no longer confined by the magnetic and

electric fields of the Penning trap. A small fraction of the Ps^* moves in the direction of the cloud of trapped antiprotons. A collision of a Ps^* atom and a trapped antiproton can produce Rydberg-states of antihydrogen ($\bar{\text{H}}^*$) via a second charge exchange.

1.7 New ATRAP Apparatus

After successfully producing antihydrogen by these two methods, the ATRAP collaboration designed and constructed a new apparatus with the intent of not only creating antihydrogen, but of capturing it as well. The new apparatus still uses a Penning trap to load, confine and manipulate the charged-particle constituents of antihydrogen. The addition of a Ioffe trap (a magnetic neutral atom trap in which the Zeeman shift of the atom is used to attract atoms to a local minimum of magnetic field magnitude) enables the potential of capturing cold antihydrogen atoms.

Figure 1.3 shows the new ATRAP apparatus. The axial magnetic field of the Penning trap is produced by the superconducting solenoid shown in the figure. The electrostatic potentials for the Penning trap are produced by biasing the stack of hollow cylindrical electrodes positioned near the bottom of the apparatus and the Ioffe trap surrounds the top half of the stack. The antiprotons are loaded through a thin titanium window from the bottom of the apparatus. The positrons are loaded from the top, as will be described in detail in this dissertation.

1.7.1 ATRAP Electrode Stack

Figure 1.4 shows the ATRAP electrode stack, along with the naming convention for each electrode. The stack consists of 36 gold-plated copper cylindrical electrodes. In-

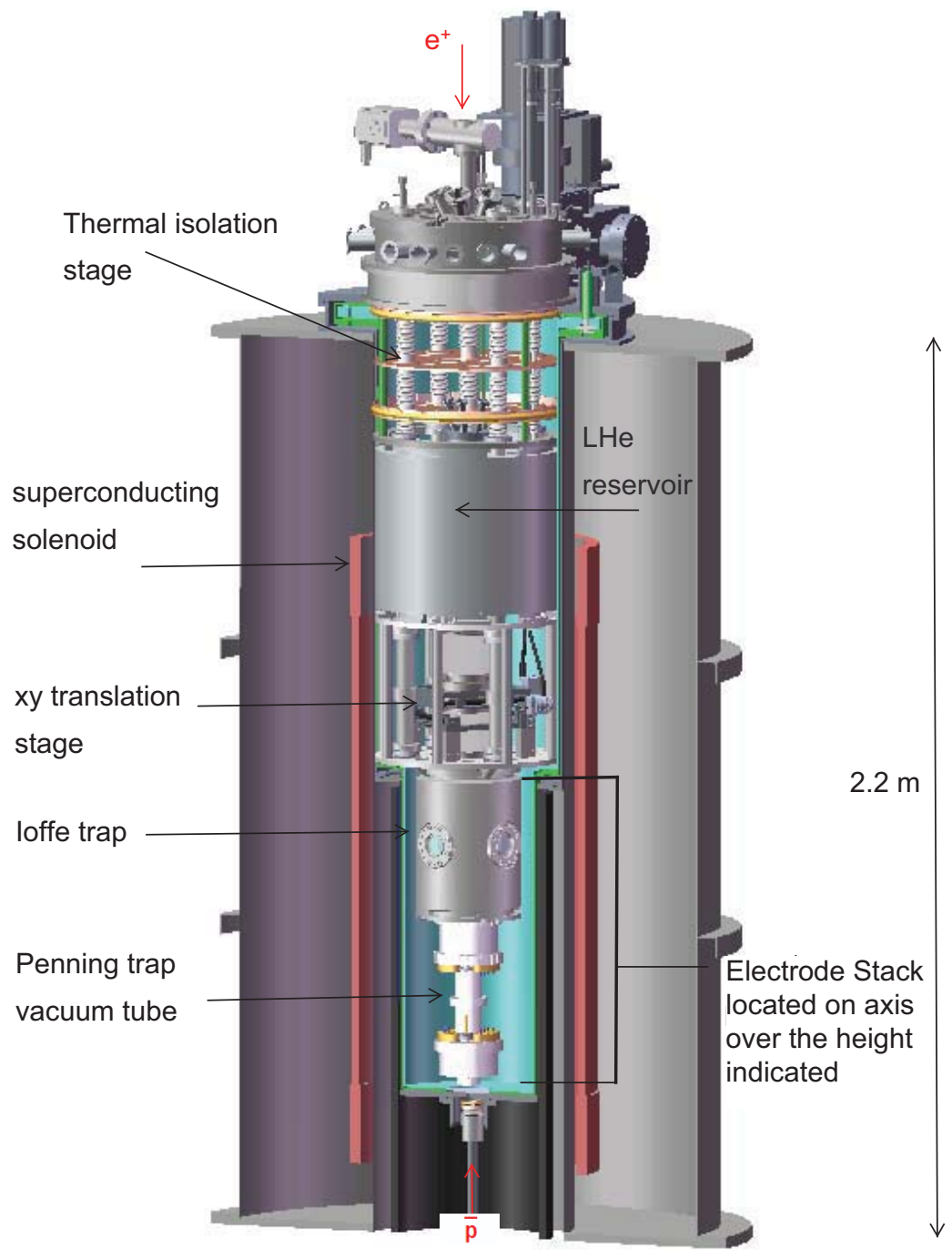


Figure 1.3: The new ATRAP apparatus

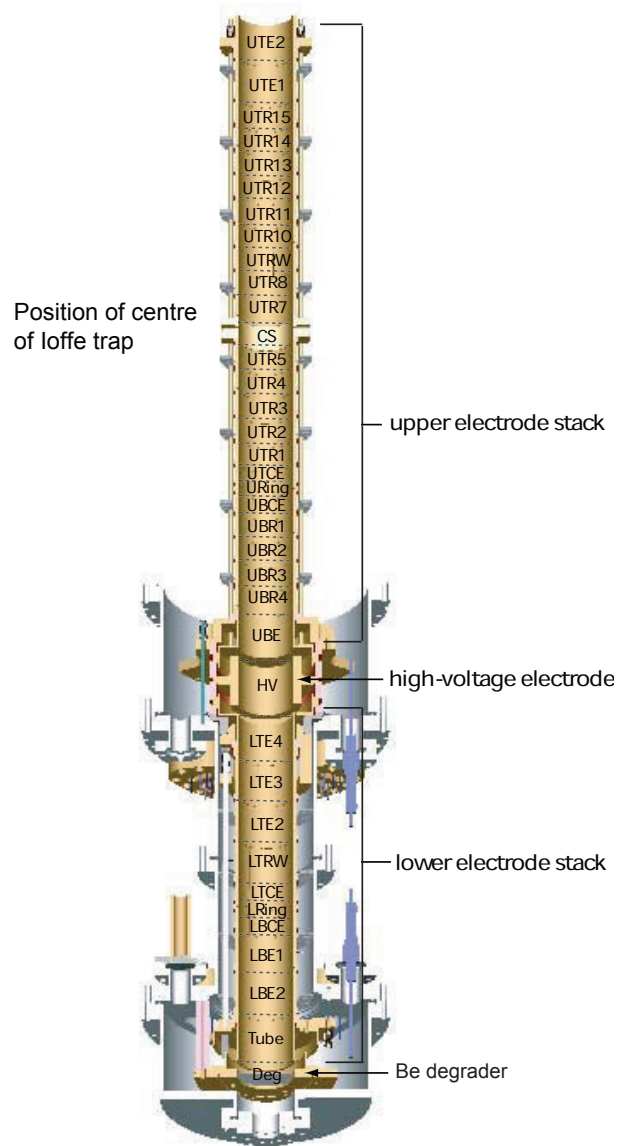


Figure 1.4: Cut away showing the interior of the ATRAP electrode stack

insulating macor spacers are placed between the electrodes so that each electrode can be individually biased. The entire electrode stack resides in the vacuum chamber near the bottom of the ATRAP apparatus, at the location indicated in Figure 1.3. The electrode stack is kept at a temperature of 4 kelvin by thermal contact with the liquid-helium reservoir shown in Figure 1.3. The low temperature is important for cooling the charged particles, and also provides the exceptional vacuum that is imperative for long-term antimatter confinement.

There are two main regions in the ATRAP electrode stack: the upper electrode stack and the lower electrode stack, as labelled in Figure 1.4. The lower stack is primarily used for capturing antiprotons, while the upper stack is used for trapping positrons and for combining the two species to create antihydrogen. Because the upper stack is the region of antihydrogen production, the Ioffe trap is located in this region, as shown in Figure 1.4. Without the Ioffe trap, when antihydrogen is produced inside the Penning trap, the neutral atom is not confined by the Penning trap, and therefore drifts out to the cylindrical electrodes and annihilates. The Ioffe field gives a possibility for neutral atom trapping within the low-pressure region of the ATRAP apparatus.

1.8 Previous ATRAP Method of Positron Loading

Prior to the method described in this dissertation, the ATRAP collaboration had been capturing positrons since 1999. Positrons were loaded into the ATRAP Penning trap by field ionization of strongly-magnetized Rydberg positronium [20].

A transmission moderator, made from a 2- μm -thick tungsten crystal, W(100), was placed at the top of the electrode stack inside the magnetic field of the Penning trap. Attached to the other end of the electrode stack was a 2-mm-thick W(110) crystal which

acted as a reflection moderator. A ^{22}Na radioactive source capsule (similar to the one that will be described in Section 2.1) was mechanically lowered into the magnetic field to a position directly above the electrode stack, but outside the vacuum system. The high-energy positrons entered the vacuum system through a thin titanium window at the top of the vacuum chamber of the electrode stack. Most of the positrons from the source capsule had enough energy to traverse the window and enter the exceptionally good vacuum in the electrode-stack region.

Once the positrons passed through the window, they encountered the tungsten transmission moderator. The key to this loading technique is for a positron to capture a secondary electron from the surface of the moderator upon leaving the W crystal and for the electron and positron to bind into a highly-magnetized, weakly-bound state of Rydberg positronium. The positronium could subsequently be Stark-ionized by applying a voltage on one of the cylindrical electrodes. The resulting positron can be captured in the potential well created by the applied voltage, while the excess energy is carried off by the electron. The key benefit of this method of positron loading is that it enables loading directly into a closed, cryogenic vacuum chamber, which, in a similar apparatus [10], has been shown to have an exceptionally good vacuum of 5×10^{-17} torr. Extremely low pressures are required for antihydrogen studies to ensure long lifetimes of antiprotons and antihydrogen, since both can annihilate with background gas.

The Rydberg positronium method produced a peak loading rate of 4×10^4 (e^+ /hr) per mCi of ^{22}Na in the radioactive source [20]. Currently, the largest ^{22}Na source available is 50 mCi, so loading 5-million positrons required 2.5 hours. Furthermore, the loading rate was dramatically reduced when the magnetic field was lowered. The old experiments were done in a 5-tesla magnetic field, while the new apparatus requires a much smaller

field of only 1 tesla in order to allow for a Ioffe-trap field and this smaller field would reduce the 4×10^4 (e⁺/hr)/mCi loading rate by more than an order of magnitude.

1.9 Overview

This report details the method in which the rate at which positrons are provided to the ATRAP experiments has increased by a factor of 200 using a buffer-gas positron accumulator. This increased rate has dramatically changed the experimental procedure for creating antihydrogen for the ATRAP collaboration and has enabled many new experiments that were not possible with the old technique of positron loading. Chapter 2 describes the buffer-gas accumulator apparatus that initially traps the positrons emitted from a ²²Na source with an efficiency of 0.4%. This apparatus was York University's contribution to the ATRAP collaboration. It was a team effort from the research groups of Dr. Eric Hessels and Dr. Cody Storry. Chapter 3 describes the method in which positrons are ejected from the accumulator. Chapter 4 describes the apparatus designed and built to transfer the positrons from the accumulator to the ATRAP antihydrogen apparatus. The Positron Guide was my main contribution to the collaboration. I was responsible for the initial design, building, testing and the ultimate success of this section of the experiment. Chapter 5 describes the method in which the positrons are efficiently caught in the ATRAP Penning trap, where they are subsequently used for antihydrogen experiments. The final chapter discusses the results obtained with the new positron loading technique.

Figure 1.5 shows an overall view of the new buffer-gas accumulator, the transfer section and the ATRAP antihydrogen trap.

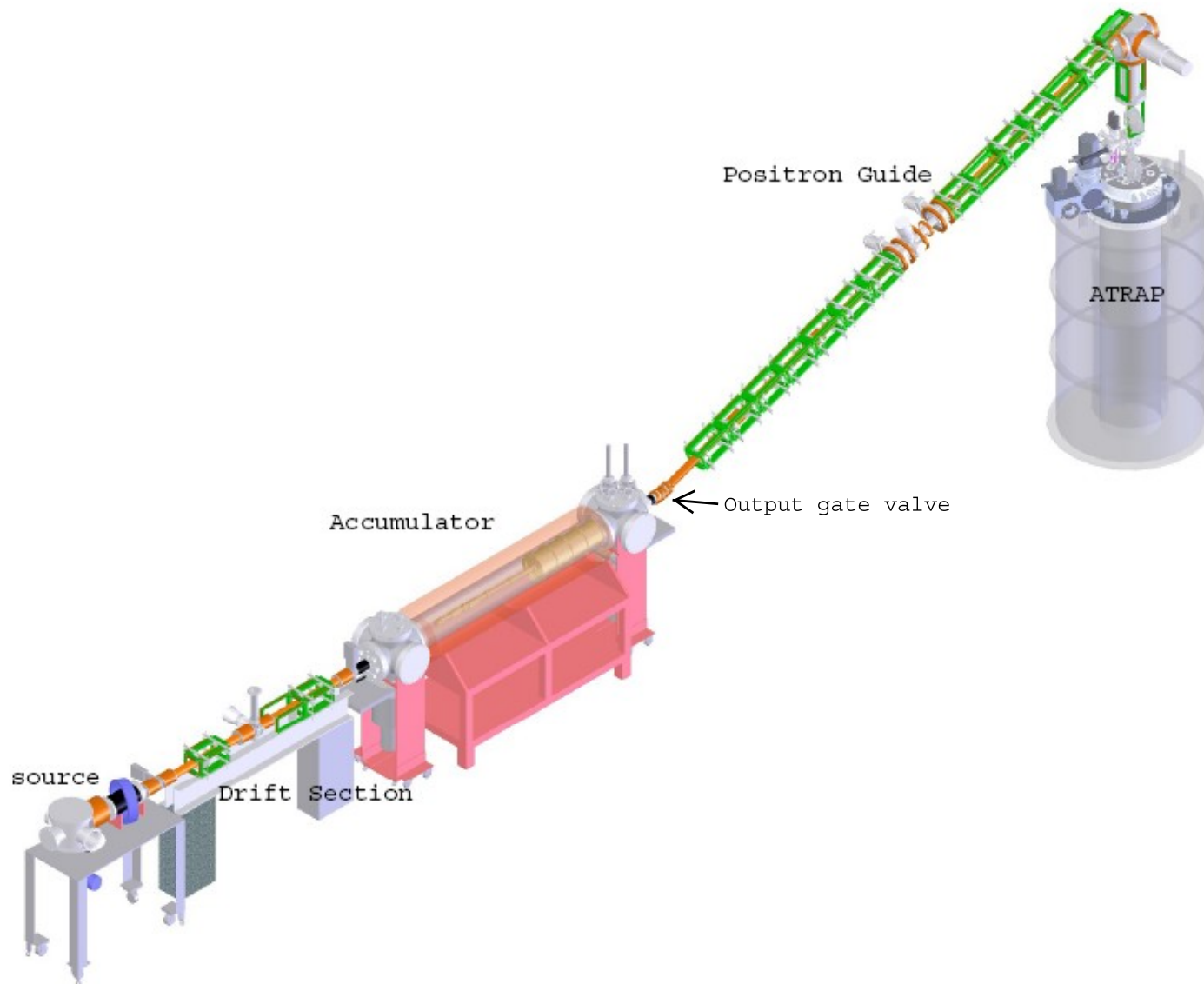


Figure 1.5: Schematic of entire apparatus

Chapter 2

Buffer-Gas Accumulator

The design of the buffer-gas accumulator is based on the apparatus designed and built by the Surko group at the University of California, San Diego [21, 22, 23, 24]. This type of apparatus was already used by the ALPHA collaboration (another antihydrogen project working out of the AD) for antihydrogen production. The apparatus consists of three sections, as shown in Figure 2.1: a source of positrons, a moderating material to slow down the positrons, and a capture region made up of a Penning trap where the buffer gas is introduced. It is in the accumulator Penning trap that the positrons are captured, cooled and stored until they are transferred into the ATRAP Penning trap.

2.1 ^{22}Na Source

The source of positrons is a 50-mCi ^{22}Na salt sealed within a titanium capsule with a 5- μm -thick titanium window at the front of the capsule. Positrons are produced when the radioactive ^{22}Na undergoes a nuclear transition, changing one proton into a neutron:



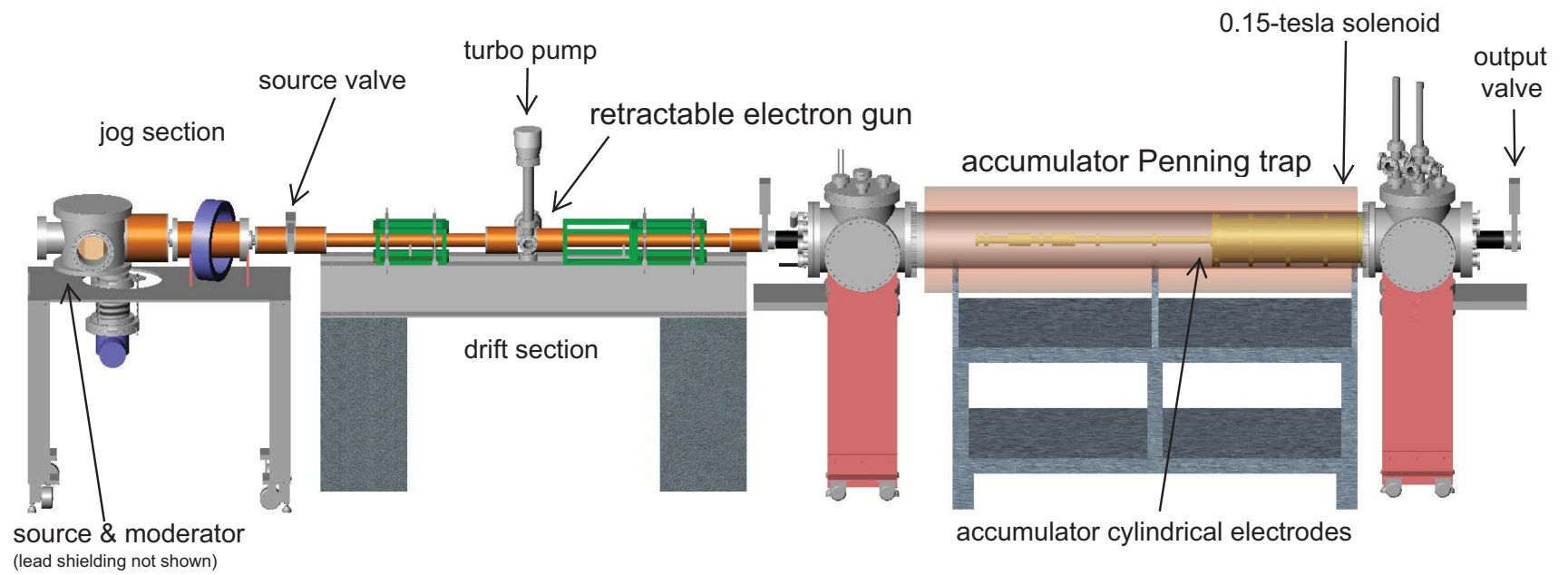


Figure 2.1: Schematic of accumulator

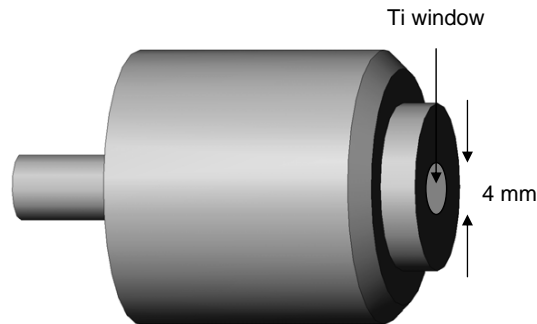


Figure 2.2: Source capsule for ^{22}Na

The resulting positron and electron neutrino share the 546 keV of energy available from the decay. The source therefore produces positrons at a range of energies between 0 and 546 keV.

The ^{22}Na source was manufactured by iThemba LABS and had an initial radioactivity of 52.5 mCi (1940 MBq) measured on October 20, 2006. The capsule in which the ^{22}Na salt is enclosed is shown in Figure 2.2. A ^{22}Na salt solution is dried onto a piece of tantalum at the back of the source capsule [25]. The source is then sealed with a 5- μm -thick, 4-mm-diameter titanium window [26].

^{22}Na has a half life of 2.602 years. Figure 2.3 shows the decay scheme for ^{22}Na to ^{22}Ne . When ^{22}Na decays, 90.57% of the time it emits a positron and 9.43% of the time it decays by electron capture (EC) and does not produce a positron. Since the source produces positrons isotropically, only 50% of the positrons are travelling towards the thin titanium window and thus in the direction of the Penning trap. An additional yield of 25% is due to the backscattering off of the tantalum backing [25]. The backing is chosen to be a high-Z material, specifically tantalum, because the backscattering coefficient increases with higher Z (since elastic scattering of positrons of this energy increases faster with Z

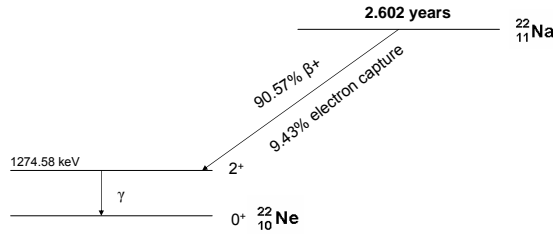


Figure 2.3: Decay scheme for ^{22}Na . ^{22}Na decays by either β^+ decay or electron capture.

than inelastic scattering [27]).

Of the positrons directed towards the Penning trap, approximately 50% are lost due to self-absorption inside the source material itself and another 28% are absorbed within the 5- μm titanium window [28]. Therefore, approximately 27% of the positrons that are created by ^{22}Na decay leave the window and can be used for moderation (approximately 24% of the disintegrations). Table 2.1 shows the strength of the iThemba ^{22}Na source as it decays over time. From the table, it can be seen that at the time of construction (November, 2006) the source had 471 million e^+/s emerging from its front window.

2.2 Neon Moderator

For the positrons that are emitted from the source to be useful for our accumulator, they must be in the form of a low-energy beam that has a small energy spread. Such a beam is produced by passing the high-energy positrons through a moderator and using a magnetic field to guide the resulting low-energy positrons. The efficiency of the moderator is defined as the ratio of the number of slow positrons in this beam to the number of positrons emitted by the source. The most efficient material used for moderating positrons is solid neon [29] and we have implemented a cryogenic solid neon moderator

Date	Activity (mCi)	Total e+ from source (x10 ⁹) /s	Usable e+ (x10 ⁶) /s
2006/11/01	52.0	1.73	471
2006/12/01	50.9	1.70	461
2007/01/01	49.8	1.66	450
2007/02/01	48.7	1.62	440
2007/03/01	47.7	1.59	431
2007/04/01	46.6	1.55	422
2007/05/01	45.6	1.52	413
2007/06/01	44.6	1.48	403
2007/07/01	43.6	1.45	395
2007/08/01	42.6	1.42	386
2007/09/01	41.7	1.39	377
2007/10/01	40.8	1.36	369
2007/11/01	39.9	1.33	361
2007/12/01	39.0	1.30	353
2008/01/01	38.1	1.27	345
2008/02/01	37.3	1.24	337
2008/03/01	36.5	1.22	330
2008/04/01	35.7	1.19	323
2008/05/01	34.9	1.16	316
2008/06/01	34.1	1.14	309
2008/07/01	33.4	1.11	302
2008/08/01	32.6	1.09	295
2008/09/01	31.9	1.06	289
2008/10/01	31.2	1.04	283
2008/11/01	30.5	1.02	276
2008/12/01	29.9	0.99	270
2009/01/01	29.2	0.97	264
2009/07/01	25.6	0.85	231
2010/01/01	22.4	0.74	202
2010/07/01	19.6	0.65	177
2011/01/01	17.1	0.57	155
2011/07/01	15.0	0.50	136
2012/01/01	13.1	0.44	119
2012/07/01	11.5	0.38	104
2013/01/01	10.1	0.33	91
2013/07/01	8.8	0.29	80
2014/01/01	7.7	0.26	70
2014/07/07	6.7	0.22	61
2015/01/01	5.9	0.20	53
2015/07/01	5.2	0.17	47
2016/01/01	4.5	0.15	41
2016/07/01	4.0	0.13	36
2017/01/01	3.5	0.12	31
2017/07/01	3.0	0.10	27
2018/01/07	2.7	0.09	24
2018/07/01	2.3	0.08	21
2019/01/01	2.0	0.07	18
2019/07/01	1.8	0.06	16
2020/01/01	1.6	0.05	14

Table 2.1: Table of the iThemba source strength and positron yield (usable positrons refers to the fact that only 27% of the positrons from the source make it through the titanium window).

for our positron apparatus.

2.2.1 Moderator Theory

Solid neon is a wide-band-gap insulator. As the high-energy positrons from the ^{22}Na source enter into the frozen neon, they quickly lose energy due to ionizing collisions. Since solid neon is an insulator, energy loss due to ionizing collisions can only occur if the positron has enough energy to create an electron-hole pair, an exciton, or a positronium atom. Once below the energy threshold at which these processes can occur, the only energy-loss mechanism available is phonon emission. The maximum phonon energy is very small, and therefore it is very likely that a positron that is cooled below this energy threshold will escape from the thin layer of solid neon. The positrons escape as long as they reach the surface of the neon before their energy falls below the positive positron work function of the solid neon [30].

2.2.2 Moderator Design

In order to use neon as a moderating material, the source must be cooled to below 15 kelvin, well below the freezing point of neon. Achieving this low temperature is accomplished using a Janis Research 4-kelvin coldhead. The coldhead is suspended from the underside of the source chamber, as shown in Figure 2.4. Figure 2.5 shows the copper holder which houses the ^{22}Na source. The source and holder are in thermal contact with the coldhead, but are electrically isolated from it (and thus from the rest of the vacuum chamber). This allows for a bias on the source, and thus enables the kinetic energy of the moderated positrons to be tuned to any value. The electrical isolation is accomplished with a disk of sapphire which is a good electrical insulator and has good thermal con-

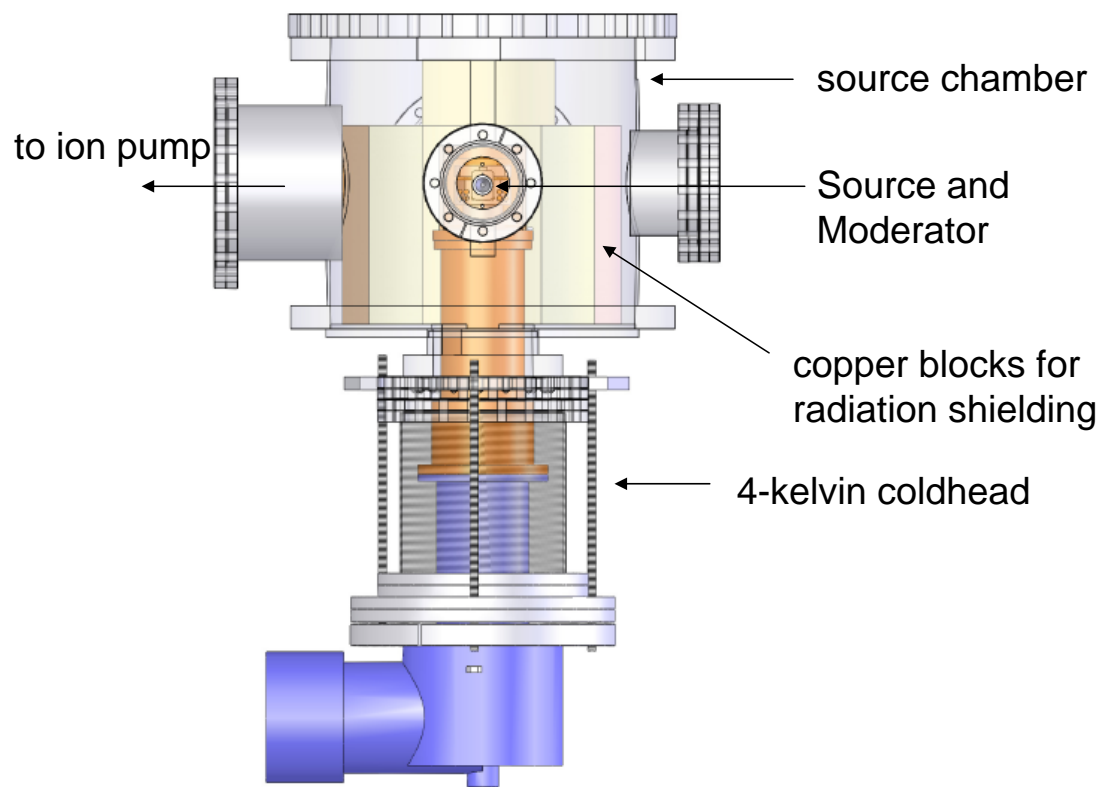


Figure 2.4: Schematic of the source chamber

ductivity. When the positrons leave the surface of the moderator, they accelerate due to a positive voltage applied to the moderator. The source is mounted in the horizontal direction with a copper cone placed directly in front of it, as shown in Figure 2.5. The solid neon moderator forms on the cold surfaces of the source capsule and of the cone. The cone geometry has been found to produce the most efficient positron moderators [31], since this geometry allows the fast positrons that failed to be moderated in the solid neon on the titanium window to have a second chance to moderate if they are directed at the cone. The source chamber is evacuated by an 8-inch ion pump directly attached to the side of the chamber. Copper blocks are placed within the vacuum chamber in the positions shown in Figure 2.4 in order to shield radiation coming from the ^{22}Na source. These blocks are not sufficient to enable a safe working environment, and therefore the entire source-end vacuum chamber is housed within a lead bunker (not shown in Figure 2.4).

2.3 Jog Section and Drift Tube

Once the positrons leave the moderator, they are magnetically guided towards the accumulator, as shown in Figure 2.6. (Guiding of positrons by magnetic fields will be discussed in great detail in Chapter 4.) The jog section serves a dual purpose: to physically offset the axis of the source and the rest of the apparatus (which reduces the need for shielding), and, more importantly, to filter the slow (moderated) positrons, which are guided by the magnetic field lines, from the high-energy, unmoderated positrons. The amount of deflection of the slow positrons is governed by the current through the jog coil of Figure 2.6.

To avoid contaminating the accumulator with neon and to avoid contaminating the neon moderator with gases from the accumulator, a two-meter tube with an inner diameter

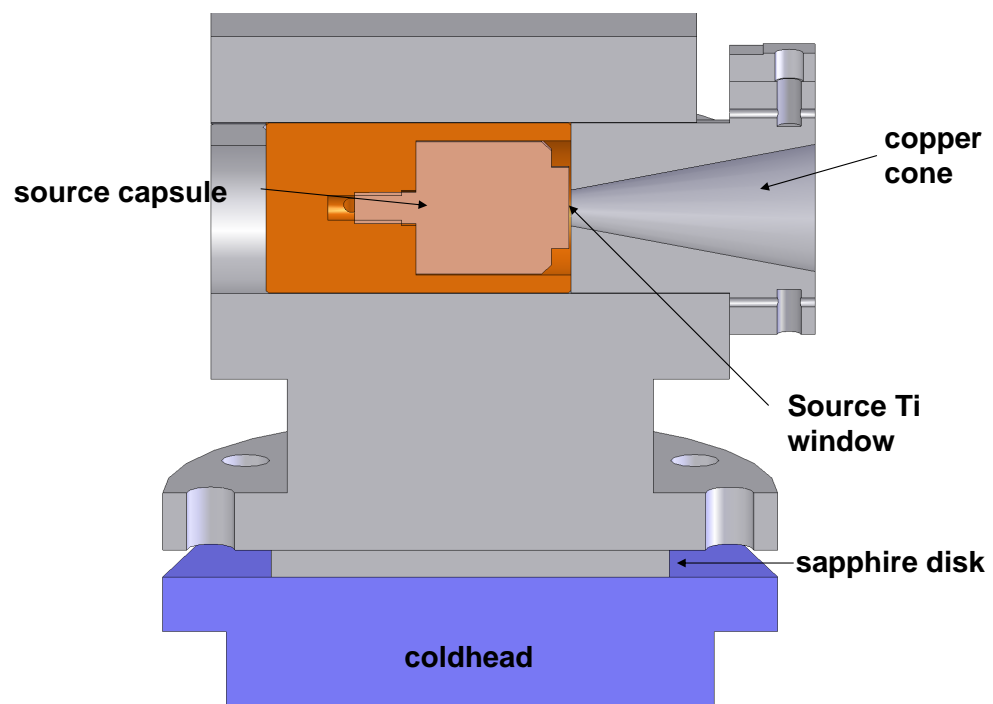


Figure 2.5: Schematic of the source and solid-neon moderator mount

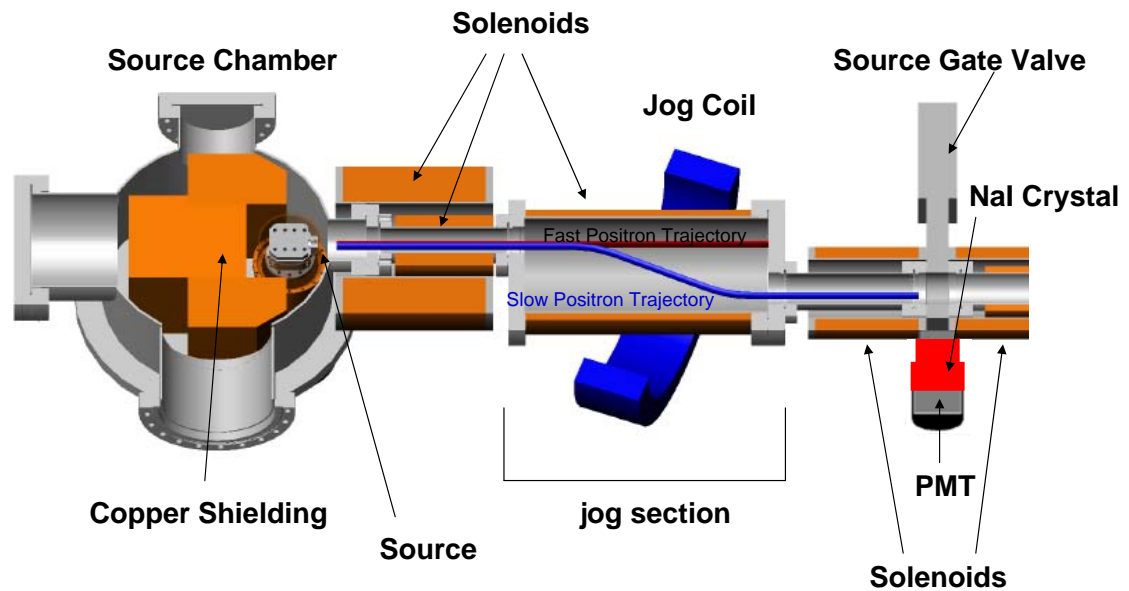


Figure 2.6: Source and jog section to filter out the unmoderated fast positrons

of 4.7 cm separates the moderator from the accumulator, as shown in Figure 2.1 and, at the half-way point of this tube, a 4.5-inch turbo pump with 1.27-cm-diameter, 20-cm-long pumping restrictions on either side further isolates the two vacuum systems. The positrons are guided along this drift tube and through these pumping restrictions by the magnetic field produced by solenoids wound directly onto the vacuum tube, and by additional coils near each of the pumping restrictions.

2.4 Scintillation Detection for Particle Counting

To measure the efficiency of the moderator, NaI crystals are used to detect the gammas produced from positron annihilations. When a positron strikes a surface, it annihilates with an electron. More than one gamma must be produced from the annihilation due to

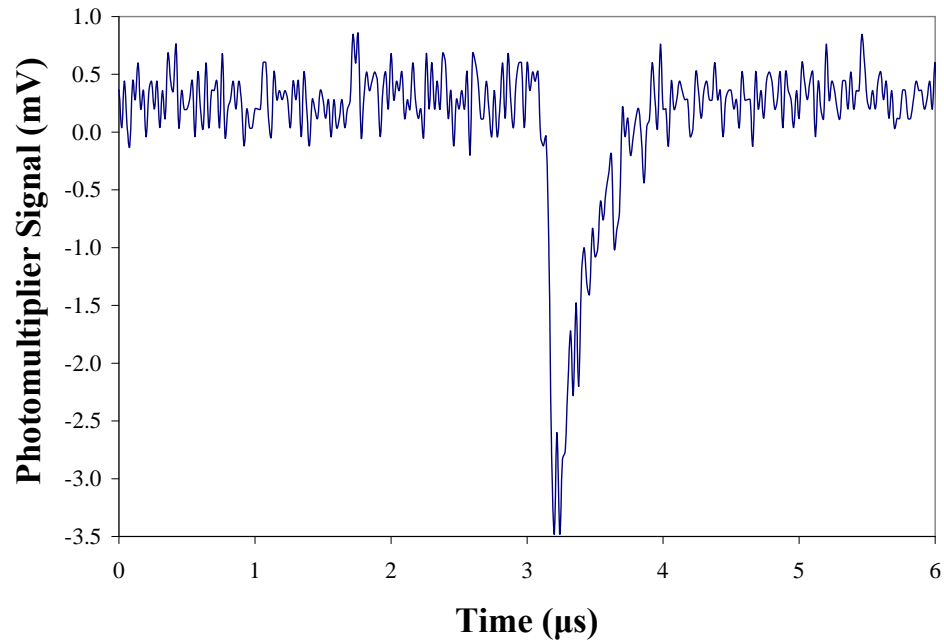


Figure 2.7: Positron annihilation signal on NaI detector and photomultiplier

conservation of energy and linear momentum. The most common case is that the annihilation will produce two gammas, each with an energy equal to the rest mass of the electron (0.511 MeV). Three or more gammas are also possible, but are much less probable. If a gamma penetrates the NaI crystal (positioned outside the vacuum chamber) and if it loses energy in the crystal (mostly from Compton scattering), scintillation photons are created inside the crystal. The crystal is abutted to a photomultiplier tube (Crismatec Scintibloc, model 12 S 20/3X) which detects the scintillation photons and amplifies the signal. 900V is typically applied to this PMT. Figure 2.7 shows the signal from the photomultiplier due to a single gamma detected by the NaI crystal. Once the signal is amplified and shaped by a discriminator it is fed into a ratemeter, from which the rate of positron annihilations can be determined.

2.5 Moderator Growth

The moderator is grown with ultra-pure neon gas (99.999%). The neon is introduced into the vacuum chamber through a mass-flow controller which controls the flow rate, and thus the neon pressure in the source chamber. The neon freezes onto all of the cold surfaces, but the positrons come into contact with only the neon which is deposited on the titanium window of the source and on the copper cone (see Figure 2.5). We find that the most efficient moderators are grown when the source chamber is not being pumped on during the growing process, contrary to what has been determined by other groups [32]. Neon is introduced at a rate such that the pressure of neon in the source chamber reaches 1 millitorr after 22 minutes.

As a diagnostic tool, a NaI detector is positioned outside of the vacuum chamber, as shown in Figure 2.6. The NaI-crystal PMT signal is fed into a ratemeter to determine the rate at which positrons annihilate at the closed gate valve of Figure 2.6 and thus the efficiency of the moderator.

Figure 2.8 shows the ratemeter signal of low-energy moderated positron annihilations during the period in which Ne gas is introduced into the source chamber. As shown in Figure 2.8, when the Ne gas is first introduced, the signal starts to climb, indicating that positrons are being moderated. After about 15 minutes, the signal starts to level off, and 22 minutes is found to be the optimum growing time. If a lower flow rate is used, a similar signal is acquired except that it takes longer to achieve the peak rate, and this peak rate is lower, indicating that a less efficient moderator is produced. Due to the equipment available, we were limited to a maximum of 10 sccm of gas flowing into the chamber (due to the range of the mass-flow controller used), so higher flow rates were not investigated.

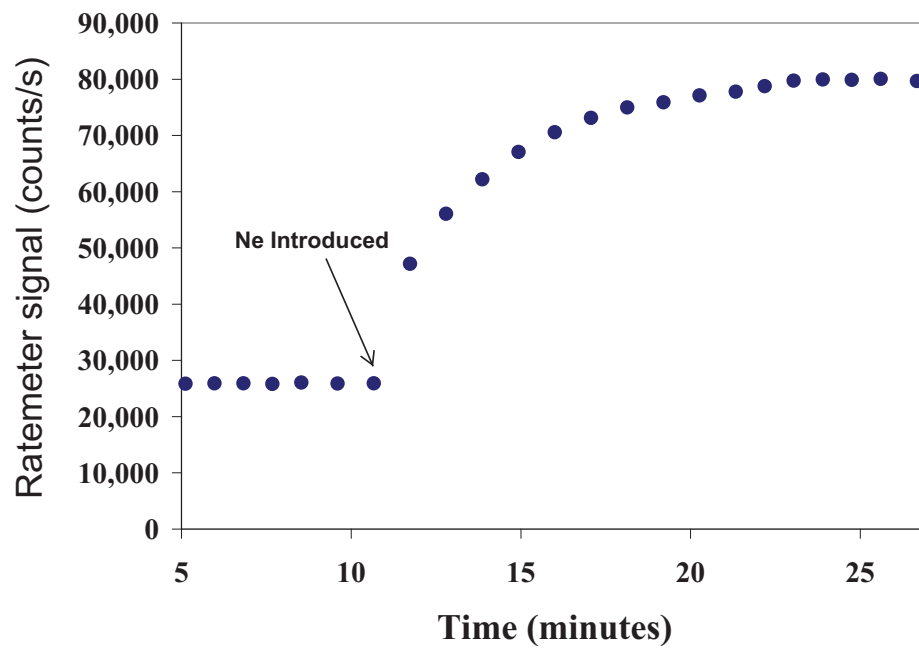


Figure 2.8: Signal from the ratemeter during moderator growth

2.6 Moderator Efficiency

To determine the moderator efficiency, the detection efficiency of the NaI detector must be estimated. This estimate must take into account the position and type of crystal used, shielding due to surrounding materials and the discriminator efficiency. To understand the first two factors, the software package GEANT4 is used to model the positron annihilations as they would occur in our apparatus. GEANT4 simulates the passage of particles through matter [33]. For our GEANT4 simulation, the material around the annihilation point is approximated by the geometry shown in Figure 2.9. The vacuum tube shown is a 304L stainless steel tube (with an outer diameter of 50.8 mm and a wall thickness of 1.9 mm) with a standard 3.375-inch-diameter Conflat flange. The simulation begins with low-energy positrons travelling through the vacuum chamber. Once they encounter the closed gate valve, they annihilate and produce gammas. The tracks of some sample gammas are shown in green in Figure 2.9. The gammas that pass through the NaI crystal and deposit energy in the crystal are counted as a signal by GEANT4. The GEANT4 simulation is run for 1,000,000 positrons that are incident on the gate valve. The fraction of positrons that produce a signal gives the simulated detection efficiency for this NaI detector. The GEANT4 simulation of 1 million positrons shows that 1 gamma is detected by the NaI crystal for each 47 positrons that hit the gate valve shown.

The discriminator efficiency takes into account the electronics that must be added into the NaI crystal/PMT/ratemeter circuit. The main electronic component used is a discriminator, which has a threshold voltage to filter out noise. The discriminator introduces an efficiency factor since some signals from the PMT are below the threshold. To calibrate the discriminator efficiency, oscilloscope traces from the NaI crystal/PMT were compared to the output of the discriminator. 10- μ s oscilloscope traces are observed with

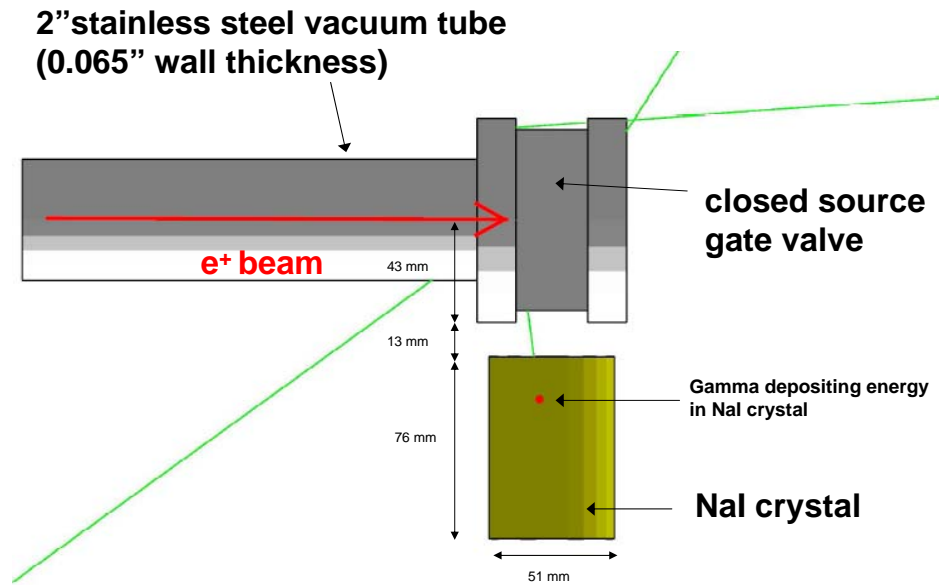


Figure 2.9: Schematic of the assumed geometry used for the GEANT4 simulation to calculate NaI detection efficiency. Green lines represent possible annihilation events.

random triggering to determine (by eye) how many counts are detected by the NaI crystal/PMT compared to how many counts are output by the discriminator. For 270 10- μ s oscilloscope traces, 175 discriminator counts corresponds to 274 counts observed on the oscilloscope. The counts and discriminator counts corresponds to an efficiency factor of 0.64(7). Experimentally, the ratemeter signal shows that there is a count rate of 6.5(1) $\times 10^4$ per second. Thus, the rate of moderated positrons is

$$\text{rate of slow positrons} = \frac{\text{ratemeter signal}}{\text{discriminator efficiency} \times \text{detection efficiency}} \quad (2.1)$$

$$= 4.8(7) \text{ million moderated positrons per second} . \quad (2.2)$$

The ratemeter measurement was taken in November 2007 when the source strength measured 40(1) mCi (see Table 2.1) and the number of β^+ particles emitted from the front

of the ^{22}Na source was $1.33(3) \times 10^9$. Thus, the moderator efficiency is

$$\text{moderator efficiency} = \frac{\# \text{ of slow positrons}}{\# \text{ of positrons from source}} = 0.36(6)\%. \quad (2.3)$$

2.7 Energy Spread of Moderated Positrons

A computer-controlled bias enables the axial kinetic energy of the moderated positrons to be adjusted. Figure 2.10 shows the energy distribution of the moderated positron beam when the moderator is set to 10 V, 20 V and 30 V. The data shown are measured by having the beam of moderated positrons annihilate on the output valve (of Figure 2.1) after passing through the accumulator Penning trap. A NaI crystal detector is positioned beside the output valve to measure the annihilation rate of positrons. A blocking potential is applied to the Penning trap, and, by varying this blocking potential, the energy distribution of the moderated positrons is determined, as shown in Figure 2.10.

The energy distribution changes dramatically when the moderator bias is changed. For larger biases, the positron number increases, but the energy spread increases more substantially. Because the energy spread is greatly increased when applying higher voltages to the moderator, and because the accumulation efficiency decreases for a wide energy spread, the optimal moderator voltage for accumulating positrons is found to be 10 V.

2.8 The Accumulator Penning Trap

Once the beam of low-energy positrons leaves the drift section shown in Figure 2.1, it enters the accumulator. The accumulator is made up of a 0.15-tesla, 2-m-long solenoid that provides radial confinement for the positrons. Inside the solenoid there is a series

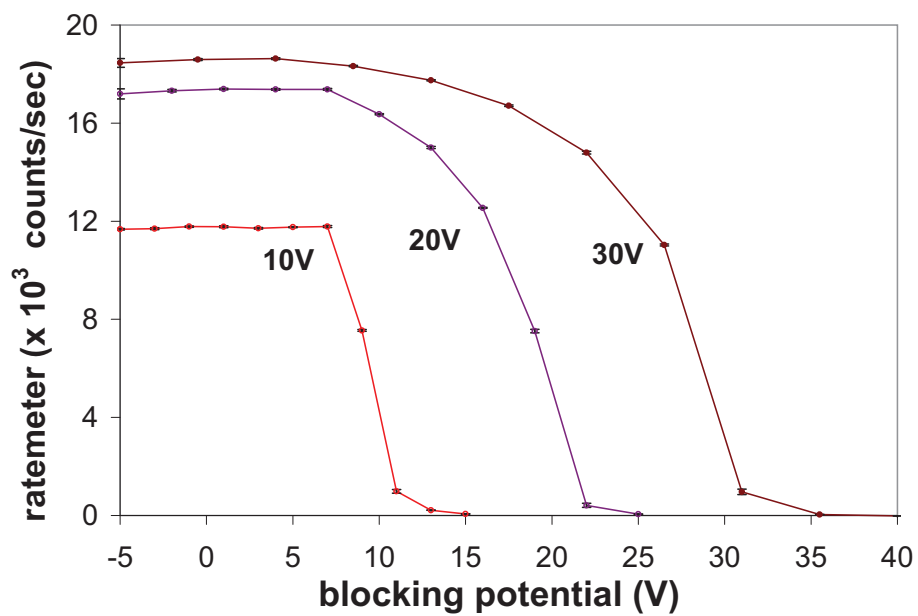


Figure 2.10: Energy distribution of the moderated positrons. The graph shows how the distribution changes when the moderator is biased at 10 V, 20 V and 30 V. The data shows that most of the positrons have axial kinetic energy of between 7 and 11 eV when the moderator is set to 10 volts, between 10 and 22 eV when it is set to 20 volts, and between 17 and 32 volts when it is set to 30 volts.

of coaxial cylindrical electrodes that provide axial confinement for the positrons. The positrons are trapped, accumulated and stored in this Penning trap until they are transferred into the ATRAP Penning trap.

2.9 Buffer-Gas Accumulation

The accumulator design is based on a three-stage accumulation scheme developed by the Surko group at the University of California, San Diego [21, 22, 23, 24]. A diagram of the accumulator is given in Figure 2.11. It is made up of a specially designed electrode stack (labelled Stage 1, 2 and 3 in Figure 2.11) inside of a 0.15-T axial magnetic field. The slow beam of moderated positrons enters the accumulator electrodes from the left of the figure. The three stages have high ($P \approx 10^{-3}$ torr), medium ($P \approx 10^{-4}$ torr) and low ($P \approx 10^{-6}$ torr) pressures, respectively, as shown in Figure 2.11. The high pressure is obtained by introducing nitrogen gas into Stage 1. The increased pumping speed obtained by the larger inner diameter of the Stage 2 and Stage 3 electrodes gives the lower pressures in these two regions. As discussed in Section 2.9.2, the positrons are initially captured via inelastic collisions with the nitrogen gas in the high-pressure region and are then stored in the low-pressure region, where they are less likely to annihilate with the electrons in the nitrogen gas.

2.9.1 Magnetic Field

The 0.15-T axial magnetic field of the accumulation Penning trap is produced by a copper solenoid wound by New England Technicoil. The solenoid is wound with square copper tube to enable cooling water to flow through the coils to dissipate the 15 kW of

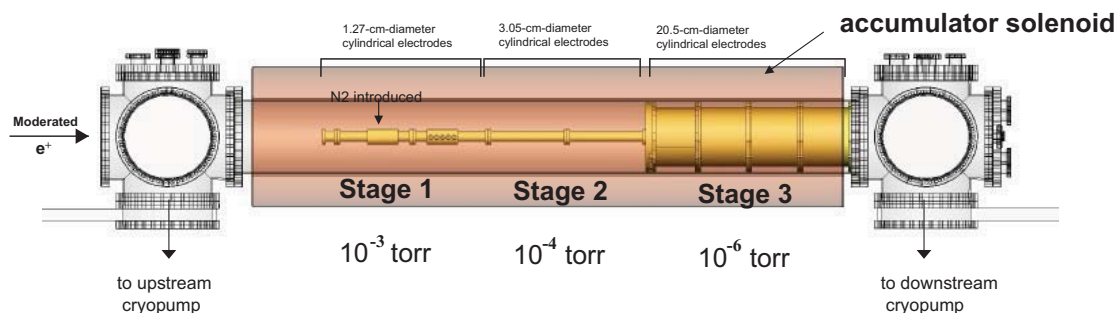


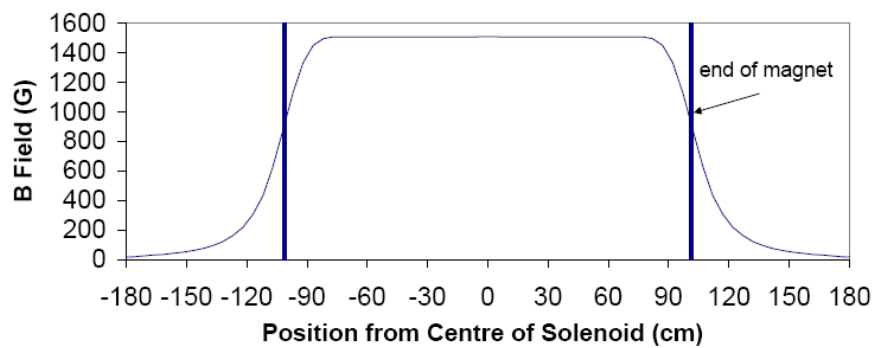
Figure 2.11: Schematic of the accumulator. The accumulation electrode stack is designed to produce the approximate pressures shown.

heat produced. The solenoid produces a field of 0.15 tesla with a current of 400 A (which requires a voltage of 38V). The magnetic field on-axis is shown in Figure 2.12a. The solenoid was designed by Dr. Matthew George to theoretically produce an axial field that varies in magnitude by $\leq 0.0015\%$ over the central 1.5 m of the solenoid.

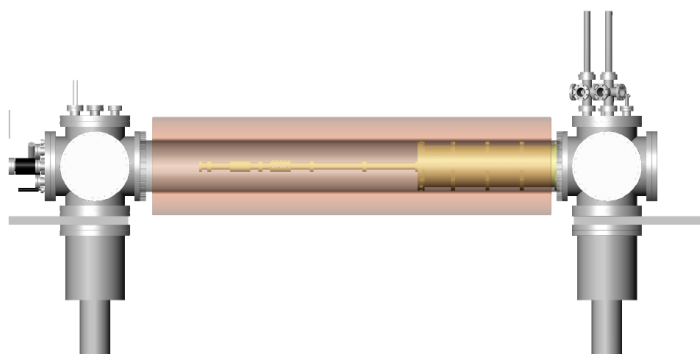
2.9.2 Positron Interactions with Nitrogen Molecules

Low-energy positrons can interact with nitrogen molecules in several ways. They can lose energy to the nitrogen molecules via both inelastic collisions (ionization, electronic excitation, dissociation, vibrational excitation, rotational excitation, or charge exchange) and elastic collisions (momentum transfer). The rate at which each of these processes occurs depends on the positron energy, but each (except for elastic collisions) has an energy threshold below which the process is forbidden. Murphy and Surko have shown [21] that the dominant energy-loss mechanism in a nitrogen buffer-gas accumulator is the excitation of a nitrogen molecule, which has an average energy loss of 9 eV per collision, and a lower threshold of 7 eV. For higher-energy positrons the presence of vibrational modes of the electronically excited state creates a large increase in the number of available

a)



b)



c)

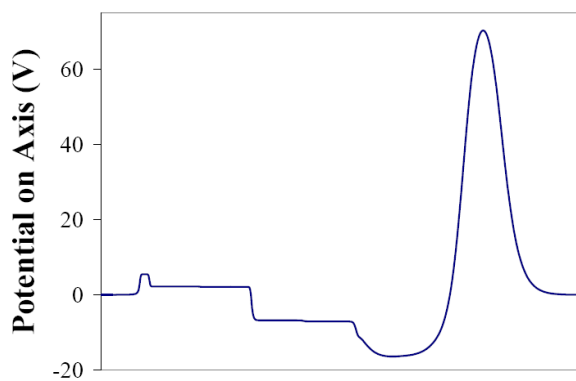


Figure 2.12: The on-axis axial magnetic field produced by the resistive solenoid, the electrode stack, and potential on axis during accumulation.

states.

The positron can also directly annihilate with an electron in the nitrogen molecules or form positronium, which also leads to the positron annihilating. The threshold for positronium formation is 8.8 eV. When the positron energy is 11 eV, the efficiency of positron formation and electronic excitation are equal. At higher energies, loss due to positronium formation dominates.

2.9.3 Pressures in the Accumulator

The electrode stack of Figure 2.11 is divided into three stages, each having a different inner diameter, with the diameters chosen to produce the desired pressures along the axis of the trap. The nitrogen buffer gas is introduced into the electrode stack in Stage 1, where the inner diameter of the electrodes is small (1.27 cm). The last electrode in Stage 1 (to the right of the electrode in which nitrogen is introduced, shown in Figure 2.11) has radial holes drilled into it to provide an alternate path for the nitrogen to be pumped out other than axially through the open end of Stage 1 (at the left side of Figure 2.11), or through Stages 2 and 3. The inner diameter of Stage 2 is larger (3.05 cm) to produce an intermediate pressure region between the high pressure of Stage 1 and the low pressure of Stage 3. The inner diameter of the electrodes in Stage 3 is made as large as possible (20.5 cm) to provide the largest pumping conductance from the downstream cryopump (shown to the far right of Figure 2.11). Table 2.2 shows the length and inner diameter of the electrodes in each stage of the accumulator.

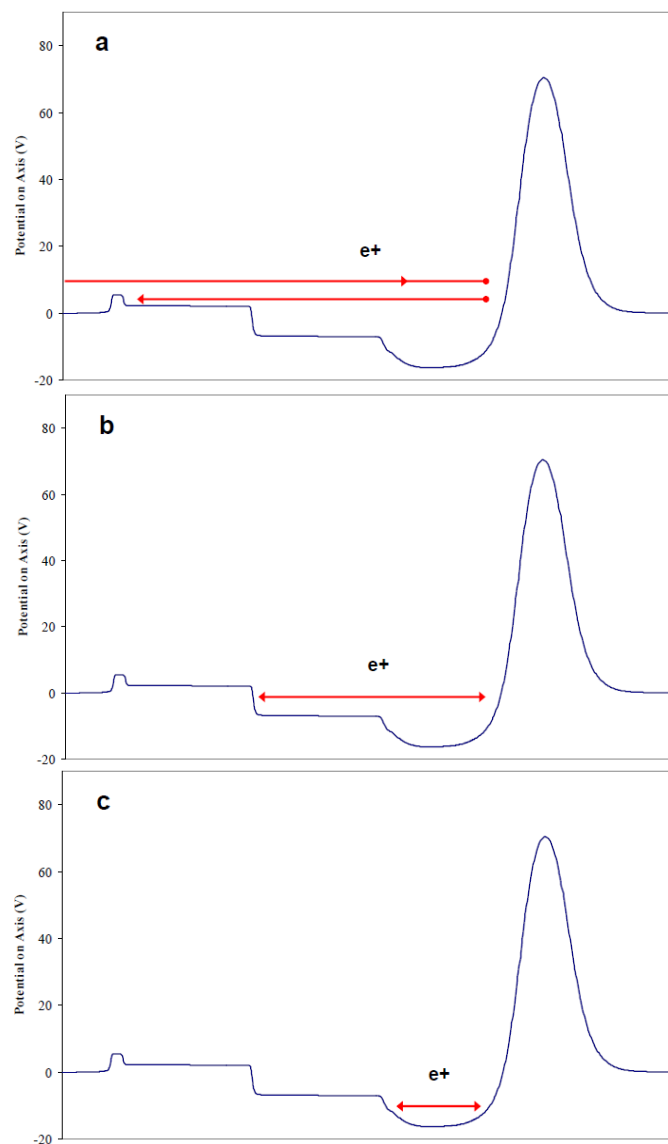


Figure 2.13: Positron range of motion during each step of accumulation

	# of electrodes	Total Length (m)	Inner Diameter (mm)	Approx. Pressure (torr)
Stage 1	3	0.57	12.7	1×10^{-3}
Stage 2	3	0.565	30.5	1×10^{-4}
Stage 3	4	0.681	205	1×10^{-6}

Table 2.2: The dimensions of the electrodes in each stage of the accumulator.

2.9.4 Electrostatic Potentials in the Accumulator

The electrode stack is designed to utilize the electronic excitation of nitrogen as the energy loss mechanism within the electrode stack. An energy-loss mechanism is required because any positron that has enough kinetic energy to enter the Penning trap also has enough energy to leave the trap. To be trapped within the electrode stack, the positrons must lose axial kinetic energy within one round trip through the accumulator electrodes. Figure 2.12b shows the electrode stack and Figure 2.12c shows the on-axis potentials produced by the potentials applied to the electrodes during accumulation.

The three-stage accumulation process is shown in Figure 2.13. The low-energy positrons (from the moderator) enter the Penning trap from the left with an average kinetic energy of 10 eV, as shown in Figure 2.10. They travel through the electrode stack until they encounter the large positive potential applied to the final electrode. This large potential reflects the positrons back towards the source end (as shown in Figure 2.13a). The positrons must undergo one collision with a nitrogen molecule during this return trip to be trapped (otherwise the reflected positrons continue back to the moderator and annihilate) and the 10^{-3} torr pressure in the Stage 1 is chosen to ensure that the majority of the 10-eV positrons experience this one collision.

After a positron loses approximately 9 eV of kinetic energy from this first collision, it

is axially trapped within the electrode stack. After a second collision, the positron loses approximately another 9 eV of energy and is then held in the region of Stage 2 and Stage 3, as shown in Figure 2.13b. After the positron loses another 9 eV of kinetic energy due to a third collision, it becomes trapped within Stage 3, as shown in Figure 2.13c. At this point, the positron energy is below the threshold of positronium formation. With this low kinetic energy, a positron trapped in Stage 3 of the accumulator, where there is very little background gas, can survive for a long time as shown in section 2.11.2.

2.10 Rotating Wall

In an ideal Penning trap, the confinement time for charged particles is infinite. In reality, whether it is due to mechanical asymmetries, non-uniformity in the magnetic or electric fields or misalignment of the electric and magnetic fields, clouds of charged particles tend to expand [34]. The rate of such expansion is increased in our trap due to the presence of nitrogen gas. Both the nonidealities of the trap and the background gas break the cylindrical symmetries of the Penning trap and cause a drag on the rotating plasma. The drag causes the plasma to expand and subsequently causes particle loss. The drag can be counteracted by a rotating electric field, which imparts angular momentum to the plasma, thus spinning it up and reducing its diameter.

2.10.1 Rotating Wall Theory

The coupling between the rotating electric field and the plasma [35] can only occur if the cloud of particles constitute a well-defined plasma. To be a well-defined plasma, the

Debye length must be much smaller than the length and radius of the the plasma:

$$\lambda_D \ll L_p, r_p, \quad (2.4)$$

where

$$\lambda_D = \left(\frac{\epsilon_0 k T}{n_e e^2} \right)^{1/2}, \quad (2.5)$$

k is Boltzmann's constant, T is the temperature of the plasma and n_e is the density of the plasma. Additionally, to be a well-defined plasma, it is required that

$$n_e \lambda_D^3 \gg 1. \quad (2.6)$$

The cloud radius in our accumulator (without the rotating wall present) is measured to be $R_p = 6.2$ mm (using the technique described later in Section 2.11.1). The length of the cloud is not measured, but, due to the geometry of the electrode stack and the shape of the potential applied during accumulation, it is estimated to be approximately 15 cm. For a typical accumulation of positrons, the particle number is 20 million by the end of the accumulation period. The density (which should be approximately uniform) is therefore $n_e \approx 1.1$ million e^+/cm^3 . The apparatus is at room temperature, so that $kT = 0.025$ eV, and from Equation 2.5, the Debye length is $\lambda_D \approx 1.1$ mm, and therefore the condition set out in Equation 2.4 is met. Additionally, the condition set out in Equation 2.6 is met since $n_e \lambda^3 \approx 1500$. Therefore, the cloud can be considered a plasma and the rotating wall can be expected to effectively spin-up the cloud.

While spinning up the plasma, the rotating electric field also heats up the particles. To counteract the heating, a cooling mechanism is required. One possible cooling mechanism is synchrotron radiation that is given off by the positrons as they undergo cyclotron

orbits. However, the cyclotron cooling time γ_c^{-1} is given by

$$\gamma_c^{-1} = \frac{3\pi\epsilon_0 mc^3}{e^2\omega_c^2}, \quad (2.7)$$

where ω_c is the cyclotron frequency of the positron, and, in the 0.15-T magnetic field of the accumulator, γ_c^{-1} is 115 seconds, much too long to be considered as an efficient cooling mechanism. The method employed instead to counteract the heating of the positrons is the use of a neutral buffer gas. This gas should have a low annihilation cross section since it is being introduced into the region where the positrons are being stored. As well, a large cross section for low-energy inelastic processes (such as vibrational and rotational excitation) is required to provide an efficient cooling mechanism. Finally, the gas should have a low elastic-collision cross section in order to avoid cross-field transport.

Since nitrogen is already introduced as a buffer gas for the accumulation process, it is an obvious choice to use as this cooling gas as well. Some groups have chosen to use nitrogen, but it has been found [35] that SF_6 and CF_4 have lower annihilation rates and much shorter cooling times. In the present accumulator, SF_6 is introduced at pressures as low as 8×10^{-8} torr (as measured at the top of the downstream cryopump shown in Figure 2.11).

2.10.2 Rotating Wall Implementation

To apply a rotating electric field, the first electrode in the third stage of the accumulator is split into four quadrants, as shown in Figure 2.14. The quadrants are electronically isolated from each other with sapphire rods and can be independently biased. The DC component (to all 4 quadrants) produces the potential on axis shown in Figure 2.12c. A sinusoidal AC component is added to each segment, with a phase offset of 90° between

adjacent quadrants. The rotating wall is applied during the entire accumulation process, and thus the positrons interact with the rotating wall electric field during the entire time that they spend in Stage 3 of the accumulator.

2.11 Plasma Compression with Rotating Wall

The most important function of the rotating wall is to decrease the plasma radius. This reduction not only reduces losses by counteracting plasma expansion, but also a small plasma radius will be essential for transferring of positrons into the ATRAP Penning trap, as will be discussed in Chapter 3.

2.11.1 Plasma Radius Measurement

The radial plasma size is measured using a skimmer that is positioned after the final electrode (within the accumulator vacuum chamber, as shown in Figure 2.15). The skimmer is positioned in the fringing field of the 0.15-T accumulation solenoid, where the magnetic field is approximately 0.02 tesla. The skimmer is constructed out of aluminum attached to a linear translation stage. When the plasma of positrons is released from Stage 3 of the accumulator, they must pass by this skimmer. The number of positrons that pass the skimmer can be measured using a Faraday cup. As the skimmer is lowered, the total number of positrons making it to the Faraday cup is measured and therefore the vertical profile of the positrons can be determined.

Since the skimmer is in a smaller magnetic field than the electrode stack, the positrons are expected to have an expanded radial profile at the position of the skimmer. The expansion is due to the conservation of magnetic flux ϕ through the cross sectional area (A)

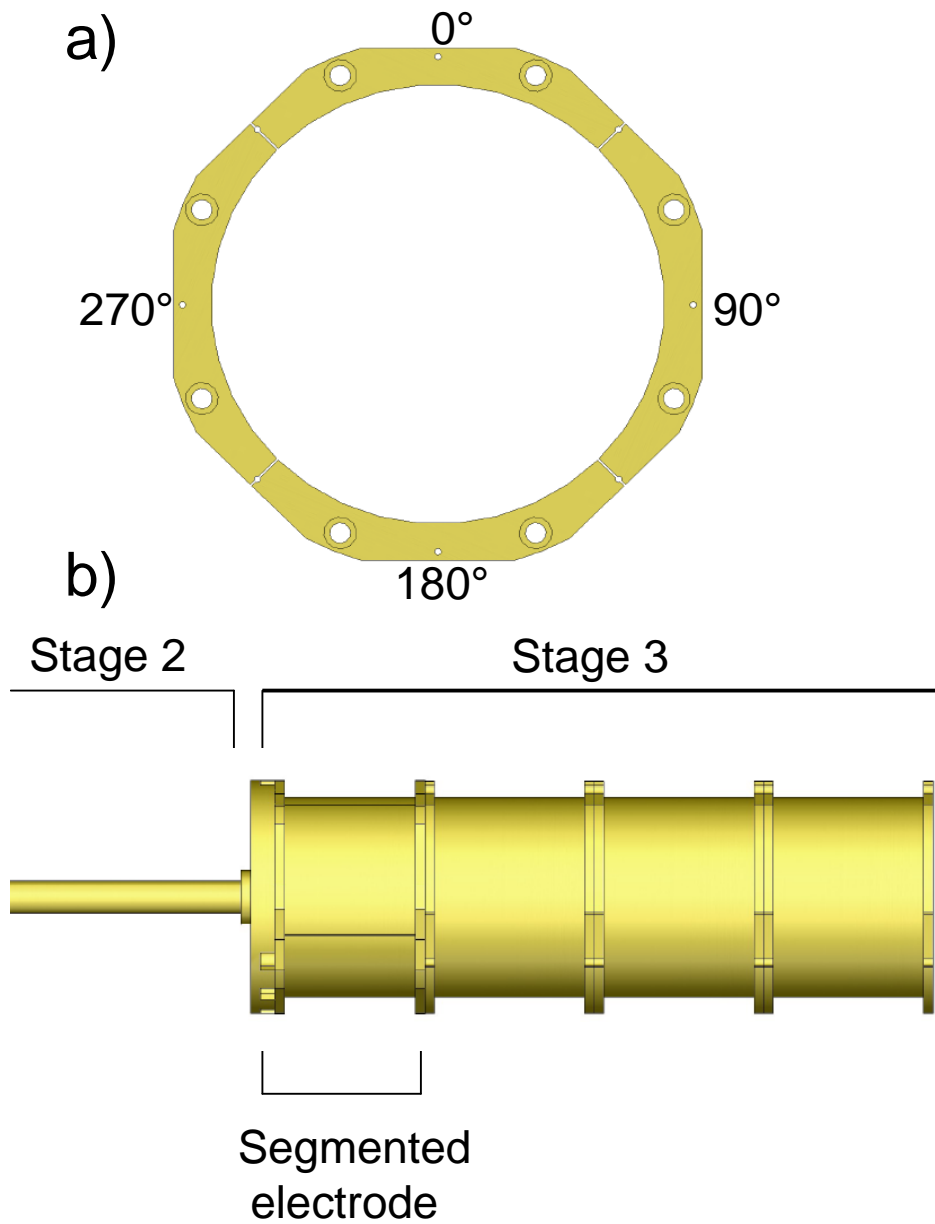


Figure 2.14: a) Axial view of the segmented electrode that produces the rotating wall. b) Position of the segmented electrode in Stage 3.

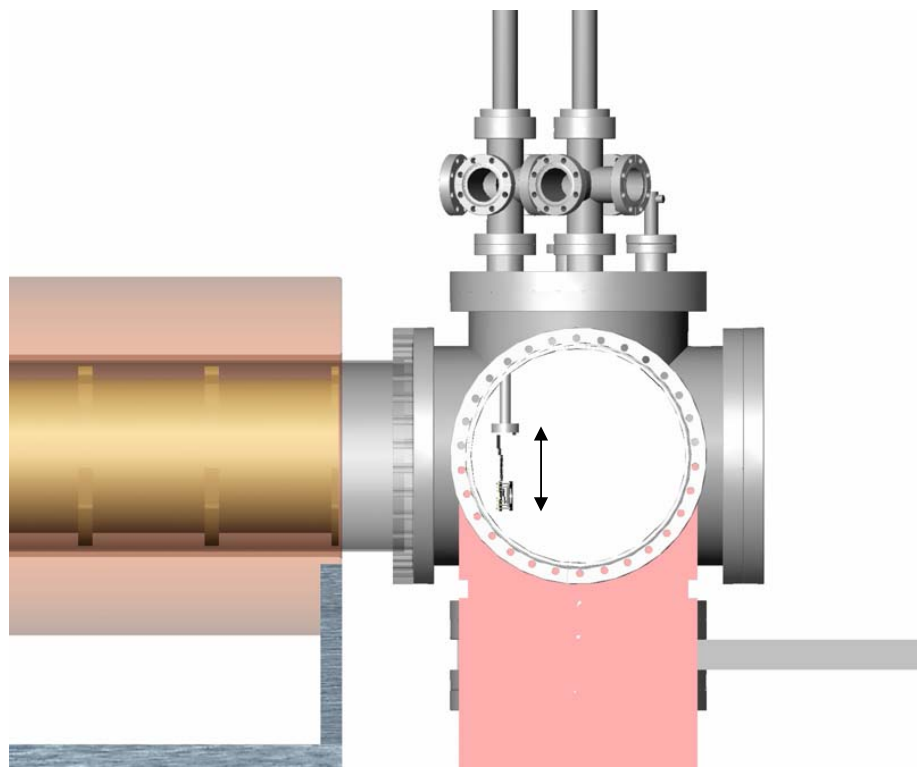


Figure 2.15: Picture of skimmer used to make plasma radius measurements. The skimmer can be moved vertically outside of vacuum using a translational stage.

of the positron cloud, where

$$\phi = \frac{B}{A}. \quad (2.8)$$

Thus, as a plasma moves between two different magnetic fields, the cross-sectional area of the plasma scales as the ratio of the magnetic fields, and thus the diameter is proportional to the square root of the ratio of the magnetic fields.

The magnetic field at the skimmer is 7.5 times smaller than in the accumulation solenoid, and thus the positron cloud diameter is $\sqrt{7.5}$ times smaller inside the accumulation solenoid than it is at the skimmer where it is measured.

Without the rotating wall applied, the vertical extent of the positrons is measured to be 33.6 mm at the position of the skimmer, as shown in Figure 2.16. This would correspond to a plasma diameter of 12.4 mm in the accumulation magnetic field.

When the rotating wall is applied, the vertical extent of the positrons is measured to be 6.2 mm at the skimmer (see Figure 2.16), thus giving a diameter of 2.3 mm inside the accumulation solenoid. The rotating wall decreases the radius of the plasma by a factor of 5.4 and increases the central density of the positron cloud by a factor of 30.

2.11.2 Number of Accumulated Positrons Versus Accumulation Time

Because the rotating wall is effective in reducing plasma expansion, it allows for increased load times. Figure 2.17 shows the number of accumulated positrons versus load time. The number of accumulated positrons is measured by ejecting them and observing them on a Faraday cup that is situated three meters away. For the positrons to make it to the Faraday cup, they must have a radial extent (diameter) of less than 4.8 cm (in a 0.02-T field). Plot (a) shows the number of positrons counted on the Faraday cup when

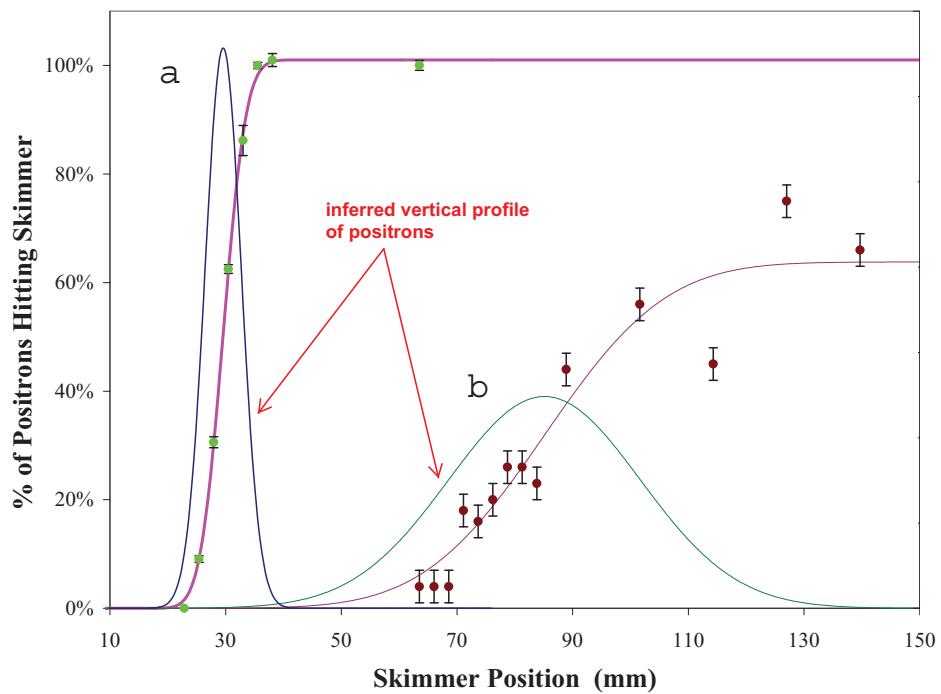


Figure 2.16: a) Vertical profile measurement at the skimmer with rotating wall applied. The vertical extent (FWHM) is measured to be 6.2 mm. b) Vertical profile measured at the skimmer without the rotating wall. The vertical extent (FWHM) is measured to be 33.6 mm.

the rotating wall is turned off. Plot (b) shows the number of positrons counted on the Faraday cup when the rotating wall is applied and shows that accumulation is improved when the rotating wall is used. Even at 20 seconds, when the number of particles is <10 million, there is a clear improvement due to the application of the rotating wall. With this number of positrons, the density is lower and the Debye length is large, leading to a cloud that is not a plasma because it does not satisfy the conditions defined by Equations 2.4 and 2.6. This result contradicts the widely-accepted idea that the plasma modes are being excited by the rotating wall. The group of Allan Mills [32] has also found strong evidence of non-plasma rotating wall effects, but to date, no mechanism has been found to explain the method of imparting angular momentum into a non-plasma cloud.

The fact that the accumulation number is proportional to time for the first 50 seconds (as shown in Figure 2.17) indicates that annihilation of positrons is not a major concern on this time scale.

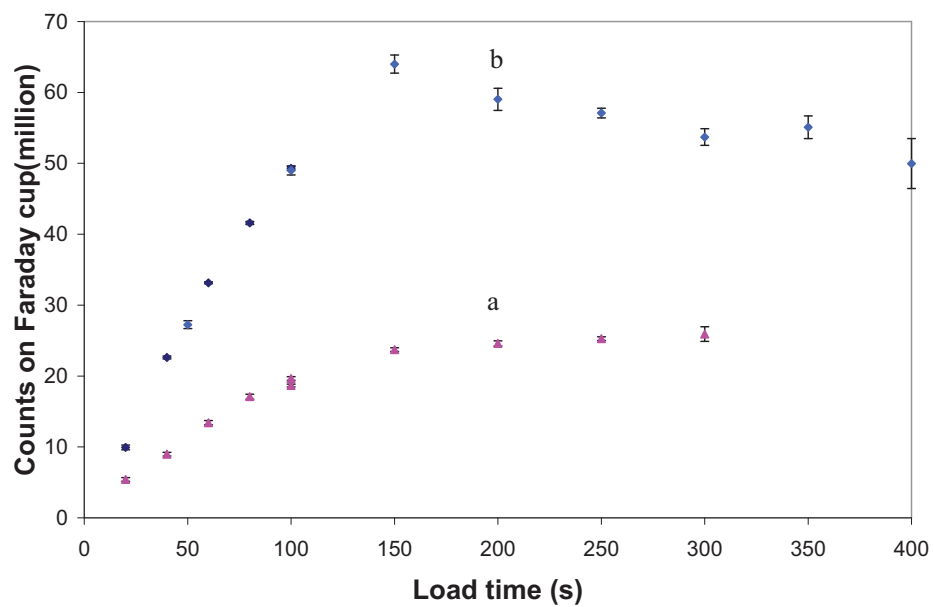


Figure 2.17: The number of positrons accumulated versus loading time a) without a rotating wall and b) with rotating wall.

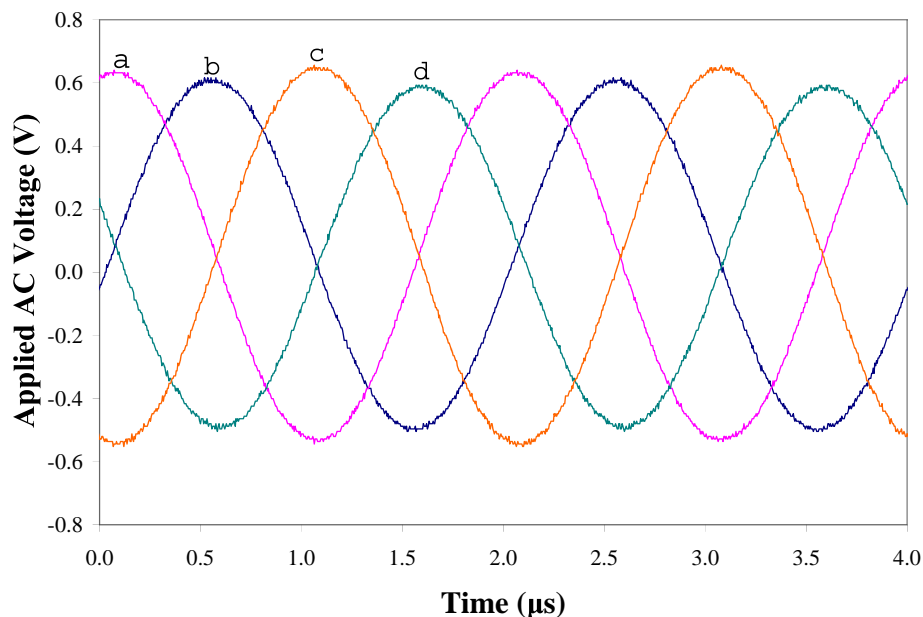


Figure 2.18: The AC component to the split electrode potentials that makes up the rotating wall. These are the standard settings used for the rotating wall. The amplitude is measured as a Peak-to-Peak voltage of 1.15 V with a frequency of 500 kHz.

2.11.3 Rotating Wall Amplitude and Frequency

The rotating wall is applied via a control box that sets the amplitude applied to each quadrant of the segmented electrode independently, and which sets a 90° relative phase shift between adjacent quadrants. The AC voltage applied to each segment is shown in Figure 2.18. The common DC and independent AC components are fed into bias tees, which are in turn attached to each of the 4 quadrants of the segmented electrode shown in Figure 2.14.

At normal running conditions, the amplitude (peak-to-peak) of each quadrant is set to 1.15 V. Figure 2.19 shows the positron number as this amplitude is changed. The pressure of SF_6 defines how much cooling is available in order to counteract the heating inherent

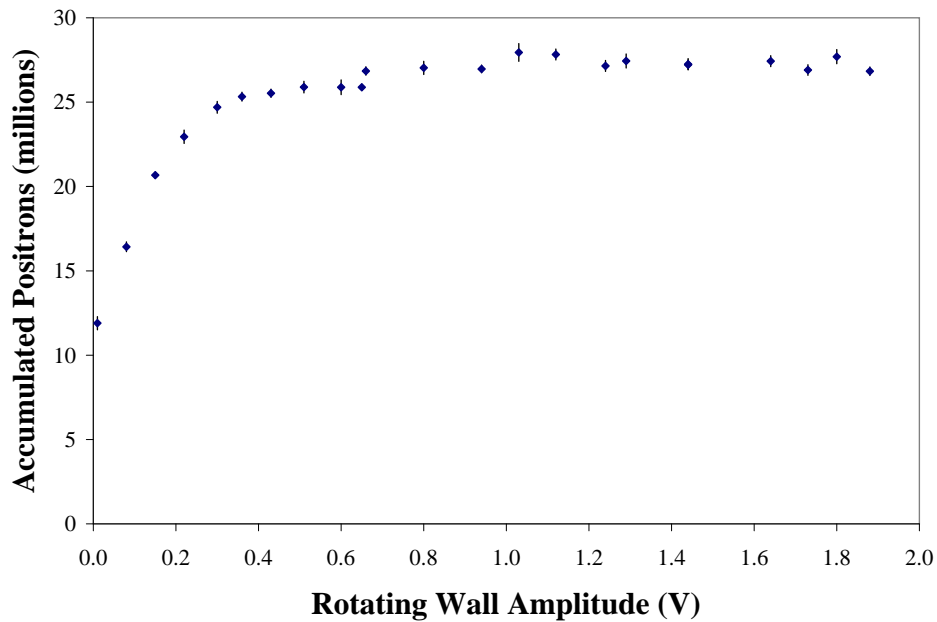


Figure 2.19: Number of positrons counted on the Faraday cup while changing the amplitude of the applied rotating wall (frequency set to 500 kHz and SF₆ pressure at 8 x 10⁻⁸ torr).

in the application of the rotating wall electric field. During normal running conditions, the SF₆ pressure is set to 8 × 10⁻⁸ torr as measured in the 14-inch supercross that is downstream of the accumulator.

As can be seen in Figure 2.20, the response to the rotating wall is rather broadband in character. Optimally, the rotating wall is set to a frequency of 500 kHz.

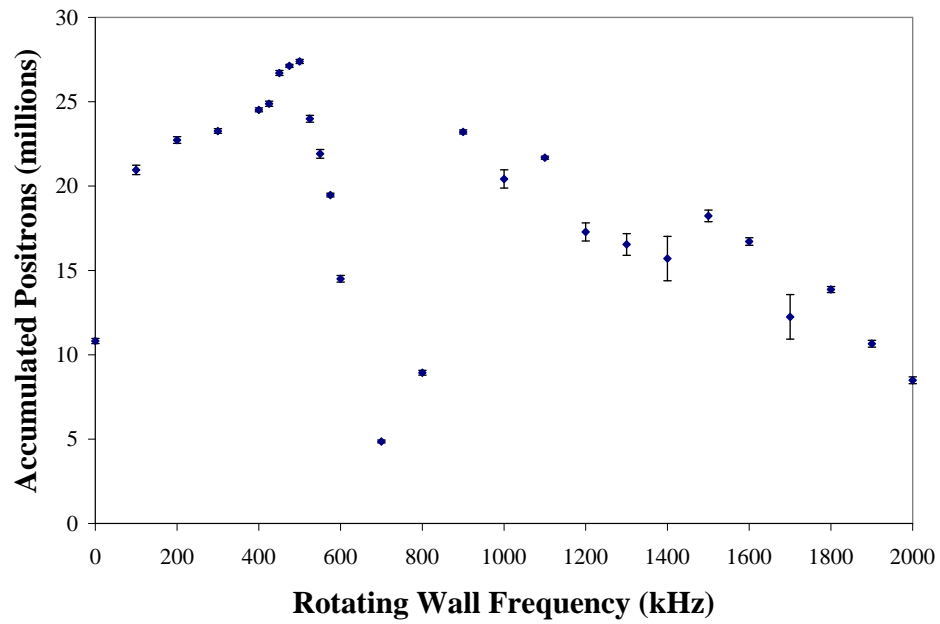


Figure 2.20: Number of positrons counted on the Faraday cup while changing the frequency of the applied rotating wall (amplitude set to 2V and the SF₆ pressure at 8.3 x 10⁻⁸ torr).

Chapter 3

Transferring Positrons

3.1 Pulsing Positrons Out of the Accumulator

Once positrons have been accumulated for approximately 50 seconds, they are transferred from the accumulator into the ATRAP Penning trap. The positrons accumulate into a negative well in Stage 3, as shown in Figure 2.13c. The positrons are guided magnetically through a grounded positron guide into the ATRAP apparatus (see Figure 1.5). In order to travel through this grounded guide, the positrons must start at a positive potential, and thus, after accumulating, the potential well containing the positrons is offset by a positive potential, as shown in Figure 3.1a. The positrons can then be launched into the positron guide by pulsing up the voltage of the well containing the positrons, as shown in Figure 3.1b.

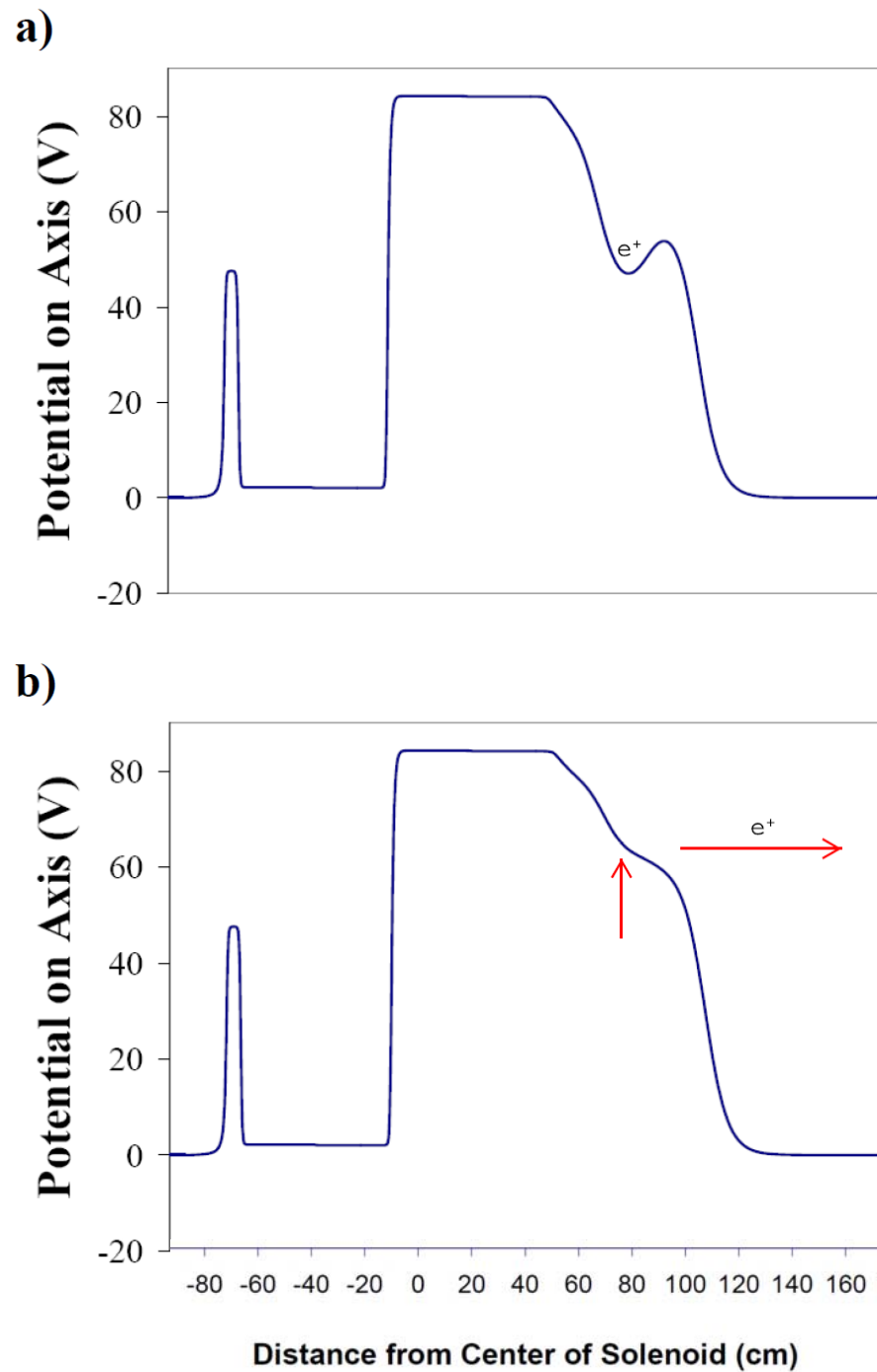


Figure 3.1: a) Potential applied immediately before the positrons are pulsed out of the trap. b) Potential applied during the pulsing.

3.1.1 Timing Sequence

To prepare the positrons for pulsing, they must be moved between the final accumulation well (shown in Figure 2.13c) and the positively-offset single-electrode well shown in Figure 3.1a. The sequence of potentials used for this move is shown in Figure 3.2. After completing the typically 50 seconds of positron accumulation, the potential on the first electrode is raised (Figure 3.2b) to prevent more positrons from entering the electrode stack. The positrons are then moved into a single-electrode potential well from the longer potential well used for accumulation (Figure 3.2c). Next, the positrons are moved into the electrode from which they will be pulsed (Figure 3.2d-g). Finally, this potential well is offset by a positive potential, so that the positrons are ready to be transferred (Figure 3.2i-j).

The steps shown in Figure 3.2b-j take approximately 5 seconds due to the time constant of the voltage source used. (This long time constant ensures that all voltages supplied to the electrodes are free of high-frequency noise.) By applying a voltage pulse to the electrode that is holding the positrons, the positrons are pushed in the axial direction away from the accumulator (to the right in Figure 3.1b). The positron kinetic energy acquired during the pulsing step can be adjusted to any level by simply offsetting the well in which they are sitting in. To avoid temporal spread of the beam, the well must be raised as quickly as possible during the pulsing stage and this is achieved using an Avtec saturated switch with a rise time of 10 ns, which is triggered by a Stanford Research DG535 pulse generator. An oscilloscope trace of the Avtec pulse is shown in Figure 3.3. The length of the pulse is not important, as the positrons are all pulsed out during the very short rise time near $t=0$ in the figure. Once the positrons leave the electrode stack, they are shielded from any electric fields by the grounded stainless steel vacuum chamber of the positron

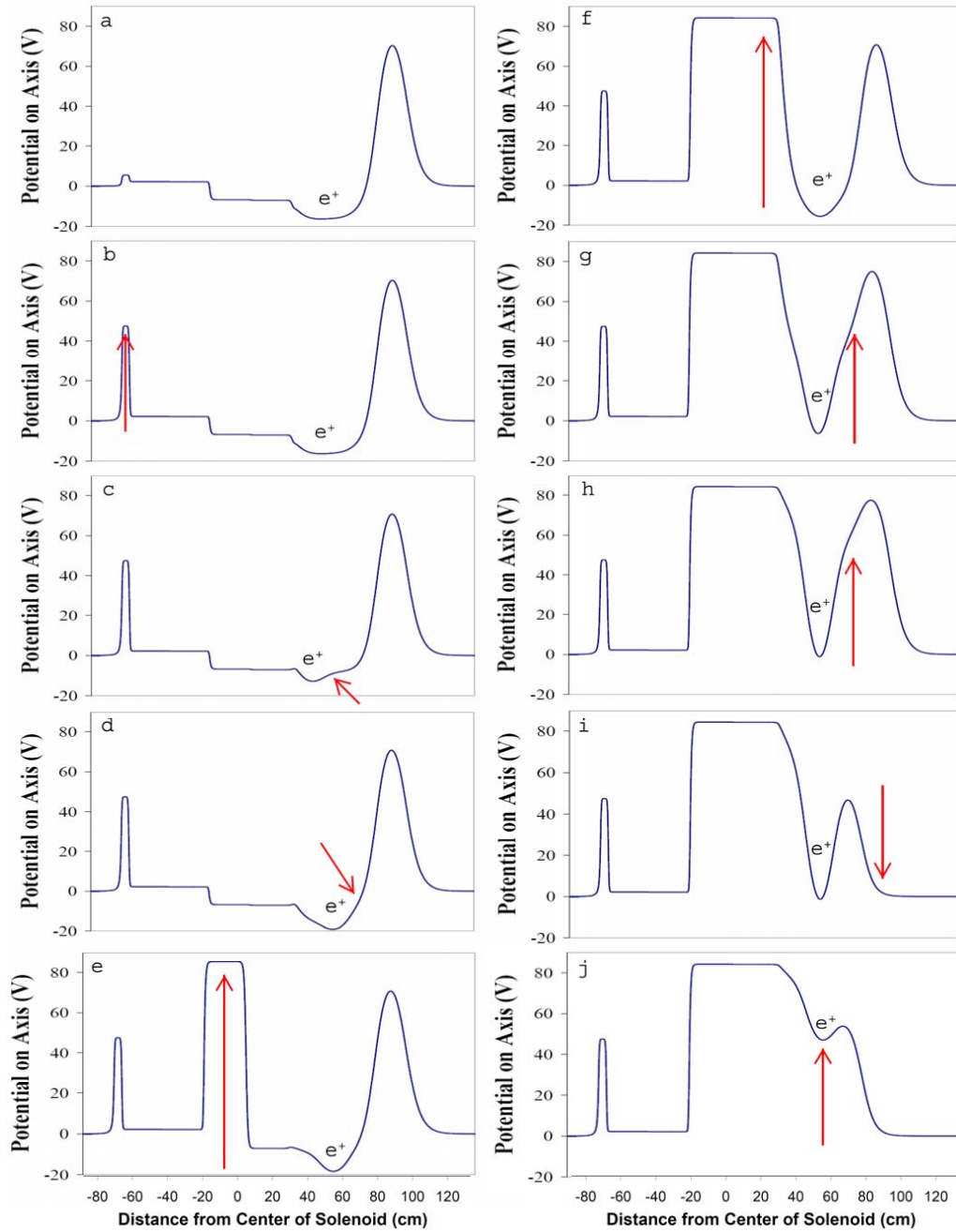


Figure 3.2: The on-axis potentials applied to prepare the accumulated positrons to be pulsed. For each step, the position of the positron cloud and the potential change is labelled.

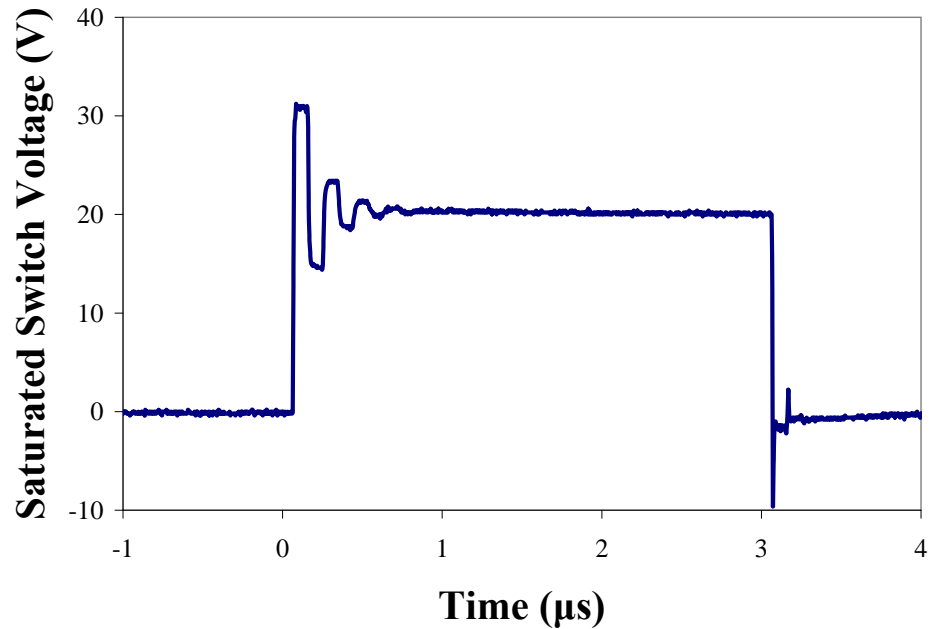


Figure 3.3: Potential applied by the Avtec saturated switch ($t=0$ corresponds to the time that the switch is triggered). The ringing between 0 and $0.5 \mu\text{s}$ and the voltage spike at $3.1 \mu\text{s}$ result from the switching hardware and are not expected to affect the launch of the positrons.

guide and are guided solely by magnetic fields (as will be discussed in Chapter 4.)

3.2 Counting Accumulated Positrons

To study the number of positrons that are accumulated, two destructive counting techniques are used. Both techniques rely on the fact that the positrons are ejected from the Penning trap in a very short time window. The first technique is based on counting the charge resulting from the positrons striking a Faraday cup. The second technique uses a NaI detector to look at the annihilation gammas generated when the positrons hit a surface.

3.2.1 Charge Measurement

When a cloud of positrons is pulsed onto the surface of a Faraday cup, the positive charge deposited can be measured to determine the number of positrons. The charge measurement is accomplished by use of a charge-sensitive preamplifier designed by Andrew Speck [36]. This amplifier is composed of an operational amplifier with a 1-pF feedback capacitor. The output of the charge-sensitive preamplifier is given by $V_{out} = Q/C$, where Q is the input charge (the charge of the positron cloud). A 300-M Ω resistor is placed in parallel with the $C = 1$ -pF capacitor to allow the charge to dissipate with a time constant of 300 μ s.

3.2.2 Calibrating the Charge Amplifiers

The length of coaxial cable between the Faraday cup and the charge amplifier adds significant capacitance to the circuit and cannot be ignored. The capacitance of this input line effectively increases the capacitance in the operational amplifier feedback loop. To get an accurate measure of the effective capacitance, each preamplifier is calibrated in-situ (with the input cable attached) using the circuit shown in Figure 3.4. For test purposes, as shown in Figure 3.4, the input voltage is supplied by the DG535 pulse generator. A 40-dB attenuator is used to reduce the charge incident on the preamplifier to a Q_{in} that is within the range that it can measure. The effective capacitance (which takes into account the blocking capacitance and the cable length) is

$$C_{effective} = \frac{Q_{in}}{V_{drop}}, \quad (3.1)$$

where V_{drop} is the voltage drop as seen on the 50-ohm-terminated oscilloscope due to the pulse from the DG535. An example of such an oscilloscope trace is shown in Figure 3.5.

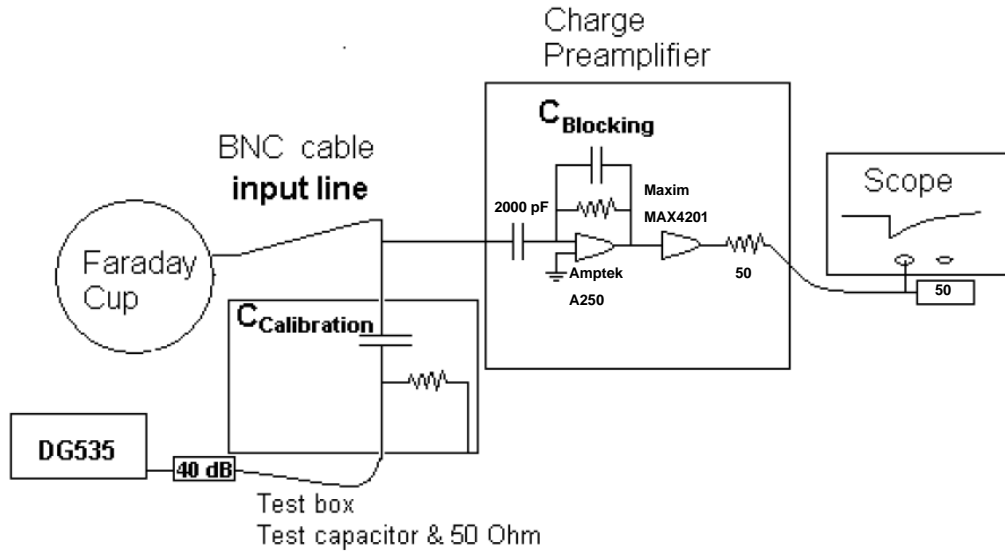


Figure 3.4: Physical setup to calibrate the charge amplifiers

When a positron hits a surface, it sometimes kicks out a secondary electron, which would appear as additional net positive charge into the charge amplifier. To prevent this additional current due to secondary electrons, all Faraday cups are biased positively at a potential lower than the energy of the incoming positrons so that any electron that leaves the surface is attracted back onto the Faraday cup, while incident positrons are still able to overcome the potential barrier and hit the Faraday cup. From the observed signal on the 50-ohm-terminated oscilloscope shown in Figure 3.5, the voltage drop $V_{observed}$ gives a measure of the charge accumulated on the Faraday cup:

$$Q = \frac{V_{observed}}{C_{effective}}. \quad (3.2)$$

The number of positrons hitting the Faraday cup is proportional to the charge:

$$N = Q/e. \quad (3.3)$$

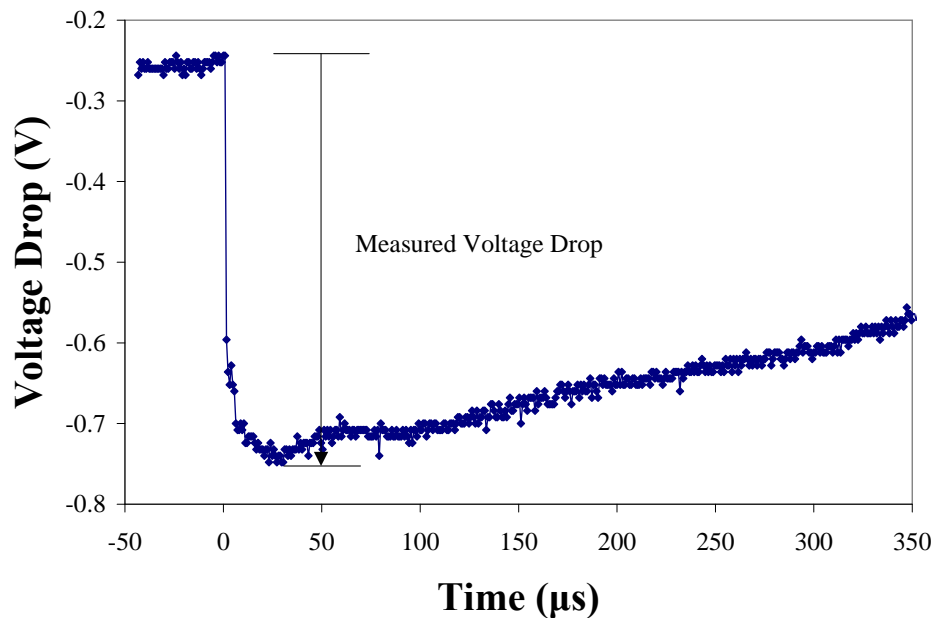


Figure 3.5: Positron signal on charge preamplifier

3.2.3 NaI Integral Counting

To use the charge-sensitive preamplifiers to count the positrons (as shown in Figure 3.5), it is necessary that there be little electrical noise. Near the accumulator electrode stack, capacitive pick-up of the pulsed potential shown in Figure 3.3, which is used when pulsing the positrons out of the accumulator, is a large source of noise that prevents the use of the preamplifiers. A secondary detection technique was developed for use at this location. A NaI crystal detector is used to measure the number of positrons hitting the output gate valve shown in Figure 2.1. The signal from the NaI detector is viewed on an oscilloscope. Since there are millions of positrons annihilating at the same place, the detector is placed at a point 11.2 m away from the gate valve to avoid saturation of the signal on the photomultiplier that detects the light produced in the NaI crystal when a

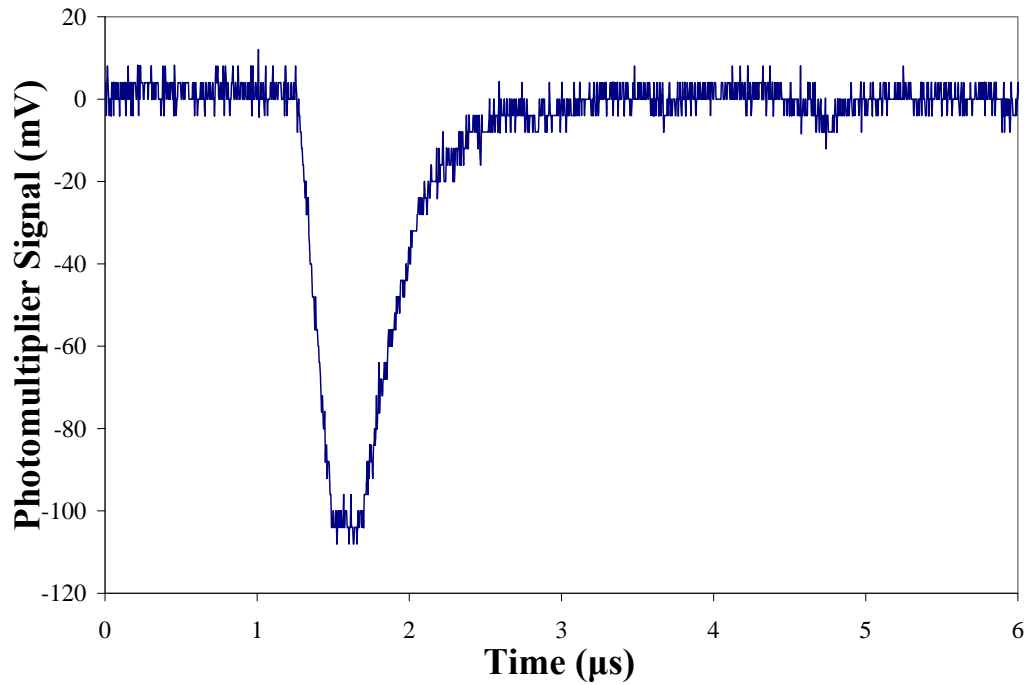


Figure 3.6: Signal on the NaI detector from 28 million positrons annihilating on the output valve. The integral of the signal is proportional to the number of positrons.

gamma passes through it. The photomultiplier signal of 28 million positrons annihilating on the output valve is shown in Figure 3.6. The integral of the signal is another measure of positron number. Figure 3.7 shows that to within an accuracy of 20%, the integral is proportional to the number of positrons (as determined from measurements using charge counting on a Faraday cup signal).

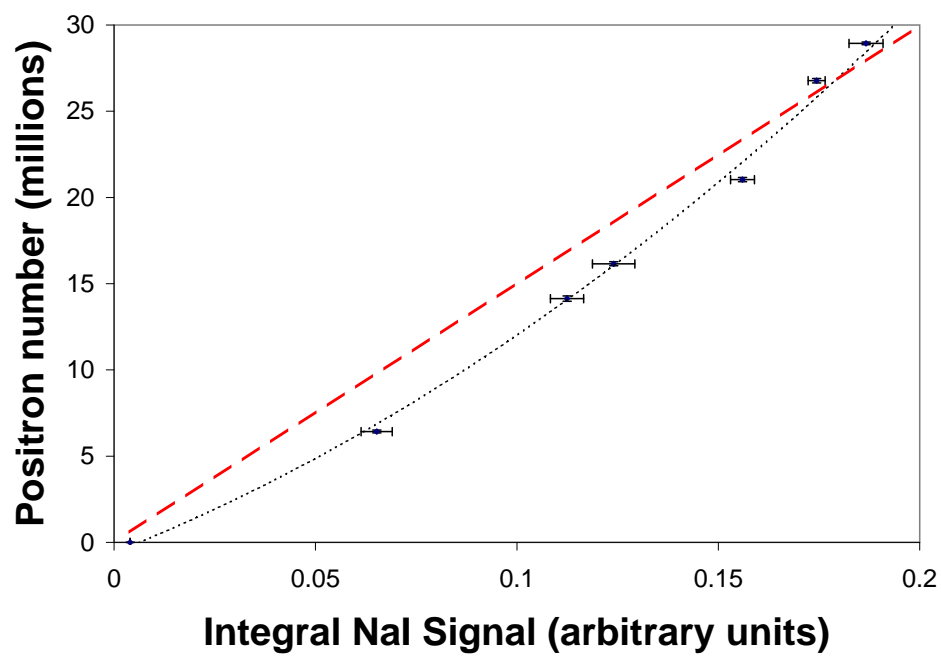


Figure 3.7: Calibration of NaI detector when annihilating at the output of the accumulator. The number on the y axis is obtained from charge counting of the positrons. The red line indicates the best-fit proportional line. The dashed line shown includes a quadratic term, which may indicate that the NaI signal is starting to saturate at larger positron numbers.

Chapter 4

Bridging the Gap: The Positron Guide

After the accumulation process is complete, the positrons must be transferred from the accumulator Penning trap into the ATRAP Penning trap, where they are combined with antiprotons to create antihydrogen. A positron guide (see Figure 4.1) bridges the gap between the two Penning traps, as shown in Figure 1.5. Positrons are first accelerated, then magnetically guided through an 8-meter-long vacuum chamber into the superconducting solenoid of the ATRAP Penning trap. Once there, they are captured to be used for antihydrogen creation. The capture process will be described in Chapter 5.

4.1 Magnetic Field of the Superconducting Solenoid

The first consideration for the design of the positron guide is the magnetic field due to the superconducting solenoid of the ATRAP Penning trap. This superconducting solenoid provides the large magnetic field required for both antiproton loading and antihydrogen creation. It has the capability of producing a central field of 3 tesla, but is normally run at 1 tesla. The total height of the superconducting solenoid is 2.2 meters, and it has an

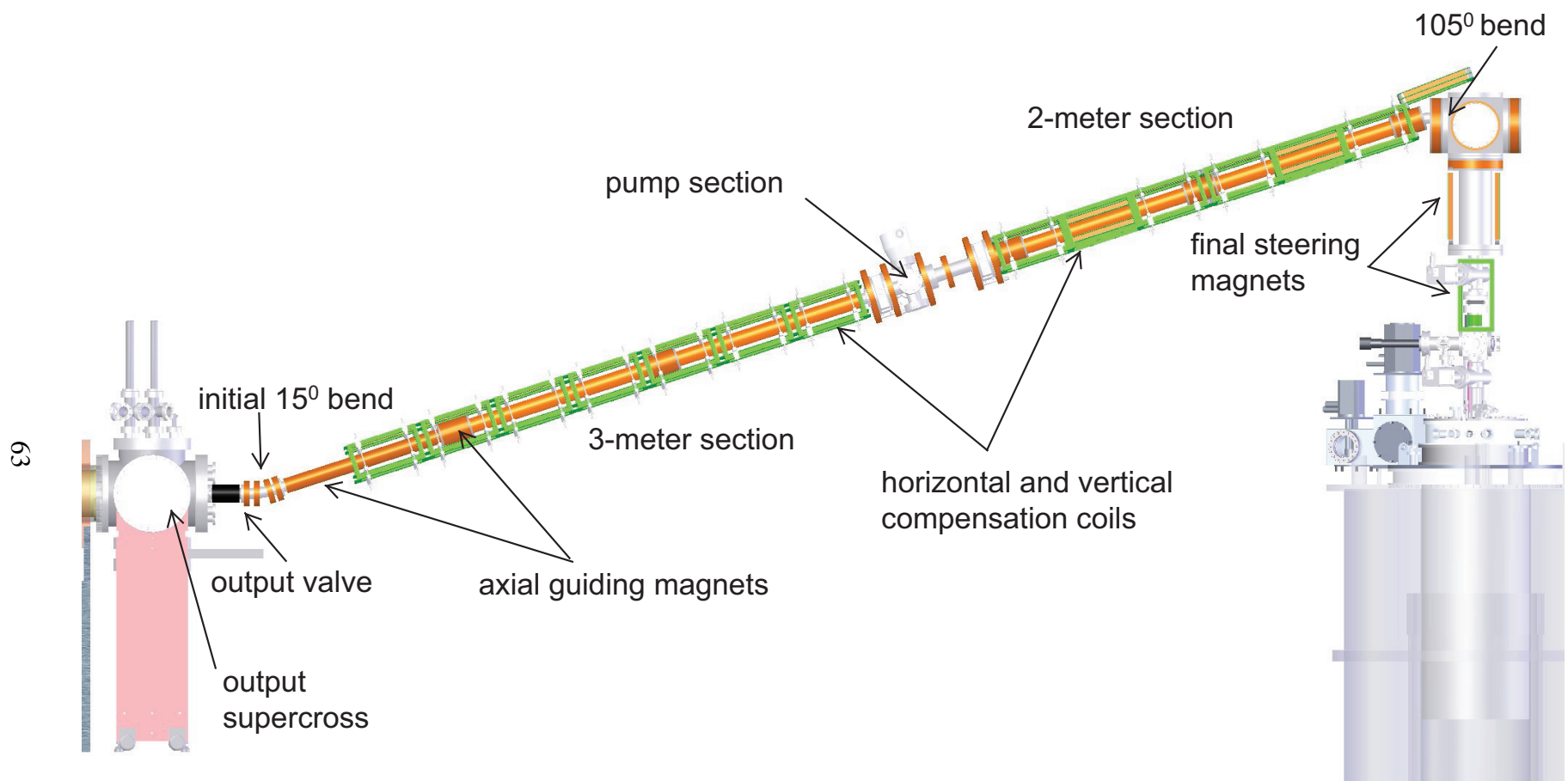


Figure 4.1: The positron guide to transfer positrons between the accumulator and the ATRAP Penning trap.

inner-bore diameter of 51.2 cm. Due to the large field and the large physical size of the solenoid, its fringing field is very large. Figure 4.2 is a contour plot of the magnetic field strength surrounding the superconducting solenoid. The positrons must travel through the fringing field, so the design of the positron guide must take it into account.

4.2 Location of the Positron Accumulator

The ATRAP Penning trap is oriented vertically, as shown in Figure 1.3. The experimental hall in which it is housed has a strict height restriction, and thus the positron accumulator could not be placed on axis with the 1-tesla superconducting solenoid. The complete positron accumulation system measures more than 4 meters in length and weighs over 2000 kg, and thus it is sensible to orient it horizontally and place it on a solid, stable surface. A new experimental area was required to house the positron accumulator, and, since the nearest area available in the AD was 5 meters away from the ATRAP Penning trap, the positron guide was required to be several meters long. The large distance between the accumulator and the superconducting solenoid also helps to reduce fringing fields at the position of the positron accumulation system that would otherwise interfere with the accumulation process.

Since the accumulator and ATRAP Penning traps are not coaxial, and since the positrons are guided along magnetic field lines, the direction of the magnetic field lines due to the 1-tesla superconducting solenoid must be considered. The ATRAP electrode stack (as shown in Figure 1.4) has an inner diameter of 3.6 cm and is positioned near the centre of the 1-tesla superconducting solenoid. For the positrons to make it into the Penning trap, they must follow field lines that pass through this 3.6-cm-diameter circle. Figure 4.3 shows some field lines due to the 1-tesla superconducting solenoid. Only the field lines

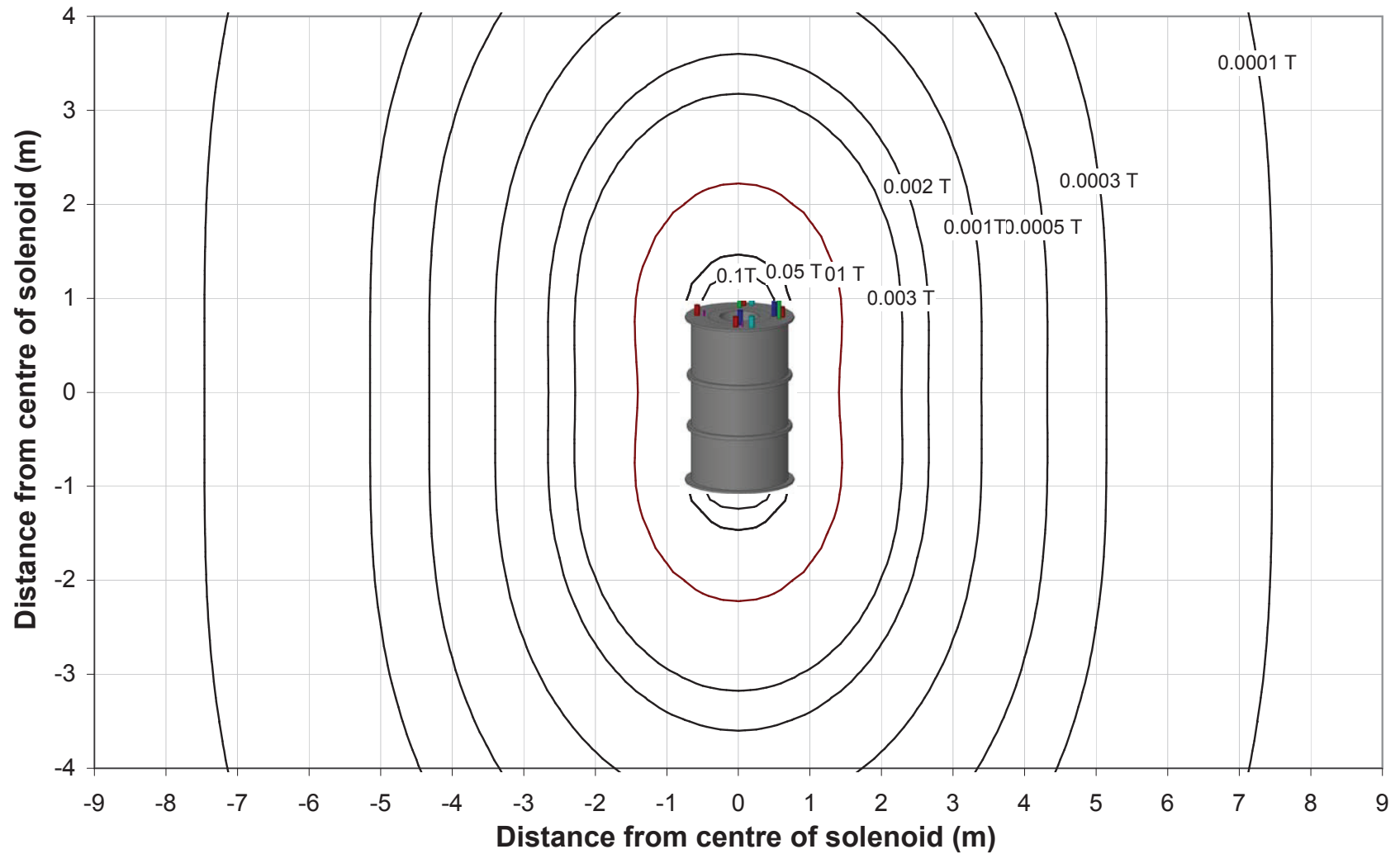


Figure 4.2: The magnitude of the fringing field from the superconducting solenoid while producing a 1-tesla field inside its bore.

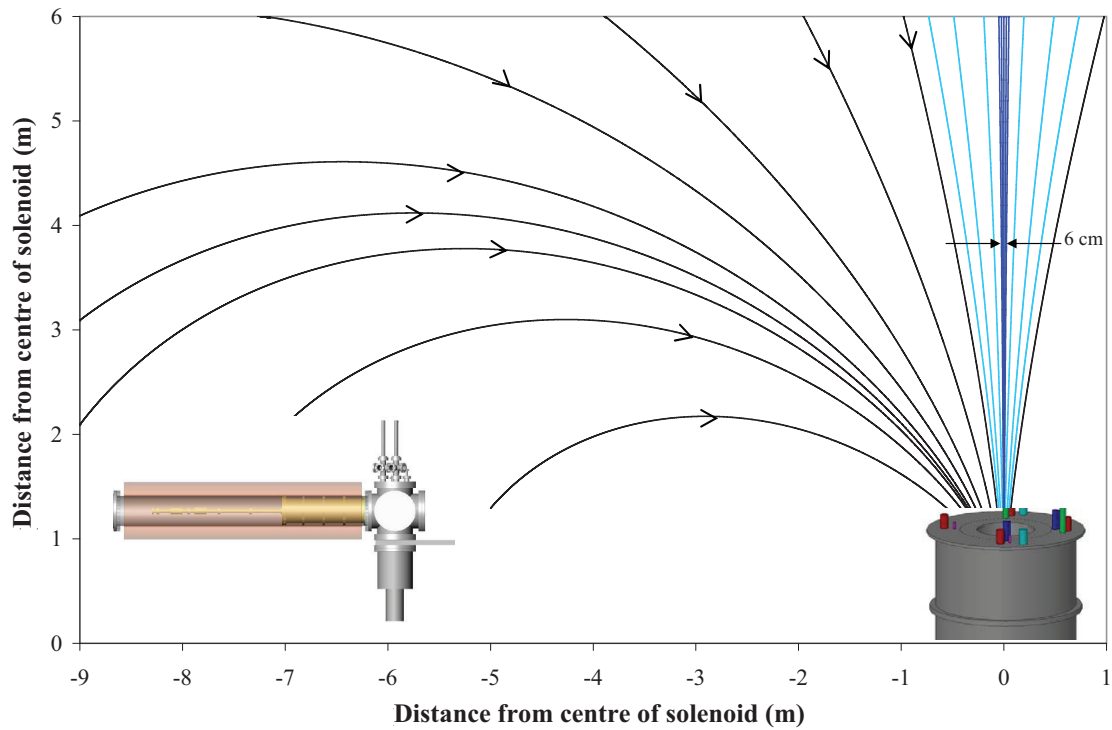


Figure 4.3: The relative position of the large 1-tesla superconducting solenoid and the accumulation Penning trap. Some field lines produced by the 1-tesla solenoid are shown. Only the field lines in blue pass through the electrode stack. The field lines in dark blue pass through the central 1-mm diameter of the superconducting solenoid.

that are almost axial (shown as the blue lines in the figure) pass through the inside the electrode stack. Thus, the positron guide must transport the positrons onto the blue field lines to get them into the electrode stack.

4.3 Vacuum Considerations

Another consideration for the design of the positron guide is the large difference in vacuum conditions for different sections of the apparatus. The pressure ranges from as high as 10^{-3} torr in Stage 1 of the buffer-gas accumulator (see Figure 2.11), to perhaps as low as 5×10^{-17} torr inside the ATRAP Penning trap (as measured in a similar apparatus to the ATRAP Penning trap [10]).

To transfer positrons between the two systems (the buffer-gas accumulator and the ATRAP Penning trap), there must be an unimpeded, evacuated path between the two, since positrons can annihilate with any residual gas that is present. Since the positrons are being transferred from the accumulator at low energies (10 eV - 400 eV) and these low-energy positrons cannot pass through even a very thin piece of material, no vacuum window can be used to isolate the ultra-low-pressure region of the ATRAP Penning trap. Instead, the vacuum chamber in the ATRAP Penning trap now has a 1-mm-diameter, 12.7-mm-long opening on axis to allow the positrons to enter into the electrode stack (as shown in Figure 1.3 with a close-up view in Figure 4.4). This opening acts as a restriction between the positron guide and the ultra-low-pressure region of the trap. The tube is placed within the 4-kelvin region of the ATRAP experiment so that both sides of the combined vacuum chamber have significant cryopumping ability. The cryopumping significantly reduces background gas near the electrode stack where it would cause significant loss of trapped positrons and antiprotons. Activated charcoal is placed above the opening (as shown in Figure 4.4) in order to increase the 4-kelvin surface area, thus increasing the cryopumping above the opening. Despite this opening, a cloud of antiprotons can be held for over fifteen hours in the ATRAP Penning trap with no noticeable loss, thus the vacuum conditions in the ATRAP Penning trap are sufficient to perform antihydrogen

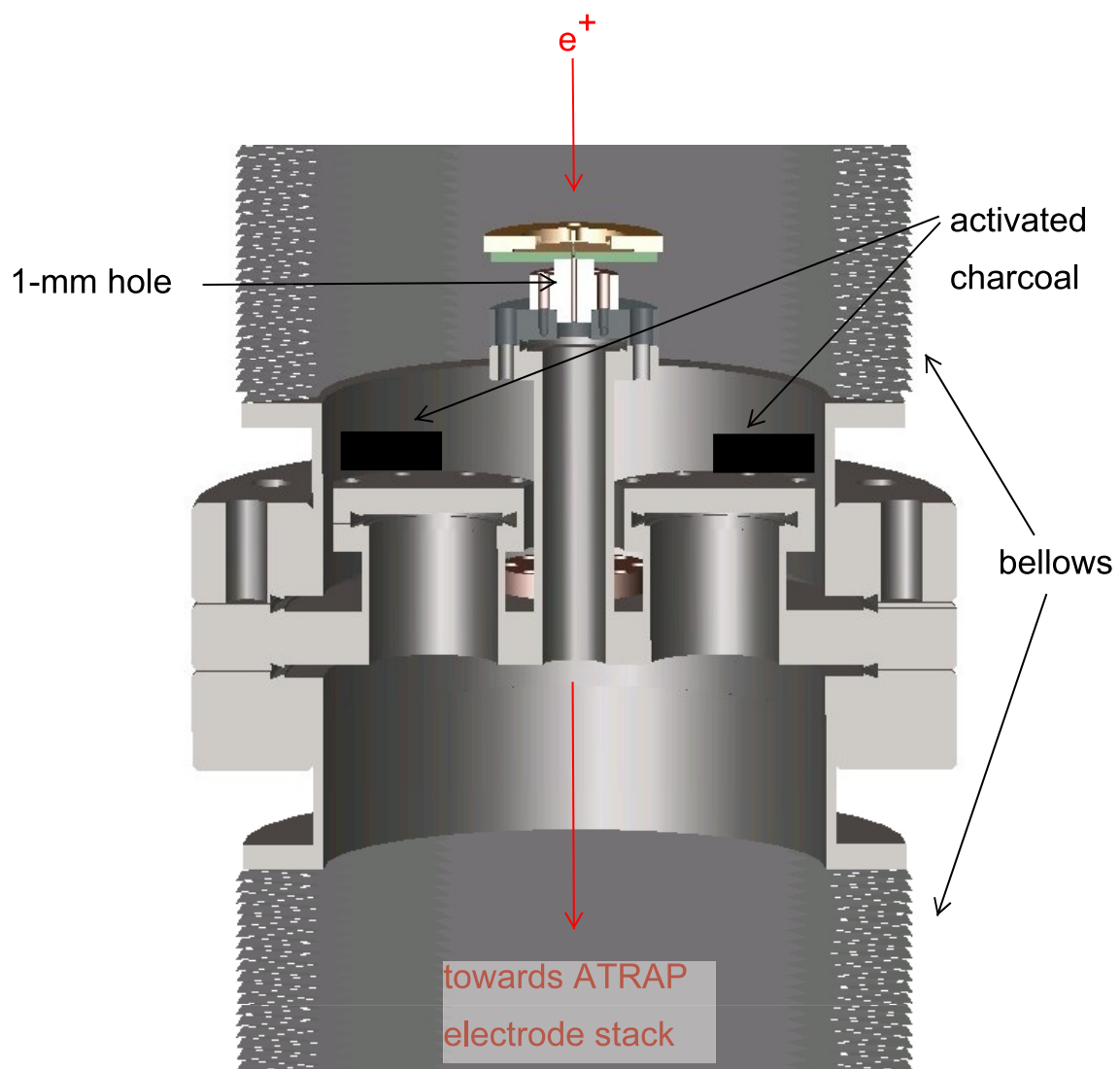


Figure 4.4: Schematic of the 1-mm tube. The entire area is at 4 kelvin.

experiments, even with the presence of the 1-mm tube.

The addition of the 1-mm opening has a dramatic effect on the possible field lines that the positrons can follow to make on their way into the electrode stack. Only the field lines due to the 1-tesla superconducting solenoid that are shown in dark blue in Figure 4.3 pass through the 1-mm tube. From the figure, one can see that these dark blue field lines expand to only a 6-cm diameter at a height of 3-m above the centre of the superconducting solenoid.

4.4 Motion of a Positron in a Magnetic Field

4.4.1 Homogeneous Magnetic Field

Once the positrons are ejected from the accumulator, they are guided by magnetic field lines. No electric field is present since there is a grounded vacuum chamber along the entire path length. The guiding fields along most of the path are applied using electromagnetic solenoids. Since the fields inside of the solenoids are approximately homogeneous, motion of a positron within a homogeneous magnetic field is considered in this section.

The Lorentz force \vec{F}_L that describes a force acting on a particle with charge Q moving with velocity \vec{v} in an external electromagnetic field is

$$\vec{F}_L = Q(\vec{E} + \vec{v} \times \vec{B}). \quad (4.1)$$

For a homogeneous magnetic field along the z-axis ($\vec{B} = B_0 \hat{z}$), $\vec{E} = 0$. The particle's velocity is divided into a component in the direction of the magnetic field and a component

perpendicular to the magnetic field,

$$\vec{v} = \vec{v}_z + \vec{v}_\perp, \quad (4.2)$$

with

$$\vec{v}_\perp = \vec{v}_x + \vec{v}_y. \quad (4.3)$$

From Equation 4.1, there is no force in the direction of the magnetic field, and thus the positron advances in the z-direction with a constant velocity

$$\vec{v}_z = \vec{v}_{oz}, \quad (4.4)$$

where \vec{v}_{oz} is the initial velocity of the particle in the direction of the applied magnetic field.

Since a magnetic force does no work on a particle, the magnetic field cannot change the magnitude of the velocity of the particle, therefore the total speed is

$$|\vec{v}| = v_o = \text{constant}, \quad (4.5)$$

where v_o is the initial speed of the particle. Since \vec{v} and v_z are constant, $|\vec{v}_\perp|$ must also be constant.

Equation 4.1 for $Q = +e$ simplifies to

$$\vec{F}_L = eB_o(\vec{v}_\perp \times \hat{z}). \quad (4.6)$$

The constant force always acts in the xy plane and is perpendicular to the direction of the velocity component in the plane. \vec{F}_L must equal the centripetal force:

$$\frac{mv_{o\perp}^2}{R} = ev_{o\perp}B_o, \quad (4.7)$$

Position	Magnetic Field (T)	Cyclotron Frequency (f _c)	Cyclotron Radius (μm)
Source and Moderator	0.011	308 MHz	48
Jog Section	0.007	196 MHz	76
Drift section	0.020	560 MHz	26
Main Accumulation Solenoid	0.150	4.2 GHz	3.5
ATRAP Superconducting Solenoid	1.0	28 GHz	0.53

Table 4.1: Cyclotron frequencies, cyclotron radius and magnetic fields at different positions

and thus the positron travels in a circular path in the xy plane with a radius of

$$R = \frac{mv_{o\perp}}{eB_o}. \quad (4.8)$$

The quantity $\frac{eB_o}{m}$ has the dimensions of frequency and

$$\omega_c = 2\pi f_c = \frac{eB_o}{m} \quad (4.9)$$

is the cyclotron frequency of a positron in a magnetic field B_0 . Table 4.1 shows the cyclotron frequencies for different positions along the path the positrons follow. The period

$$T = \frac{2\pi}{\omega_c} = \frac{2\pi m}{eB_0} \quad (4.10)$$

is the time required for a positron to complete one revolution in the xy plane. Since the motion along the direction of the magnetic field is a constant, the positron advances, for each revolution, a distance of

$$h = v_{oz}T, \quad (4.11)$$

Thus, the positron moves along a spiral (helical) trajectory and after passing a distance h, returns to the same field line on which it started.

The magnitude of the magnetic moment,

$$\mu = \frac{KE_{\perp}}{B}, \quad (4.12)$$

is a constant of the motion, where $KE_{\perp} = \frac{mv_{\perp}^2}{2}$ is the kinetic energy in the direction perpendicular to the magnetic field vector.

4.4.2 Non-Homogeneous Magnetic Field

Most of the positron guide is constructed using long solenoids and other electromagnets in order to produce as nearly homogeneous magnetic fields as possible. Figure 4.5 shows the magnetic field gradient seen by the positrons as they travel between the accumulator and the ATRAP Penning trap. As the positrons leave the 0.15-T field of the accumulation solenoid, they travel from the high field of the accumulator into a low fringing field and then into the 0.02-T field of the positron guide. Along the positron guide, the field is made as uniform as possible, but between solenoids there is a increase in the magnetic field magnitude due to additional electromagnets at the junctions. As the positrons make it to the end of the positron guide field and take a 105° bend (see Figure 4.1) into the fringing field of the 1-tesla superconducting solenoid, they encounter a magnetic field minimum inside the vacuum cube at the bend location. After the positrons have made it around the bend, they travel down the central axis of the 1-tesla superconducting solenoid, and they encounter the largest field gradient along this downward path to the superconducting solenoid. Because the large field is required inside the ATRAP Penning trap, this significant field gradient is inevitable. At points along the positron path where the magnetic field gradient is not zero, the positrons are not travelling in the simple motion discussed in the previous section. More analysis must be done to understand the

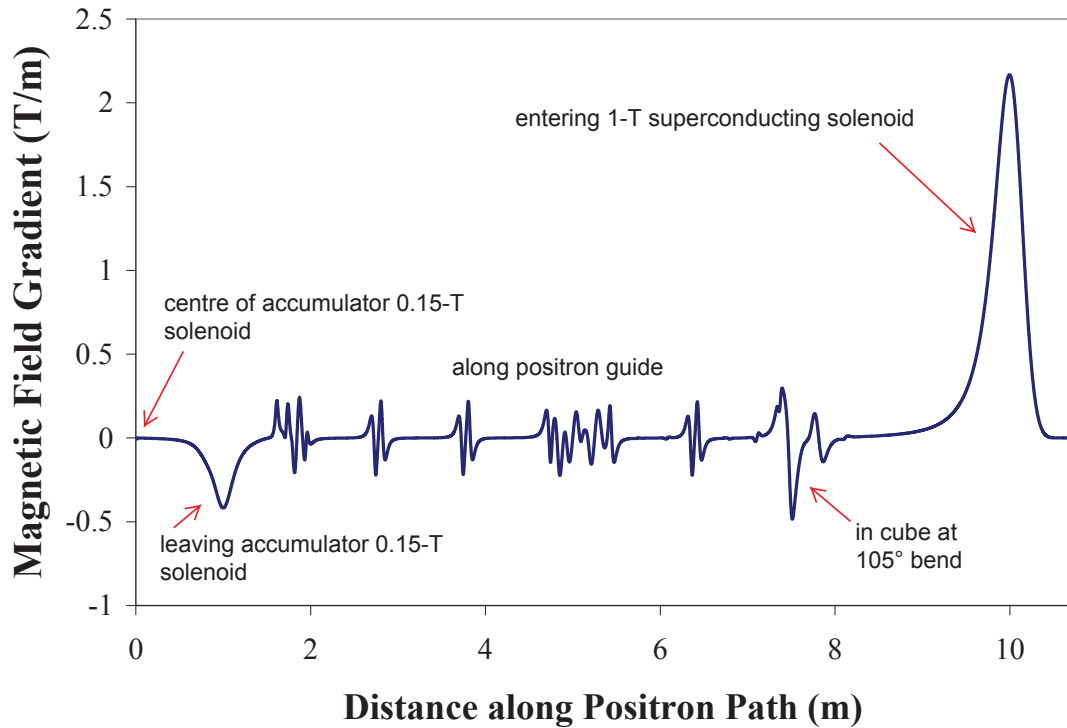


Figure 4.5: The magnetic gradient along the positron path between the accumulator and the 1-tesla superconducting solenoid.

positron's motion while travelling through these non-homogeneous magnetic fields.

As a particle traverses a magnetic field gradient, the magnitude of the angular momentum (or, equivalently, the magnetic moment of Equation 4.12) is conserved. To achieve this conservation, the perpendicular kinetic energy must increase in proportion to the increase of magnetic field. Since a magnetic field does no work on the charged particle, speed v is constant as the particle traverses a magnetic field gradient.

The pitch angle Φ , shown in Figure 4.6, is defined as the angle between the positron velocity \vec{v} and the magnetic field $\vec{B} = B_0 \hat{z}$. A consequence of the invariances in μ (Equation 4.12) and v is that, as the particle encounters an increasing magnetic field, the

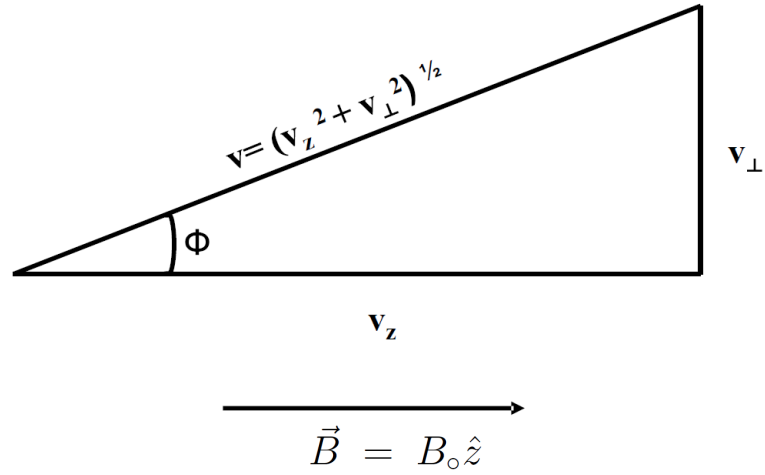


Figure 4.6: The pitch angle Φ is the angle between the particle velocity and the magnetic field. The magnetic field is along the z-axis.

perpendicular component of speed (v_{\perp}) increases with a resulting decrease in the axial component of speed (v_z). If the magnetic field increase is large enough, the particle will lose all of its v_z and turn around. This effect is known as magnetic mirroring.

From the definition of the pitch angle in Figure 4.6,

$$v_{\perp} = v \sin \Phi. \quad (4.13)$$

Inserting v_{\perp} into Equation 4.12 for a positron travelling from a field B_1 to a field $B_2 > B_1$,

$$\mu = \frac{mv^2 \sin^2 \Phi_1}{2B_1} = \frac{mv^2 \sin^2 \Phi_2}{2B_2}. \quad (4.14)$$

Magnetic mirroring will occur if the angle in the large magnetic field Φ_2 equals 90° . To avoid magnetic mirroring there is a maximum pitch angle Φ_1 at which the particle must start with when it is in the smaller magnetic field B_1 . Rearranging Equation 4.14 leads to

$$\sin \Phi_1 < \sqrt{\frac{B_1}{B_2}}. \quad (4.15)$$

Incorporating the definition of the pitch angle leads to an initial velocity equation that must be met in order to avoid magnetic mirroring for positrons travelling from the positron guide ($B_1 = 0.02$ T) to the 1-tesla superconducting solenoid ($B_2 = 1$ T),

$$\frac{v_z}{v_\perp} > \sqrt{\frac{B_2}{B_1}} - 1 = 2.38. \quad (4.16)$$

If the initial velocity ratio of $\frac{v_z}{v_\perp}$ in the positron guide is 2.38 or less, the particles will be magnetically mirrored and therefore never make it into the ATRAP Penning trap. The condition of Equation 4.16 is very easy to achieve as long as the kinetic energy of the positrons, acquired during the pulsing stage described in Section 3.1, is aligned with the magnetic field. Accurate alignment is accomplished by ensuring that the accumulation electrode stack is physically aligned with the magnetic field produced by the accumulation solenoid, as shown in Figure 2.11. The inner bore of the solenoid is 5 cm larger in diameter than the vacuum chamber in which the electrode stack is positioned and thus orientation of the solenoid can be adjusted relative to the electrode stack to ensure proper alignment.

4.5 Additional Design Considerations

If the accumulator solenoid and the ATRAP 1-tesla superconducting solenoid were coaxial, a solenoidal field would be sufficient to guide the positrons from one solenoid to the other. Since the two solenoids are not coaxial, as shown in Figure 1.5, a much more complicated set of guiding electromagnets must be used. These magnets must guide the positrons onto one of the dark blue field lines of Figure 4.3. Once guided onto one of these field lines, the 1-tesla superconducting solenoid will guide the positrons into the ATRAP Penning trap. To get the positrons onto the correct field lines, the fringing

field of the 1-tesla solenoid must be cancelled, leaving only the 0.02-tesla solenoidal field of the positron guide until it reaches the required field line. The cancelling can be accomplished in one of two ways. Magnetic shielding could be used to surround the positron guide field. Such shielding would attract the fringing field of the 1-tesla solenoid into the high permeability material of the shielding, effectively removing the effect of the fringing field. The magnetic shielding method was explored and rejected because the shielding can saturate, thus a very large amount of shielding material is needed to adequately shield along the entire length of the positron guide. Another reason magnetic shielding was avoided is because the entire path cannot be shielded, and an interface between the shielded and unshielded regions would cause very large local fields.

The other method for dealing with the fringing fields is to produce fields that cancel out the fringing field of the 1-tesla solenoid. Producing an opposing field is accomplished by adding a series of rectangular coils along the entire length of the positron guide. The current through each coil is independently controlled so that the field can be adjusted to approximately cancel out the fringing field thus leaving only the guiding field.

To determine the best path to take between the accumulator and the ATRAP Penning trap, the magnitude of the fringe field shown in Figure 4.2 must be taken into account. Since the fringing field is strongest near the superconducting solenoid, it is advantageous to be as far away as possible from the 1-tesla superconducting solenoid in the vertical direction before letting the fringing field guide the particles the rest of the way. Thus the guiding solenoidal field ends at the highest vertical point possible (determined by the height restrictions due to the building in which the experiment is housed) at 2.2 m from the top of the superconducting solenoid (see Figure 4.1). At this height, the fringing field is 0.003 tesla (in the vertical direction). The rectangular coils are designed to allow

the ATRAP superconducting solenoid to be run at 3 tesla, the maximum field that it can produce. At 3 tesla, the fringing field is three times larger than it is at 1 tesla, meaning that the field at 2.2 m is 0.09 tesla.

4.6 Modelling

Before constructing the electromagnets of the positron guide, the magnetic fields and particle trajectories were modelled.

4.6.1 Magnetic Field Modelling

As explained in Section 4.4, if the magnetic field is homogeneous, the positrons will spiral along magnetic field lines at a constant speed. In a non-homogeneous field, as long as the condition of Equation 4.16 is met, the positrons will still approximately follow magnetic field lines, but not at a constant speed. Thus, by plotting the magnetic field lines along the entire positron guide, the approximate trajectory of the positrons can be determined. The calculation of magnetic fields is done with a software package for Mathematica called Radia. Radia is a magnetostatic computer code which produces accurate and fast computations of three-dimensional magnetic fields for any defined set of electromagnets. Radia is used to create the field lines in Figure 4.3 and the contour plot in Figure 4.2.

Using the Radia software, a wide variety of positron guide magnet-coil geometries could be explored and optimal coil designs are used to produce a robust and reliable method of transferring positrons between the buffer-gas accumulator and the ATRAP Penning trap.

4.6.2 Trajectory Modelling

To get a more accurate trajectory calculation, a Fortran program was written by Dr. Eric Hessels. The program calculates the positron trajectory using first principles. To make this calculation, the magnetic field must be known at all points in space. The same Mathematica program used in the previous section is used to create a grid of magnetic field vectors. A three-dimensional grid of 1-mm spaced magnetic field vectors is produced throughout the entire vacuum chamber of the beam line. Figure 4.7 shows a close-up of the grid around the position of the positron. For each position, there exists a set of eight magnetic field vectors which surround the point in the form of a cube. These eight points enable the magnetic field to be interpolated for any point within the cube.

For the trajectory calculations, the positron is assigned an initial velocity vector and position. The only force acting on the positrons is the Lorentz force (Equation 4.1), so the acceleration for any point in space is given by

$$\vec{a} = \frac{e}{m}(\vec{v} \times \vec{B}). \quad (4.17)$$

To evaluate the path that the positron takes, the fourth-order Runge-Kutta method is used to determine the next step in position and velocity. Figure 4.8 shows the calculated final axial velocity of the positrons when they are given different amounts of initial kinetic energy in the direction of motion. The perpendicular kinetic energy in this case is due solely to the thermal energy at room temperature (i.e., 0.025 eV). From the modelling, it can be seen that the positrons must have a parallel velocity component greater than 300,000 m/s which corresponds to a kinetic energy of 0.25 eV. Similar to the analysis shown in Equation 4.16, this condition is easily met as long as the pulse step imparts kinetic energy in the direction along the axis of the accumulator solenoid.

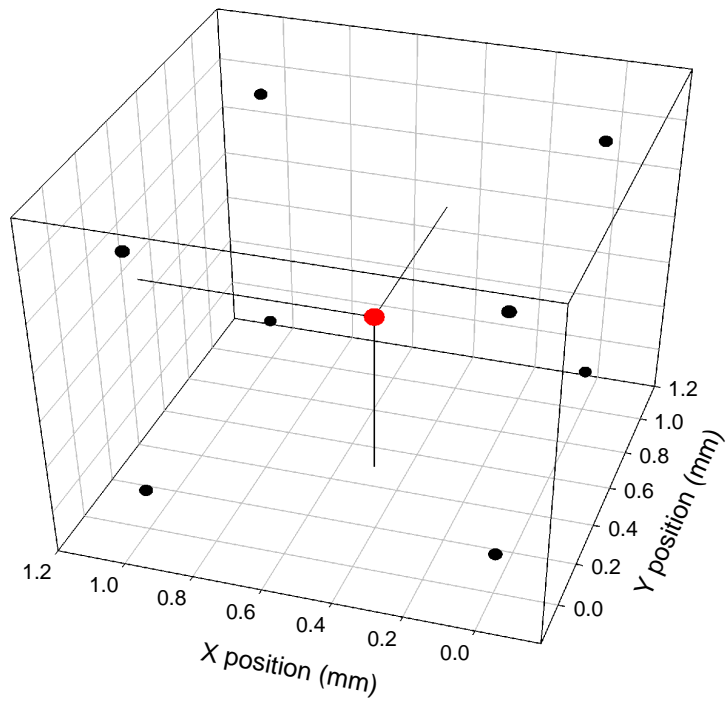


Figure 4.7: Black points represent the position of magnetic field vectors at 8 corners surrounding the point at which the trajectory is being calculated. The red point represents the position of the positron travelling through the magnetic field. The magnetic field at the red point is interpolated from the values of the field calculated by Radia for the 8 black grid points shown.

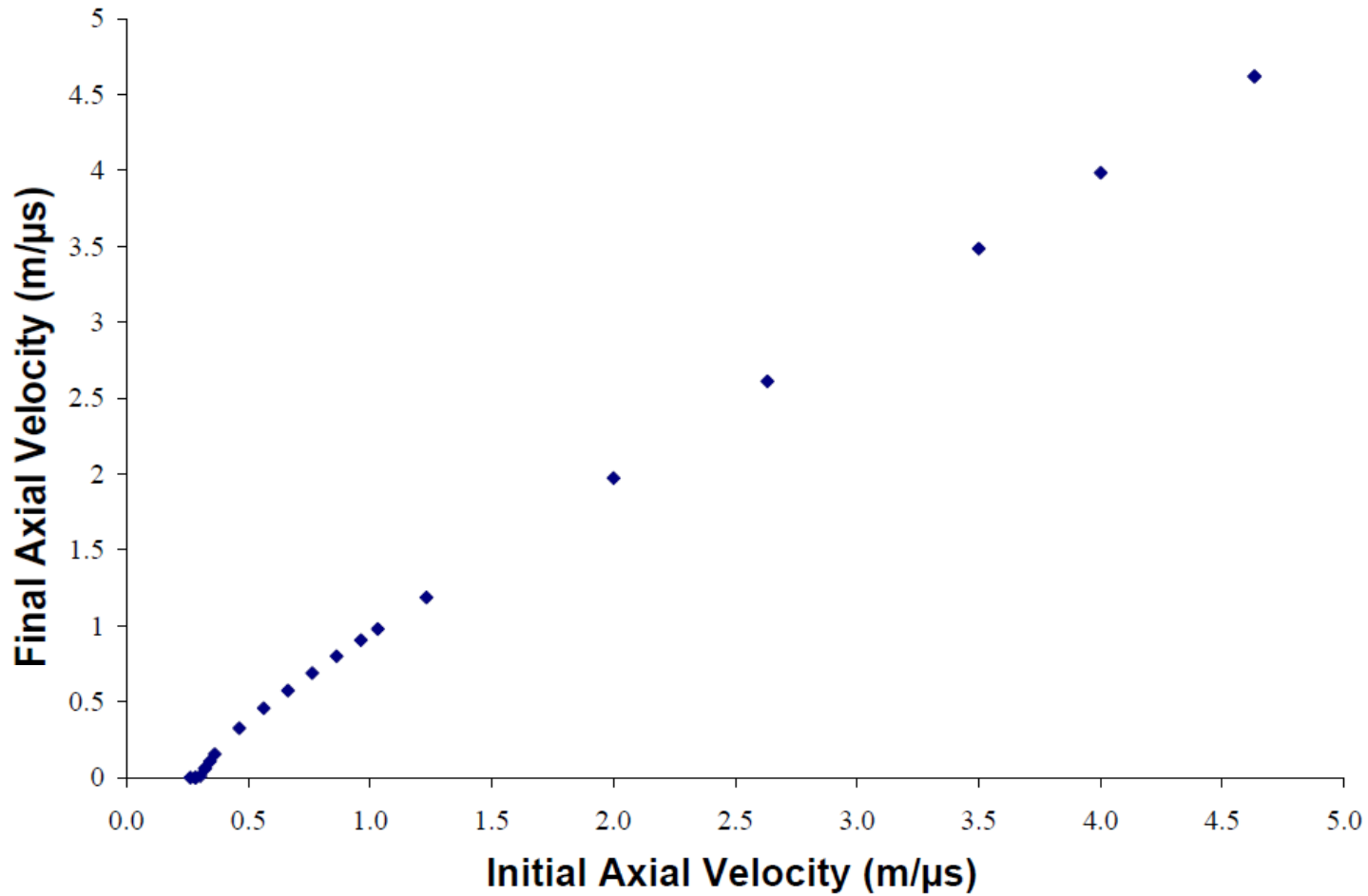


Figure 4.8: The modelled final axial velocity of the positrons when they enter the ATRAP electrode stack as the initial axial energy is changed. The perpendicular velocity is 9×10^4 m/s, which is due to thermal energy at room temperature.

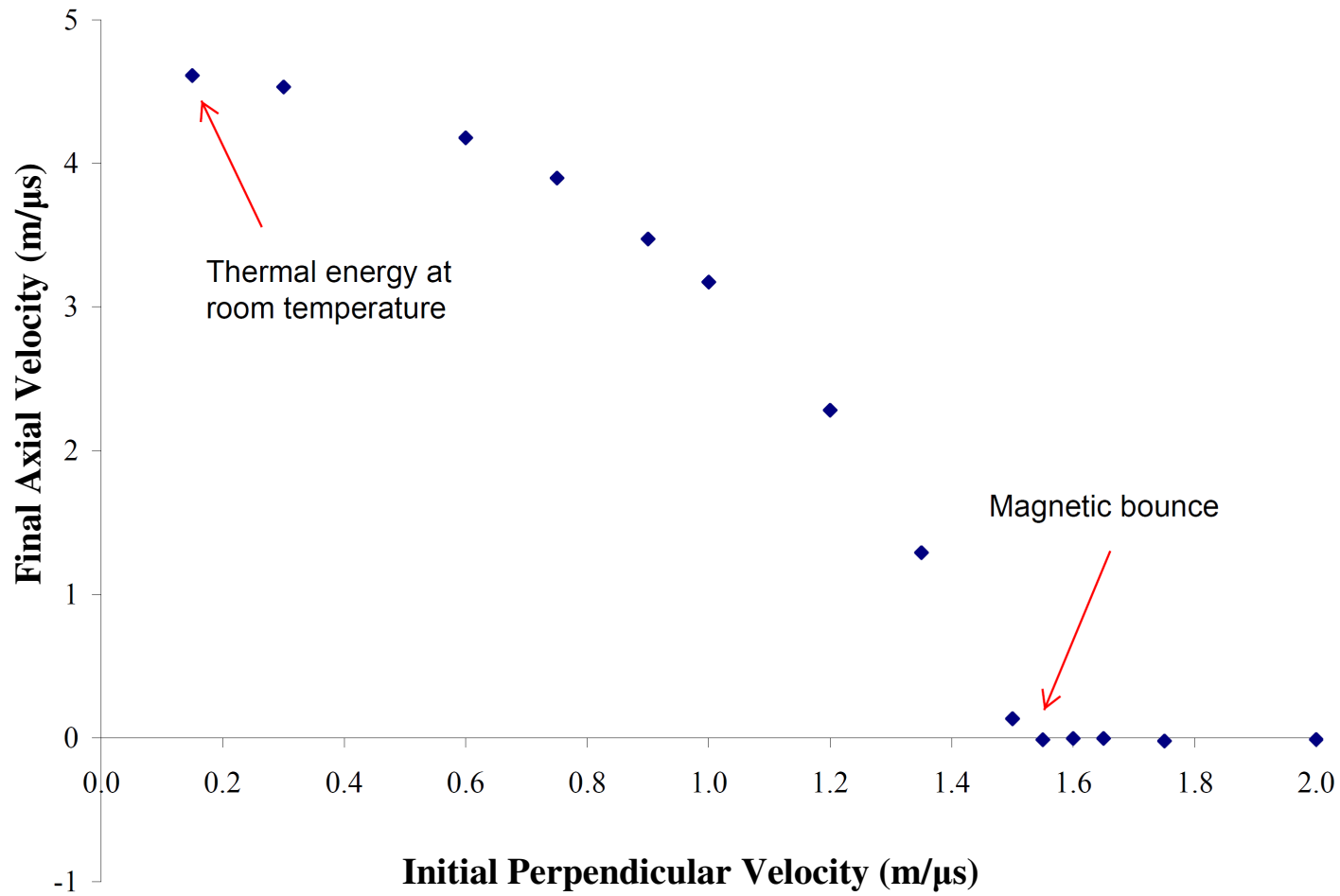


Figure 4.9: The modelled final velocity of the positrons as the initial perpendicular velocity is changed. As the perpendicular velocity is changed, the final axial velocity changes accordingly. If the perpendicular velocity is too high, the positrons will magnetically bounce.

The trajectory modelling can also explore what will happen if the perpendicular velocity component is greater than the velocity associated with the thermal energy at room temperature. This would occur if the electrode stack and the accumulator solenoid are not coaxial and the pulse step imparts kinetic energy in the direction perpendicular to the direction of motion. Figure 4.9 shows what will happen if the perpendicular velocity component is increased. An increased perpendicular velocity component implies an increased initial pitch angle (Figure 4.6). If the pitch angle is increased enough, the positrons will magnetically bounce, as shown in Figure 4.9.

Another result from the trajectory modelling is the motion in the y-direction (into and out of the page in Figure 4.1). When the positrons travel through an increasing magnetic field, they move to the left. Similarly, when the positrons travel through a decreasing magnetic field, they move to the right. Figure 4.10 shows the modelled y-position of the positrons as they travel along the transfer line. In a homogeneous field, the y-displacement would not be expected to change by more than the diameter of the cyclotron orbit. In the case of a non-homogeneous field, as shown, the y-displacement is significant enough that compensation coils must be added. The y-direction motion motivated the construction of the y-direction magnets in Figure 4.1. Based on the considerations discussed in Sections 4.1 to 4.6, the design choice for the magnetic guide included the 94 electromagnets shown in Figure 4.1. The details of this design are given in section 4.7.

4.7 Overview of Positron Guide

The positron guide, shown in Figure 4.1, uses a 0.02-tesla magnetic field to act as the guiding field for the positrons. As the positrons leave the accumulator and enter the guide, the minimum field that they encounter is 0.02 tesla (at the position of the skimmer,

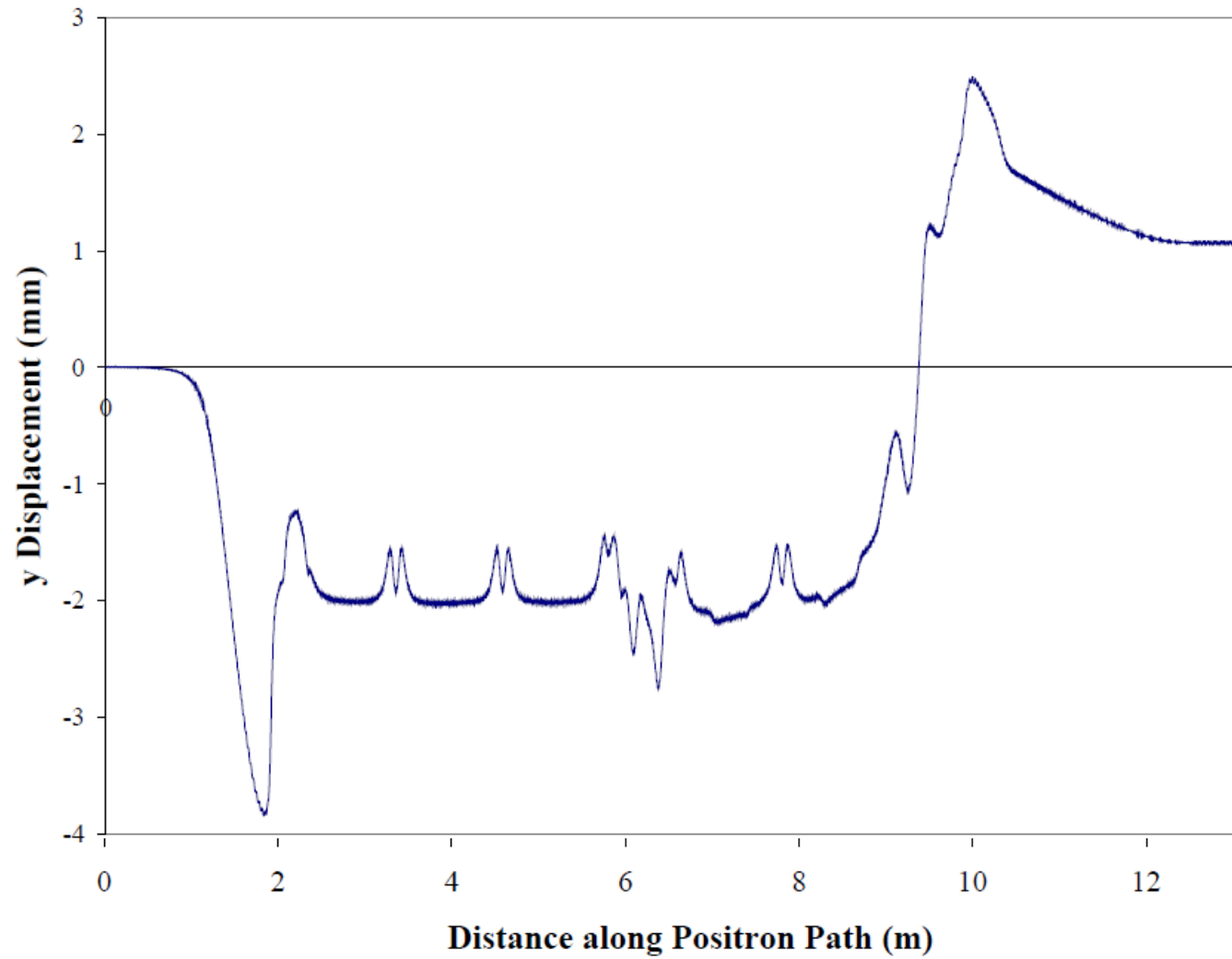


Figure 4.10: The y position of the positrons as they follow the path. The positrons will be displaced in the y direction due to magnetic field gradients.

where the cloud size is measured, as shown in Figure 2.15). Since this magnetic field matches that inside the positron guide, and, as discussed above, the radial extent of the cloud is a function of the magnetic field, the cloud will have the same radial size within the positron guide as its measured size at the skimmer. Thus, the diameter of the cloud along the positron guide is 6.2 mm.

A total of 94 electromagnets are used to create the guiding field, as shown in Figure 4.1. These electromagnets are grouped into four categories: (1) those near the initial 15° bend at the exit of the accumulator, which are used to guide the positrons into the positron guide (9 windings, as listed in Table 4.2), (2) those producing the axial guiding field along the positron guide (17 coils, as listed in Table 4.3), (3) those used to compensate for non-axial magnetic fields (mostly due to the fringing field of the 1-tesla superconducting solenoid) along the positron guide (58 coils, as listed in Tables 4.4 and 4.5), and, (4) those to do the final steering around a 105-degree bend and into the ATRAP Penning trap (9 coils, as listed in Table 4.6).

The first electromagnets (Table 4.2) are used to transfer the positrons from the 0.15-tesla field of the accumulator solenoid into the positron guide, which is angled upwards at 15 degrees. Coils SC axial, SC L/R, SC U/D are wound directly onto the flanges of downstream cross. These magnet coils have the geometries shown in Figure 4.11b and c. Coils B1 through B4 (all attached in series), provide the initial 15° bend into the positron guide. The geometry of these coils is shown in Figure 4.11a.

The main solenoidal magnets of the positron guide (S1 through S5 of Figure 4.1 and Table 4.3) are constructed by wrapping insulated copper wire directly onto the stainless steel vacuum chamber of the positron guide, as shown in Figure 4.12a. To make the entire positron guide modular and transportable, the vacuum chamber is split into five sections,

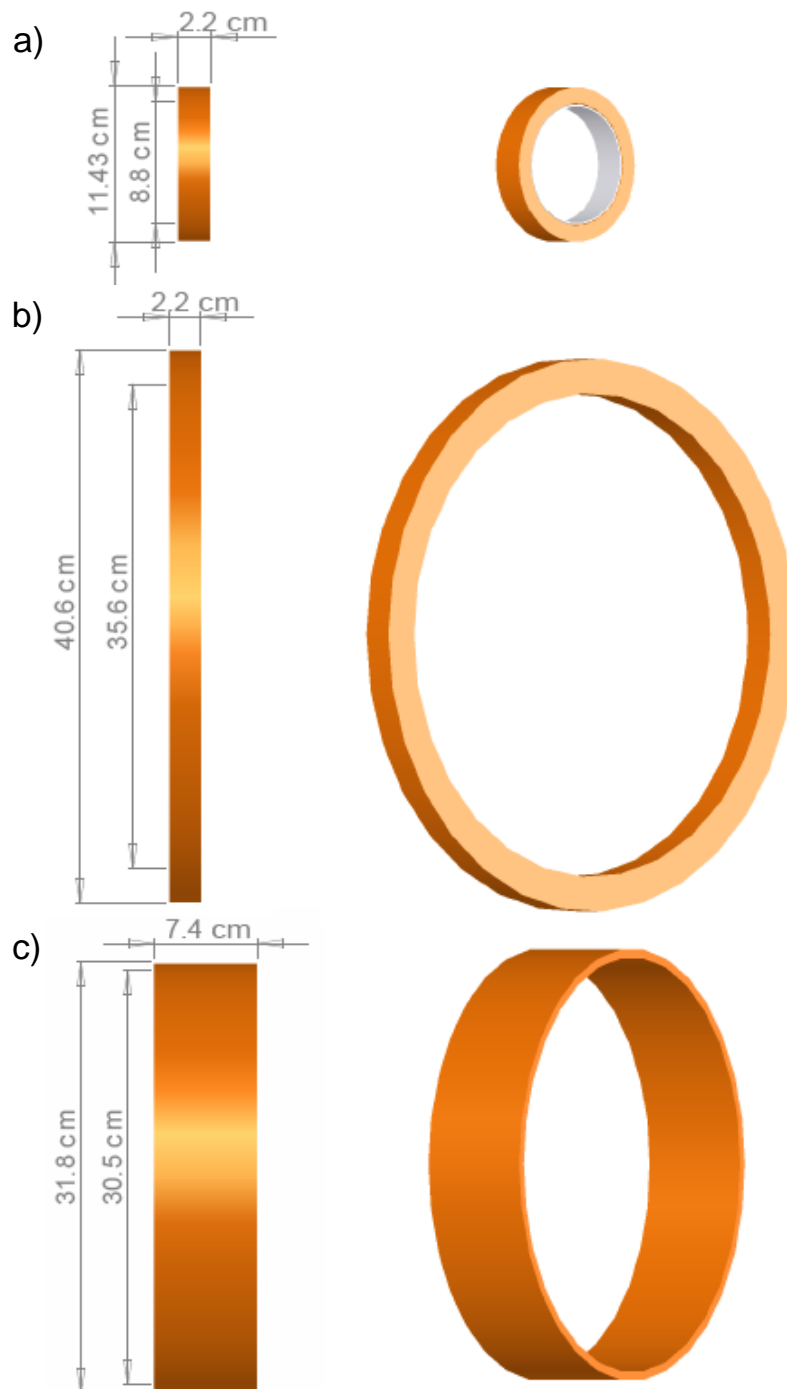


Figure 4.11: Different types of coils that make up the initial bend to transfer the positrons into the transfer guide.

each measuring 1 m in length. This leaves small gaps between the solenoids where the flanges for the vacuum chamber are situated. Additional shorter solenoids (shown in Figure 4.12b) are placed around these gaps. These shorter solenoids can slide in and out to enable the vacuum chamber to be put together.

The positron guide is divided into two sections (the 2-m section and the 3-m section, as shown in Figure 4.1). A turbo pump (shown in Figure 4.1) is installed between these two sections. Two all-metal gate valves are also installed, so that the entire system does not have to be vented each time the two sections are disconnected. Thin circular magnet coils are installed in the turbo-pump region to apply the 0.02-tesla guiding field. These coils are named P1 through P5 (see Table 4.2 and Figure 4.1) and have the geometries shown in Figure 4.12b and c.

The third category of electromagnets is for cancelling non-axial magnetic fields that are present near the positron guide. These fields are almost entirely due to the 1-tesla superconducting solenoid. This cancellation is accomplished by a series of rectangular coils along the 2-m and 3-m sections of the positron guide shown in Figure 4.1. There are three different types of rectangular coils, as shown in Figure 4.13. The rectangular coils are all constructed using insulated copper tape with a thickness of 0.25 mm and a width of 22 mm.

The rectangular coils are oriented as shown in Figure 4.14. The coil pair A & B produce fields in the vertical direction. At locations along the positron guide where large vertical magnetic fields need to be cancelled, coils with a larger number of turns (shown in Figure 4.13a) are used. Where smaller fields are required, the smaller coils (shown in Figure 4.13b) are used. The coil pair C & D of Figure 4.14 produce much smaller fields in the horizontal directions and these coils have the geometry shown in Figure 4.13c.

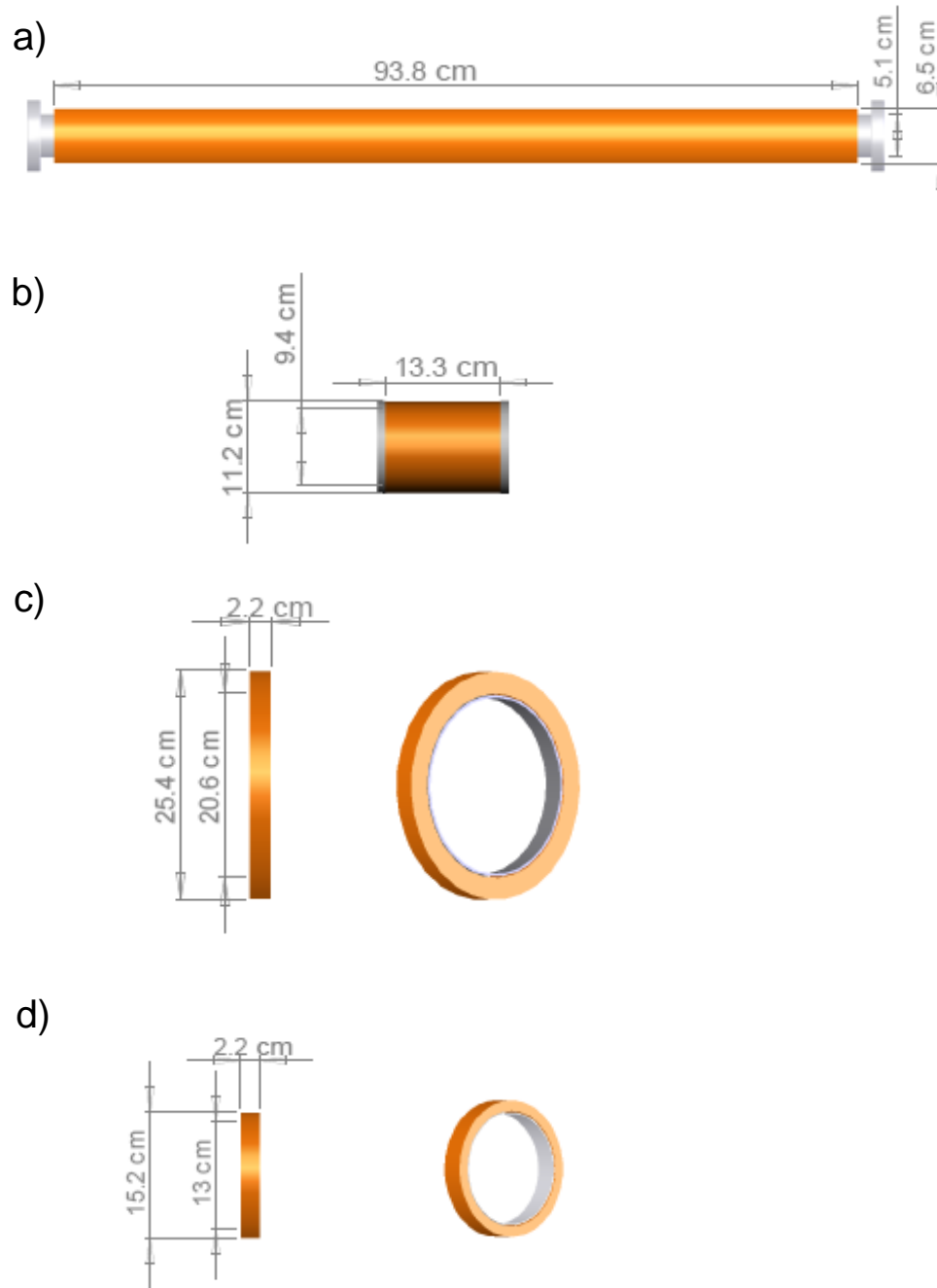


Figure 4.12: Different types of coils that produce the axial field along the positron guide.

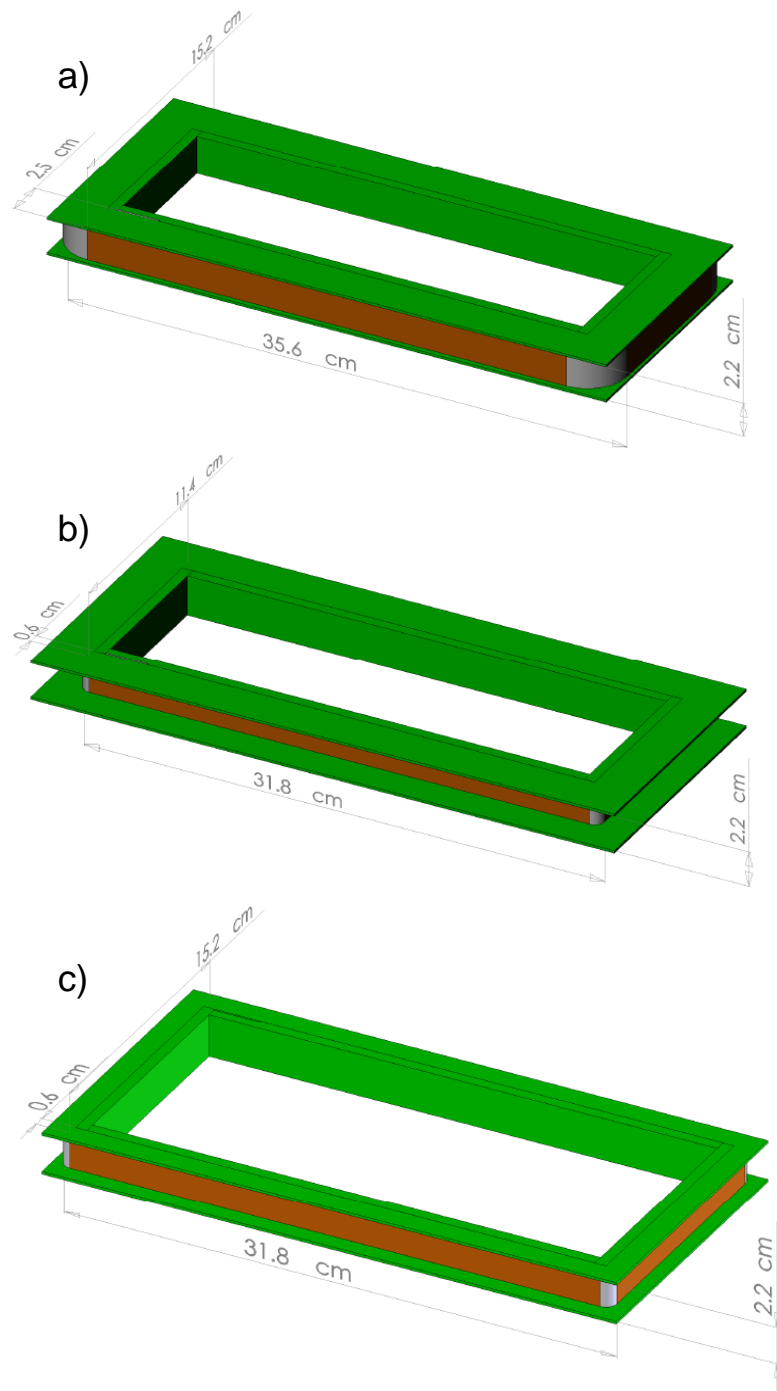


Figure 4.13: Geometry of the rectangular coils

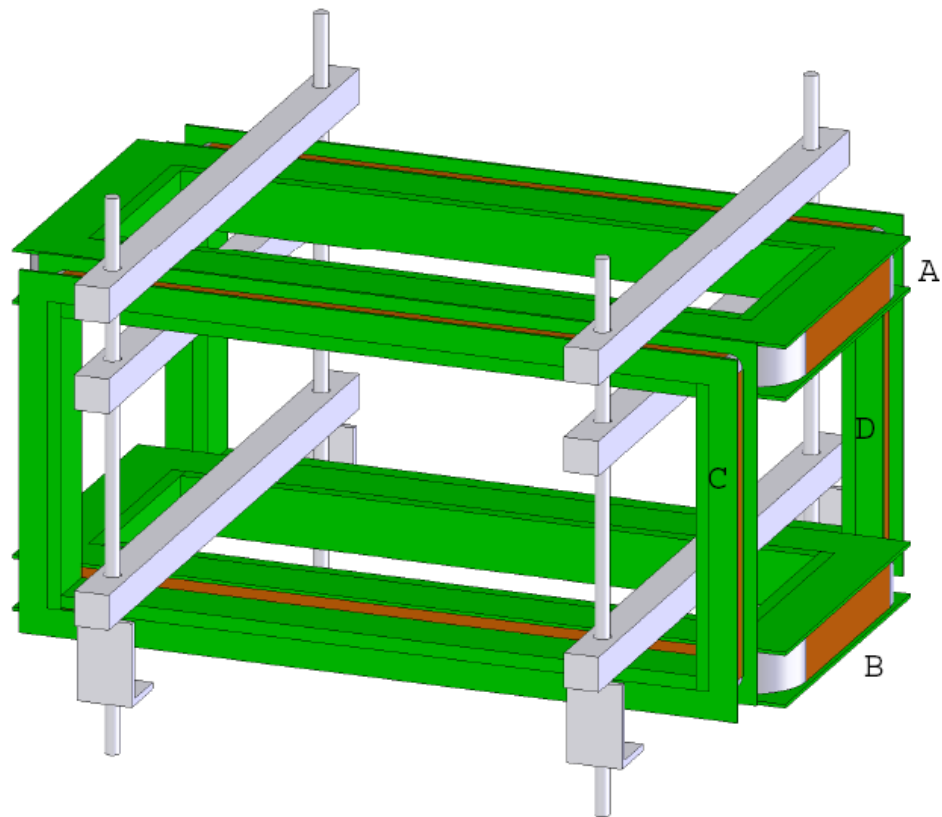


Figure 4.14: Rectangular coils used to cancel out the fringing field of the 1-tesla superconducting solenoid. Coils A and B produce a field in the vertical direction, while C and D produce a field in the horizontal direction. The main guiding solenoid fits within these coils. The entire solenoidal path is surrounded by sets of these rectangular coils.

The main purpose of the vertical magnet coils (which are labelled V0 through V14 in Figure 4.1) is to compensate for the fringing field of the 1-tesla superconducting solenoid. The main purpose of the horizontal coils (named H1 through H14) is to compensate for any stray horizontal magnetic fields. Figure 4.15 shows the offset orientation in which neighbouring rectangular coils are placed. There are two reasons for the geometry shown. Ideally, the vertical compensation magnets would be a continuous line of current bars in the direction of the solenoidal field. The bar current geometry is provided by the long sides of the rectangular coils. The short sides provide current in the perpendicular direction that cause the field to change less uniformly. To minimize the effect that the short lengths of current carrying wire have, subsequent pairs of rectangular coils are oriented as shown in Figure 4.15a. Using the geometry shown, each short side will be approximately cancelled out by the following coil since the currents will be in opposite directions. The second advantage to the offset orientation is that, in order to produce the strongest fields possible, the rectangular coils need to be as close as possible to the centre of the 1-m solenoids. A difficulty arises due to the flange coils, which are much larger in diameter than the long solenoids. Figure 4.15b shows that, using the staggered orientation allows for the placement of the flange coils in the sections where the rectangular coils are offset from the 1-m solenoids. Using the overlap geometry, the continuous fringe-field from the 1-tesla superconducting solenoid can be approximately cancelled out and the positrons travel through the vacuum chamber as if they were being guided by the 0.02-tesla solenoidal field alone.

The final category of magnet coils used to steer the positrons into the ATRAP Penning trap are labelled as final steering magnets in Figure 4.1. All of the magnets previously discussed are used to get the positrons to a position where they can be dropped on a field

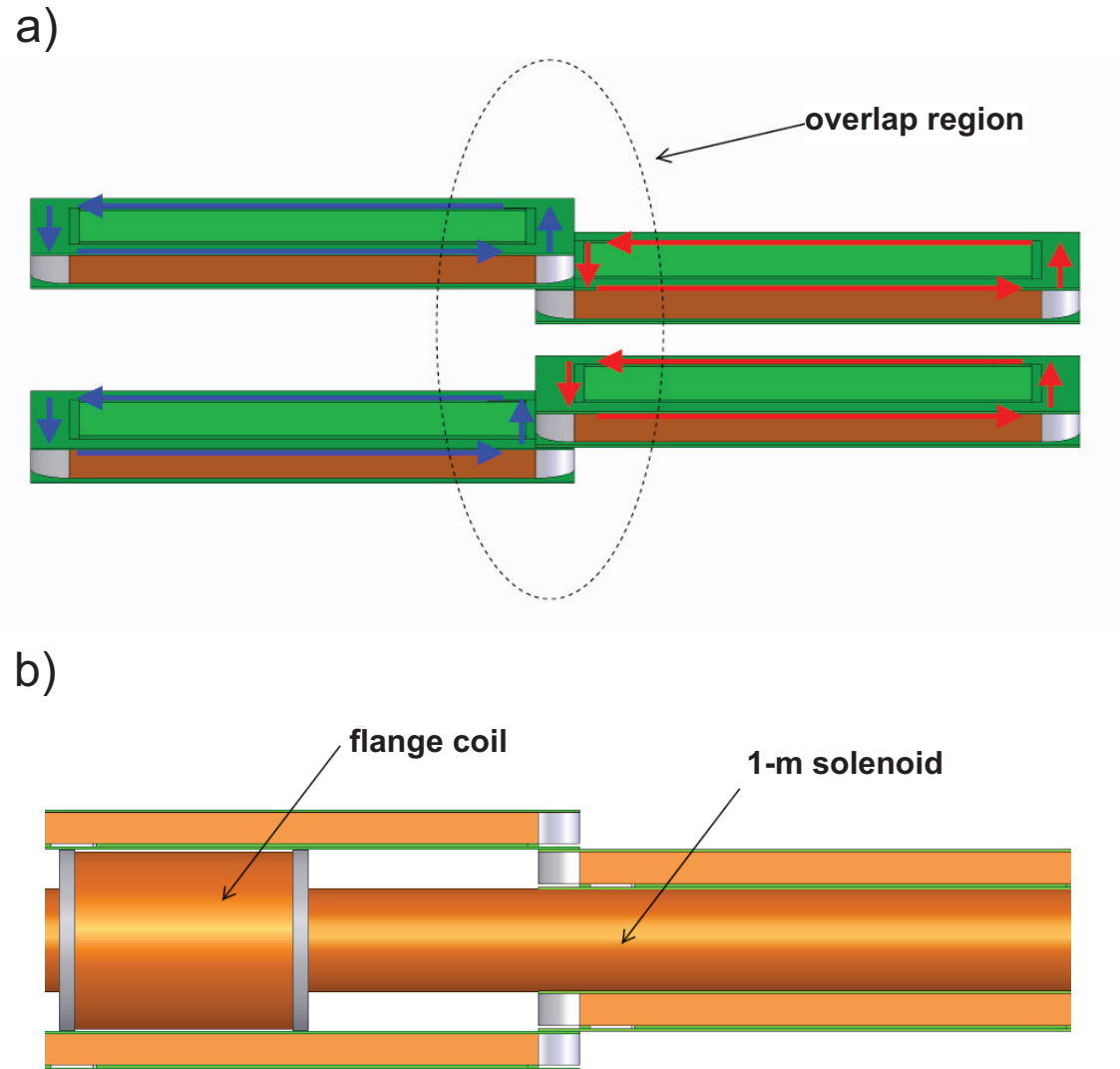


Figure 4.15: a) Overlap of rectangular vertical coils. The arrows represent the direction of the current passing through the magnets. b) The position of the flange and 1-m solenoids inside the vertical magnet assembly.

line of the 1-tesla superconducting solenoid that will continue into the bore as close to the central axis as possible. Final steering is required to make certain that the positrons will make it into the ATRAP Penning trap. Three identical hoop magnets (shown in Figure 4.16) are installed on the front, back and bottom of the vacuum cube situated at the highest-most vertical point directly above the 1-tesla solenoid. The coils are named Cube Front, Cube Back and Cube Bottom. These coils are used to facilitate the 105° bend between the positron guide's solenoid guiding field axis and the axis of the 1-tesla superconducting solenoid. Following the hoop coils, four rectangular coils are positioned on the downward leg where otherwise the only field present is the fringe field from the 1-tesla superconducting solenoid. These four rectangular coils are of the type shown in Figure 4.13a. Two are used to steer the positrons in the front/back direction (named FBDeflector) and two are used to steer the positrons in the left/right direction (named L1 & L2).

4.8 Control of Current to the Magnets

The currents for the electromagnets are provided by power supplies, which can produce up to 30 A of current. Each pair of vertical coils has its current provided by one power supply. Table 4.4 shows the currents applied to each vertical coil and how they are controlled. The horizontal coils are also grouped in pairs but more often than not, more than one pair of coils is controlled by a single power supply since the fields in the horizontal direction are not large. Table 4.5 shows the currents applied to each of the coils and explains which coils are connected in series. Most other coils are controlled by an individual power supply to have control over individual magnetic fields. The solenoidal magnet currents are shown in Table 4.3, the initial bend coils are shown in Table 4.2 and

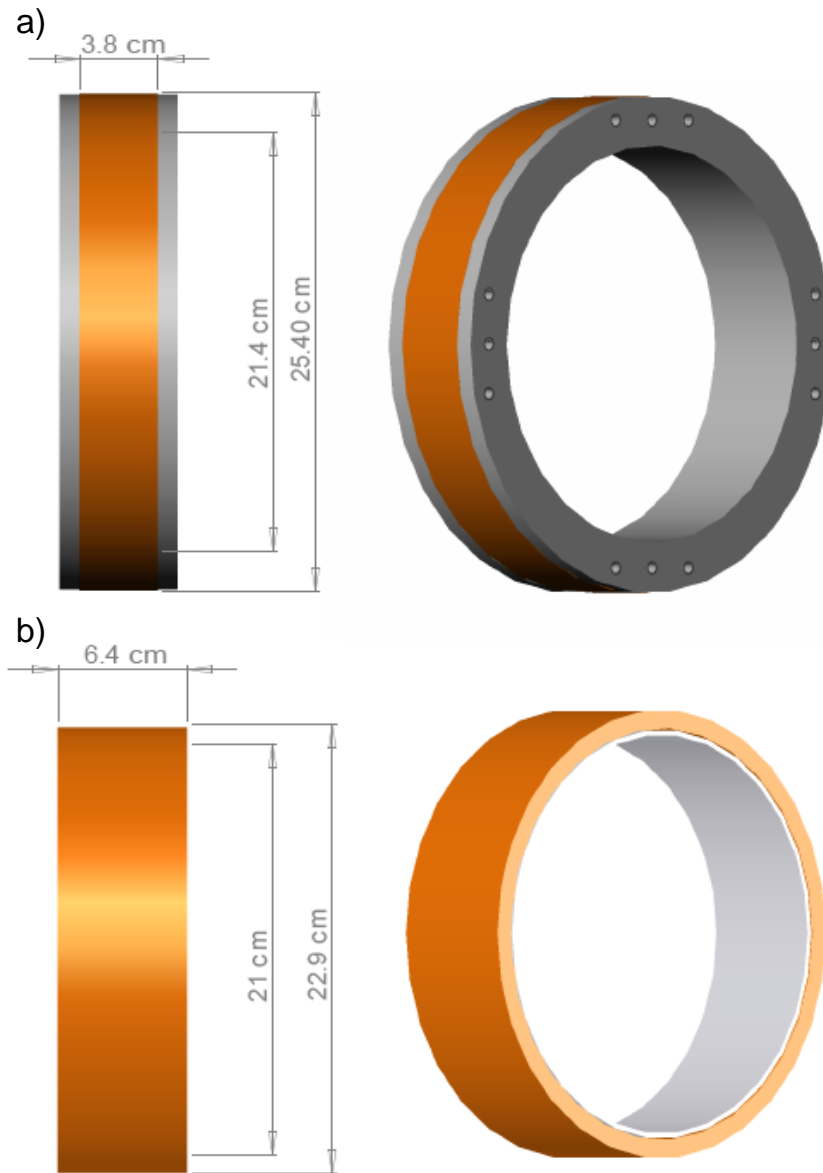


Figure 4.16: Hoop coils positioned around the vacuum cube to provide steering into the ATRAP Penning trap.

the final steering magnet currents are shown in Table 4.6. Each supply is running as a constant current source, computer controlled via an Opto22 DAC module using Labview. The current and voltage of each power supply are recorded using a data acquisition system where their values can be monitored to ensure the desired current is present. The monitoring also detects power supply failure, overheating and indicates possible shorts in the magnets. For some of the magnets along the positron guide, a change in current of as little as 0.1 A changes the positron trajectory enough so that the positrons no longer make it all the way into the electrode stack. The monitoring is critical to ensure that the positron transfer remains consistent and robust.

4.9 Optimization Tools

Magnetic field modelling using Radia aided in the design of the electromagnets and provided an estimate currents that would be needed in each magnet. The modelling is limited by how well the magnetic fields from outside sources are known. There are two other experiments in the AD Hall that use large superconducting magnets that cause small fields along the positron guide. Also, the antiprotons are guided around the AD ring by magnetic fields that change over time. These changing magnetic fields are strong enough to change the positron path drastically enough so that transfer along the guide is no longer possible during the times when these magnets are energized. The path length that the positrons must travel is over 8 meters and the field line on which they travel is defined by a total of 94 magnets powered by 50 computer-controlled power supplies. For transferring positrons between the accumulator Penning trap and the ATRAP Penning trap, the parameter space is enormous. It took many months of optimizing the positron trajectory to achieve an efficient transfer. Real-time optimization techniques were developed to aid

magnet name	magnet type	position along guide (m)	power supply name	power supply type	current(A)	current density (A/cm ²)
B1	Fig 4.11a	-0.2	ps213	20A, 30V	9.9	180
B2	Fig 4.11a	-0.15	ps213	20A, 30V	9.9	180
B3	Fig 4.11a	-0.1	ps213	20A, 30V	9.9	180
B4	Fig 4.11a	-0.05	ps213	20A, 30V	9.9	180
SC axial	Fig 4.11b	around supercross	ps203	20A, 30V	13.2	240
SC left	Fig 4.11c	around supercross	ps626	5A, 18V	0.0	0
SC right	Fig 4.11c	around supercross	ps626	5A, 18V	0.0	0
SC up	Fig 4.11c	around supercross	ps204	20A, 30V	8.0	119
SC down	Fig 4.11c	around supercross	ps204	20A, 30V	8.0	119

Table 4.2: Initial bending coils

magnet name	magnet type	position along guide (m)	power supply name	power supply type	current(A)	current density (A/cm ²)
S1	Fig 4.12a	0.50	ps306	20A, 30V	9.0	134
S2	Fig 4.12a	1.50	ps302	20A, 30V	9.0	134
S3	Fig 4.12a	3.12	ps401	20A, 30V	9.0	134
S4	Fig 4.12a	4.12	ps404	20A, 30V	9.0	134
S5	Fig 4.12a	5.12	ps305	20A, 30V	8.1	120
FC2m(a)	Fig 4.12b	0.00	ps311	20A, 30V	12.0	179
FC2m(b)	Fig 4.12b	1.00	ps311	20A, 30V	12.0	179
FC3m(d)	Fig 4.12b	2.00	ps311	20A, 30V	12.0	179
FC3m(a)	Fig 4.12b	2.62	ps212	20A, 30V	12.0	179
FC3m(b)	Fig 4.12b	3.62	ps212	20A, 30V	12.0	179
FC3m(d)	Fig 4.12b	4.62	ps212	20A, 30V	12.0	179
P1	Fig 4.12c	2.07	ps205	20A, 30V	17.1	311
P2	Fig 4.12c	2.19	ps206	20A, 30V	17.3	315
P3	Fig 4.12c	2.27	ps207	20A, 30V	14.5	264
P4	Fig 4.12d	2.35	ps208	20A, 30V	17.0	309
P5	Fig 4.12c	2.43	ps209	20A, 30V	17.0	309
P6	Fig 4.12c	2.55	ps210	20A, 30V	17.3	315

Table 4.3: Axial coils along the positron guide

magnet name	magnet type	position along guide (m)	Height along guide (cm)	power supply name	type	current(A)	current density (A/cm ²)
V0 top	Fig 4.13a	-0.18	11.5	ps301	20A, 30V	5.0	91
V0 bottom	Fig 4.13a	-0.18	9.0	ps301	20A, 30V	5.0	91
V1 top	Fig 4.13a	0.18	6.7	ps310	20A, 30V	8.3	151
V1 bottom	Fig 4.13a	0.18	-6.7	ps217	20A, 30V	11.8	215
V2 top	Fig 4.13a	0.5	4.1	ps313	20A, 30V	2.6	47
V2 bottom	Fig 4.13a	0.5	-4.1	ps313	20A, 30V	2.6	47
V3 top	Fig 4.13a	0.81	6.7	ps314	20A, 30V	4.0	73
V3 bottom	Fig 4.13a	0.81	-6.7	ps314	20A, 30V	4.0	73
V4 top	Fig 4.13a	1.16	6.7	ps309	20A, 30V	5.1	93
V4 bottom	Fig 4.13a	1.16	-6.7	ps309	20A, 30V	5.1	93
V5 top	Fig 4.13a	1.47	4.1	ps304	20A, 30V	2.2	40
V5 bottom	Fig 4.13a	1.47	-4.1	ps304	20A, 30V	2.2	40
V6 top	Fig 4.13a	1.78	6.7	ps202	20A, 30V	3.3	60
V6 bottom	Fig 4.13a	1.78	-6.7	ps202	20A, 30V	3.3	60
V7 top	Fig 4.13c	2.09	14.0	ps214	20A, 30V	7.0	127
V7 bottom	Fig 4.13c	2.09	-14.0	ps214	20A, 30V	7.0	127
V8 top	Fig 4.13c	2.4	14.0	ps201	20A, 30V	3.0	55
V8 bottom	Fig 4.13c	2.4	-14.0	ps201	20A, 30V	3.0	55
V9 top	Fig 4.13b	2.69	6.7	ps303	20A, 30V	3.2	58
V9 bottom	Fig 4.13b	2.69	-6.7	ps303	20A, 30V	3.2	58
V10 top	Fig 4.13b	2.9	6.7	ps602	5A, 18V	5.0	91
V10 bottom	Fig 4.13b	2.9	-6.7	ps602	5A, 18V	5.0	91
V11 top	Fig 4.13b	3.21	6.7	ps617	3A, 30V	2.2	40
V11 bottom	Fig 4.13b	3.21	-6.7	ps617	3A, 30V	2.2	40
V12 top	Fig 4.13b	3.52	6.7	ps605	5A, 18V	0.2	4
V12 bottom	Fig 4.13b	3.52	-6.7	ps605	5A, 18V	0.2	4
V13 top	Fig 4.13b	3.83	6.7	ps613	5A, 18V	0.0	0
V13 bottom	Fig 4.13b	3.83	-6.7	ps613	5A, 18V	0.0	0
V14 top	Fig 4.13b	4.14	6.7	ps614	5A, 18V	0.3	5
V14 bottom	Fig 4.13b	4.14	-6.7	ps614	5A, 18V	0.3	5
V15 top	Fig 4.13b	4.45	6.7	ps601	3A, 30V	1.1	20
V15 bottom	Fig 4.13b	4.45	-6.7	ps601	3A, 30V	1.1	20

Table 4.4: Rectangular vertical coils

magnet name	magnet type	position along guide (m)	height above guide (cm)	power supply name	type	current(A)	current density (A/cm ²)
H1 right	Fig 4.13c	0.18	16.5	ps611	5A, 18V	2.0	36
H1 left	Fig 4.13a	0.18	-16.5	ps611	5A, 18V	2.0	36
H2 right	Fig 4.13c	0.5	16.5	ps616	5A, 18V	0.0	0
H2 left	Fig 4.13c	0.5	-16.5	ps616	5A, 18V	0.0	0
H3 right	Fig 4.13c	0.81	16.5	ps606	3A, 30V	1.0	18
H3 left	Fig 4.13c	0.81	-16.5	ps606	3A, 30V	1.0	18
H4 right	Fig 4.13c	1.16	16.5	ps606	3A, 30V	1.0	18
H4 left	Fig 4.13c	1.16	-16.5	ps606	3A, 30V	1.0	18
H5 right	Fig 4.13c	1.47	16.5	ps606	3A, 30V	1.0	18
H5 left	Fig 4.13c	1.47	-16.5	ps606	3A, 30V	1.0	18
H6 right	Fig 4.13c	1.78	16.5	ps632	5A, 18V	0.5	9
H6 left	Fig 4.13c	1.78	-16.5	ps632	5A, 18V	0.5	9
H9 right	Fig 4.13c	2.69	16.5	ps604	3A, 30V	0.0	0
H9 left	Fig 4.13c	2.69	-16.5	ps604	3A, 30V	0.0	0
H10 right	Fig 4.13c	2.9	16.5	ps615	3A, 30V	1.1	20
H10 left	Fig 4.13c	2.9	-16.5	ps615	3A, 30V	1.1	20
H11 right	Fig 4.13c	3.21	16.5	ps625	3A, 30V	0.0	0
H11 left	Fig 4.13c	3.21	-16.5	ps625	3A, 30V	0.0	0
H12 right	Fig 4.13c	3.52	16.5	ps625	3A, 30V	0.0	0
H12 left	Fig 4.13c	3.52	-16.5	ps625	3A, 30V	0.0	0
H13 right	Fig 4.13c	3.83	16.5	ps625	3A, 30V	0.0	0
H13 left	Fig 4.13c	3.83	-16.5	ps625	3A, 30V	0.0	0
H14 right	Fig 4.13c	4.14	16.5	ps625	3A, 30V	0.0	0
H14 left	Fig 4.13c	4.14	-16.5	ps625	3A, 30V	0.0	0
H15 right	Fig 4.13c	4.45	16.5	ps625	3A, 30V	0.0	0
H15 left	Fig 4.13c	4.45	-16.5	ps625	3A, 30V	0.0	0

Table 4.5: Rectangular horizontal coils

magnet name	magnet type	height above magnet (m)	x position (cm)	y position (cm)	power supply name	type	current(A)	current density (A/cm ²)
front cube	Fig 4.16a	2.07	12.7	0.0	ps307	20A, 30V	4.9	73
back cube	Fig 4.16a	2.07	-12.7	0.0	ps308	20A, 30V	8.6	128
bottom cube	Fig 4.16a	1.92	0.0	0.0	ps312	20A, 30V	11.4	170
left cube	Fig 4.16b	2.07	0.0	12.7	ps623	20A, 30V	0.2	3
right cube	Fig 4.13b	2.07	4.1	-12.7	ps623	20A, 30V	0.2	4
front deflector	Fig 4.13a	1.23	10.2	0.0	ps218	20A, 30V	4.0	73
back deflector	Fig 4.13a	1.23	-10.2	0.0	ps218	20A, 30V	4.0	73
L1	Fig 4.13a	1.23	0.0	-10.2	ps403	20A, 30V	6.1	111
L2	Fig 4.13a	0.89	0.0	2.5	ps402	20A, 30V	7.7	140

Table 4.6: Control of all of the Final steering coils

in efficiently transferring the positrons.

4.9.1 Faraday Cup Detection

The first technique to optimize the transfer of positrons between the accumulator and the ATRAP Penning trap utilizes a series of retractable Faraday cups placed along the positron guide shown in Figure 4.17. Using the technique as described in Section 3.2.1, the number of positrons at each Faraday cup can be determined and thus a transfer efficiency at several points along the guide can be determined.

The first Faraday cup is mounted on a linear translating stage and is referred to as the retractable 3-m Faraday cup, as shown in Figure 4.17. When inserted, it intersects the middle of the positron guide vacuum tube at a position three meters away from the output of the accumulator (at the same position as the turbo pump used to pump out the positron guide). The 3-m Faraday cup is used to make the measurements of the number of accumulated positrons (all of the Faraday-cup measurements found in Chapter 2 were done using the 3-m Faraday cup).

The second Faraday cup is positioned along the downward leg on the positron guide, along the axis of the 1-tesla superconducting solenoid (labelled as the mirror Faraday cup in Figure 4.17). This Faraday cup is also attached to a linear stage, and this linear stage also has a mirror attached to it to allow laser light into the ATRAP Penning trap during times when the positrons are not being loaded. The magnetic field magnitude at the position of the mirror Faraday cup is 0.02 tesla, thus there is no magnetic field compression between the mirror Faraday cup and the main guiding field. The mirror Faraday cup gives valuable information concerning the number of positrons that make it all the way through the positron guide and around the 105° bend. Figure 4.18 shows the

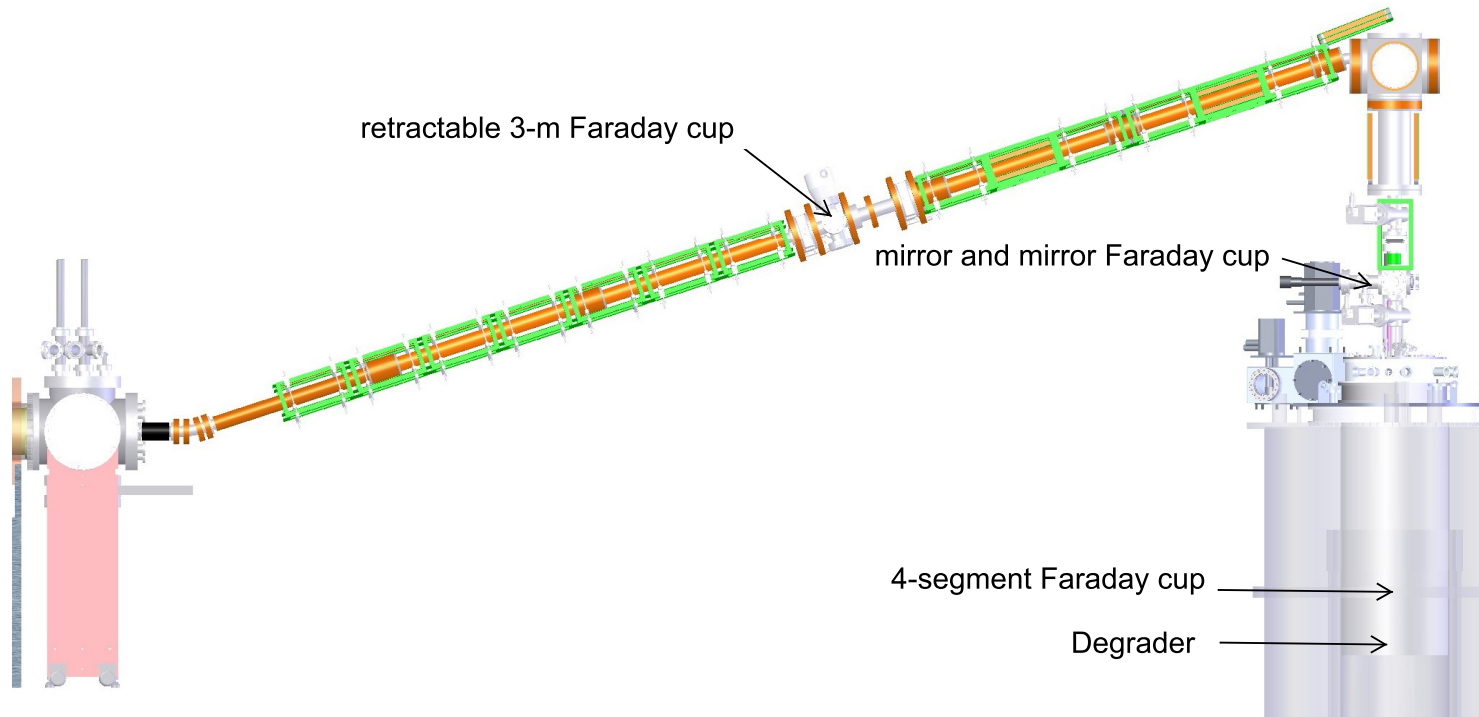


Figure 4.17: Location of the Faraday cups

positioning of the mirror Faraday cup. To allow positrons to enter the ATRAP Penning trap, the mirror and mirror Faraday cup are completely retracted, as shown in Figure 4.18a. When laser light is used to load electrons (to be discussed in Section 5.4.1), the linear stage is positioned as shown in Figure 4.18b. When the mirror Faraday cup is in position (Figure 4.18c), the positrons are prevented from going into the ATRAP Penning trap and are instead counted.

The first Faraday cup inside the 1-tesla field is positioned on top of the 1-mm opening into the ATRAP Penning trap vacuum system, as is labelled 4-segment Faraday cup in Figure 4.17. This Faraday cup (shown in Figure 4.20), is split into 4 segments with a 1-mm diameter hole through the centre. The Faraday cup is built on a printed circuit board and bolted directly onto the vacuum chamber, within the uniform 1-tesla magnetic field. The four segments of the Faraday cup are used to steer the positrons into the 1-mm tube thus into the ATRAP electrode stack.

The final Faraday cup is the degrader, a thin piece of beryllium positioned at the end of the ATRAP electrode stack, as shown in Figure 1.4. When not loading antiprotons (as described in Section 1.1.1), the degrader is attached to a charge amplifier and acts like a Faraday cup. The degrader is used to look at positrons that make it through the 1-mm opening and all the way into the ATRAP electrode stack. The degrader is an especially useful Faraday cup since it is after the ATRAP electrode stack. Using the electrodes and the degrader Faraday cup, the energy distribution (Section 5.1.1) and the temporal distribution (Section 5.1.2) of the transferred positrons can be determined.

As another diagnostic tool, an electron gun is installed in the drift tube of the accumulator, at the position indicated in Figure 4.21. Electrons are emitted by thermionic emission from a tungsten filament and magnetically guided along the same path as the

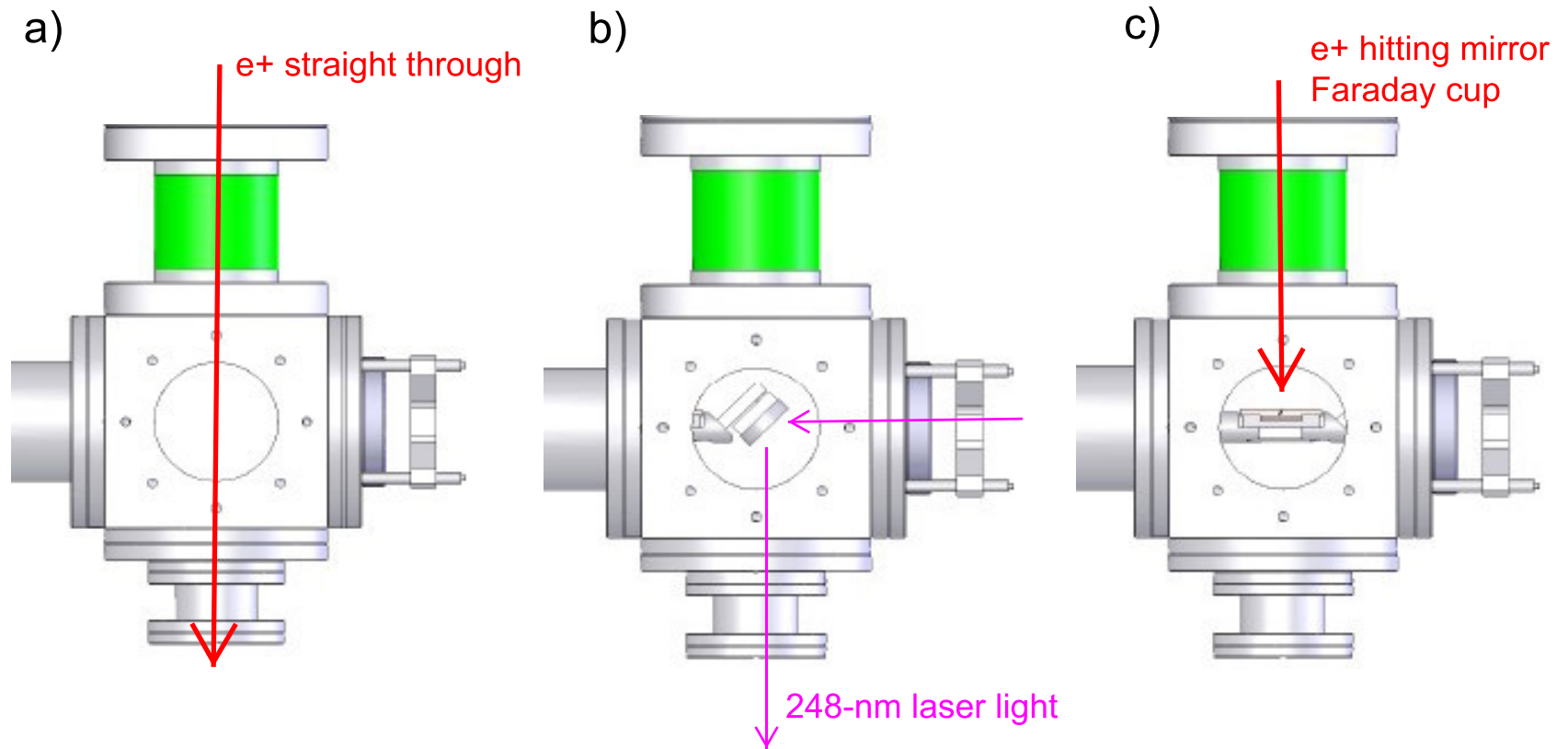


Figure 4.18: 3 positions of mirror Faraday cup

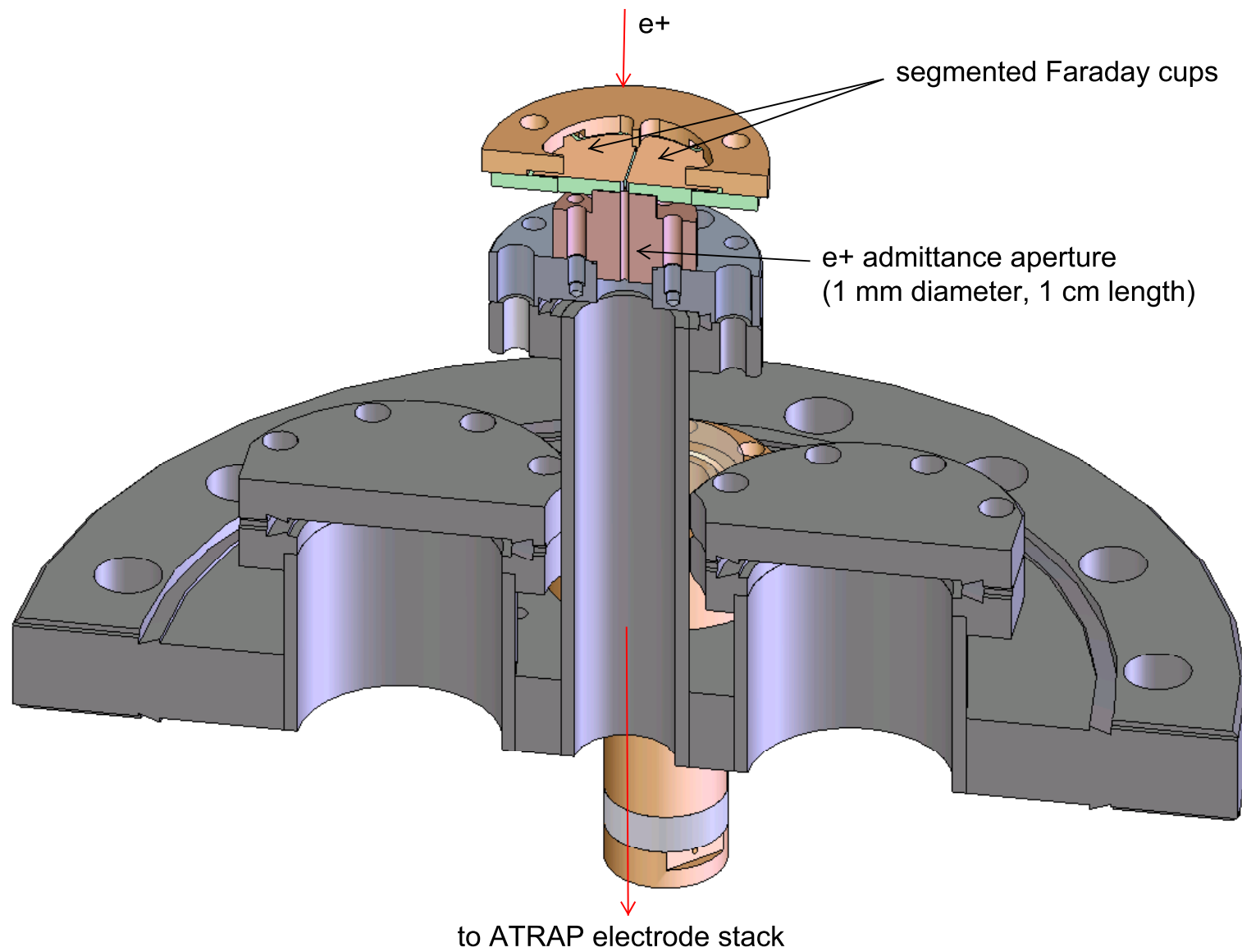


Figure 4.19: The 1-mm tube for admitting positrons into the ATRAP Penning trap

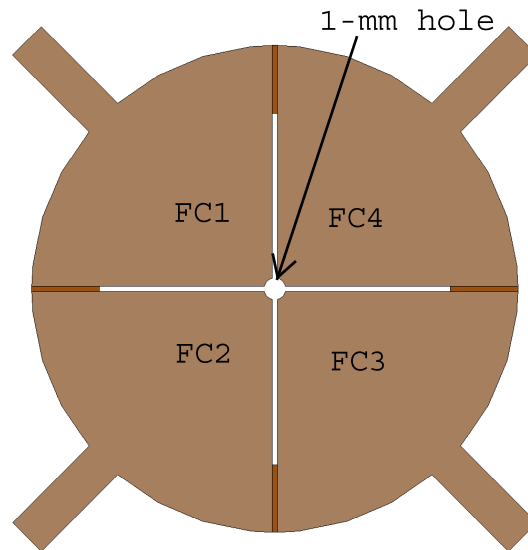


Figure 4.20: The 4-split segmented Faraday cup positioned on top of the 1-mm tube of the ATRAP Penning trap vacuum chamber. The Faraday cup is made of a printed circuit board and each segment is attached to a separate charge amplifier.

positrons. Since the electron beam is CW, it enables a real-time signal to be seen on the Faraday cups. The electron gun runs at a current of 0.52 A through the filament, which is biased to -33 V relative to ground. The back plate shown in Figure 4.21 is also biased to -33 V relative to ground. The front plate is biased at 18 V relative to the back plate. Electrons exit through a hole in the front plate in the direction of the accumulator Penning trap and through the positron guide. To acquire a CW signal, a Faraday cup is attached to a Fempto-Amp current amplifier so that the electron current can be measured. The electron gun produces a electron current of 20 μA measured on the 3-meter Faraday cup. With a CW signal produced by the electron gun, the particle trajectory (defined by the field lines produced by the series of magnets that make up the positron guide) can be adjusted much more quickly since the currents of the magnets can be adjusted and the

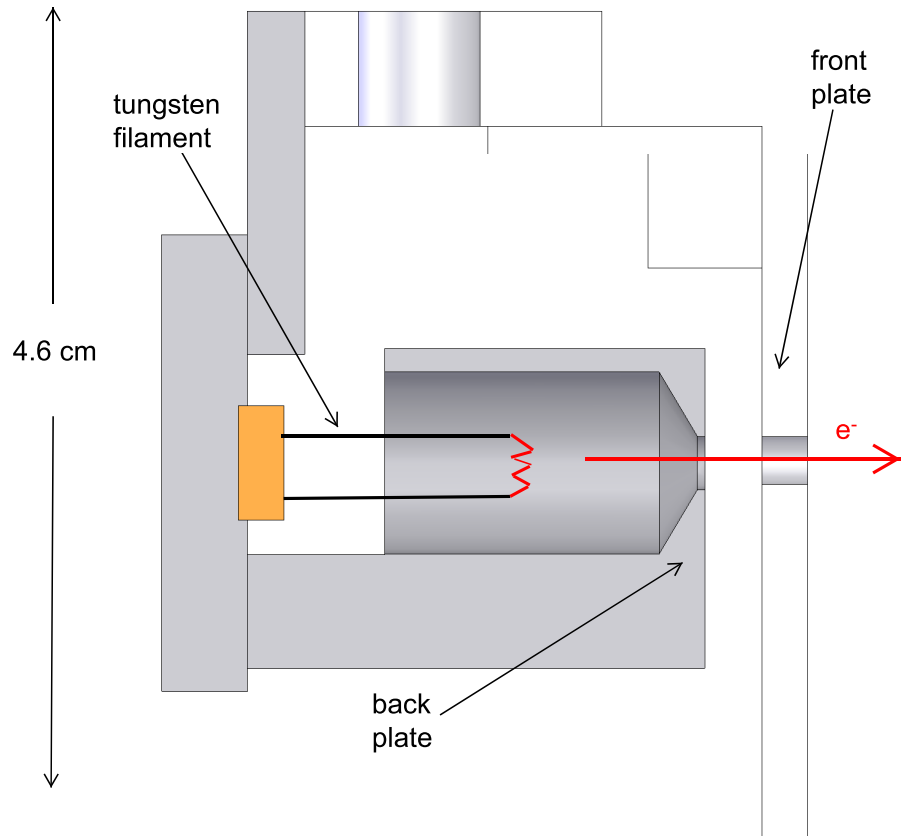


Figure 4.21: The electron gun that is placed on a retractable arm inside the drift tube of the accumulator.

result is immediately visible through either an increase or decrease in the signal seen on the Faraday cup. Since positrons need to be accumulated and transferred, the adjustment procedure is much slower when positrons are used.

Using the Faraday cups (both with positrons and electrons) works well to optimize the number of particles making it to the positions where Faraday cups are present. Optimization can be done by changing magnet currents, thus changing the magnetic field lines and the trajectories of the particles along the positron guide. When the particles are

steered considerably off target, and there is no signal present on the Faraday cups, another method must be used to direct the particles onto the Faraday cups.

4.9.2 Timing Signals

Using antimatter particles provides a unique diagnostic tool. As explained in Section 2.4, when a positron hits the side of the vacuum chamber along the positron guide, gammas are produced and can be detected using NaI detectors. The energy at which the positrons are ejected from the accumulator can be adjusted between 10 eV and 400 eV by simply changing the potential of the well in which the positrons are sitting before being transferred. Since the positrons are being given energy in the axial direction (along the positron guide axis), the speed at which they are travelling is well known. With a known speed, the annihilation position can be determined by measuring the time at which the gamma was detected on the NaI crystal. Table 4.7 shows expected delay times for various axial energies and various annihilation positions.

Using the timing information, the position where the positrons are annihilating along the positron guide can be deduced. A NaI detector (the same detector and position used in the measurements done in Section 3.2.3) positioned at 11.2 m from the accumulator is approximately equidistant from the the entire positron guide, so the annihilation signal along the entire travel path can be seen by the detector with approximately equal efficiency. Figure 4.22 shows the annihilation signal at two different points. The first annihilation point is when the output valve of the accumulator is closed so that the positrons annihilate before entering the positron guide. The second annihilation point is at the pump section shown in Figure 4.1. The gate valve that isolates the 3-m section and the pump section is closed to provide the surface on which the positrons annihilate. The distance between

Energy (eV)	Speed (m/ μ s)	Distance Travelled (m)	Delay Time (μ s)
3	1.03	1.0	0.971
		3.0	2.913
		6.0	5.825
		8.0	7.767
61	4.64	1.0	0.216
		3.0	0.647
		6.0	1.293
		8.0	1.724
100	5.94	0.6	0.101
		3.0	0.505
		6.0	1.010
		8.0	1.347
400	11.87	1.0	0.084
		3.0	0.253
		6.0	0.505
		8.0	0.674

Table 4.7: Expected delay times at different axial energies. The positron annihilation signal will be delayed for different amounts of time depending on how far along the positron guide the positrons make it before they annihilate. The energy that is used to transfer positrons is highlighted.

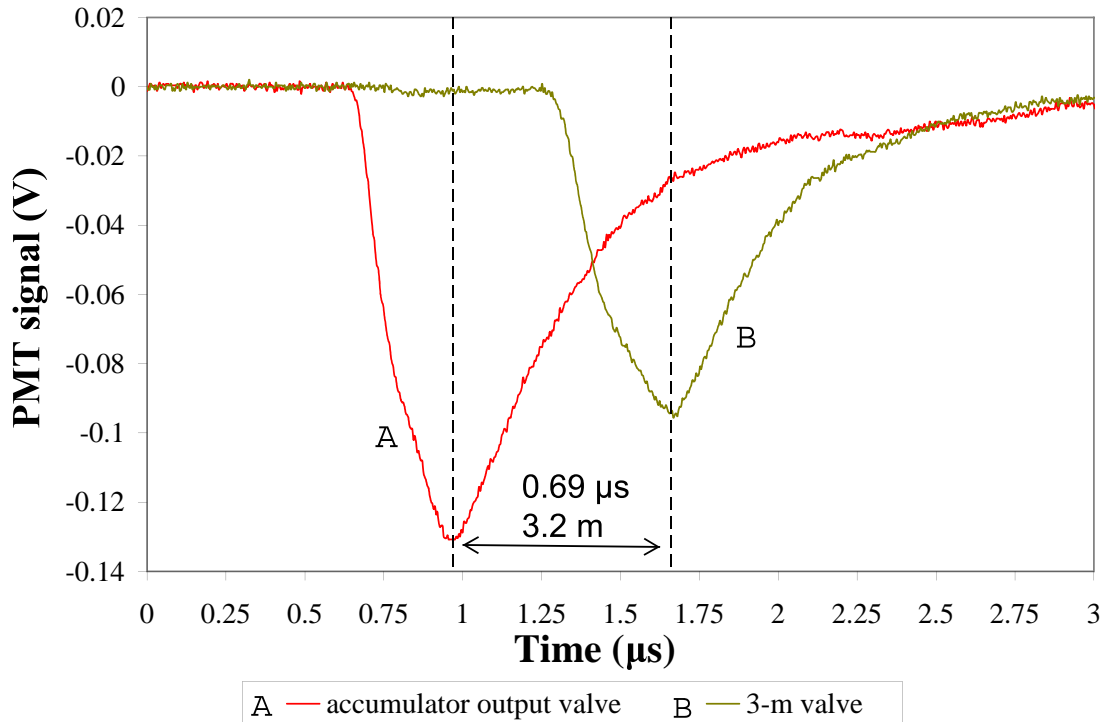


Figure 4.22: Scintillation signal at A) the output valve and B) the 3-m valve. From the spacing between the two peaks, there is a time delay of $0.69 \mu\text{s}$ between the two annihilation points, which are separated by 3.2 m along the positron guide.

the two annihilation points is 3.2 m . From Figure 4.22, the difference in the annihilation times is measured to be $0.69 \mu\text{s}$. Assuming that the positrons do not accelerate between the two points because there is no electric field present and the positrons are travelling in a mostly-homogeneous field, as shown in Figure 4.5, the positrons are travelling at a speed of $4.6 \text{ m}/\mu\text{s}$. The kinetic energy of these positrons is 61 eV .

The knowledge of the annihilation positions is a very important tool when one considers the complexity of the positron guide and the number of independently controlled magnets. When the positrons are not making it through the entire guide and into the ATRAP Penning trap, the annihilation signal gives information on the position at which

they are annihilating, and thus an indication of which magnet needs to be adjusted. Figure 4.23 shows four annihilation signals. Lines A & B are the same annihilation signals as shown in Figure 4.22. Line D shows the annihilation signal once the positrons have made it around the 105° bend and are annihilating on the mirror Faraday cup. Line C shows the annihilation signal when the positrons are not making it all the way through the positron guide and are annihilating somewhere along the guide. From the timing, it can be deduced that they are annihilating 40 cm before they enter the top of the vacuum cube (where they make the 105° bend).

The annihilation signals can also be used to diagnose if the entire positron cloud is passing through the transfer line. First, when the positrons are annihilating on the Faraday cup, the NaI signal also shows whether or not there is loss at earlier times. Any earlier signals imply that some of the positrons are annihilating somewhere along the guide before the Faraday cup. Secondly, when the Faraday cup is retracted, if there are no longer any annihilations at that point, the entire annihilation signal must be due to annihilations on the Faraday cup, thus all of the positrons are hitting the surface of the Faraday cup. As shown in Figure 4.23b, for the 3-meter Faraday cup, both of these conditions are met. The transfer efficiency to the 3-meter Faraday cup is thus considered consistent with 100%, and all of the positrons that are being ejected from the accumulator are being counted at the 3-meter Faraday cup. It can also be seen that there is no loss along the entire positron guide up until the mirror Faraday cup shown in Figure 4.23d. When the positrons are well steered, the positrons counted on the mirror Faraday cup and the 3-meter Faraday cup are equal, thus providing a 100% transfer efficiency between the accumulator and the mirror Faraday cup before entering the 1-tesla superconducting field.

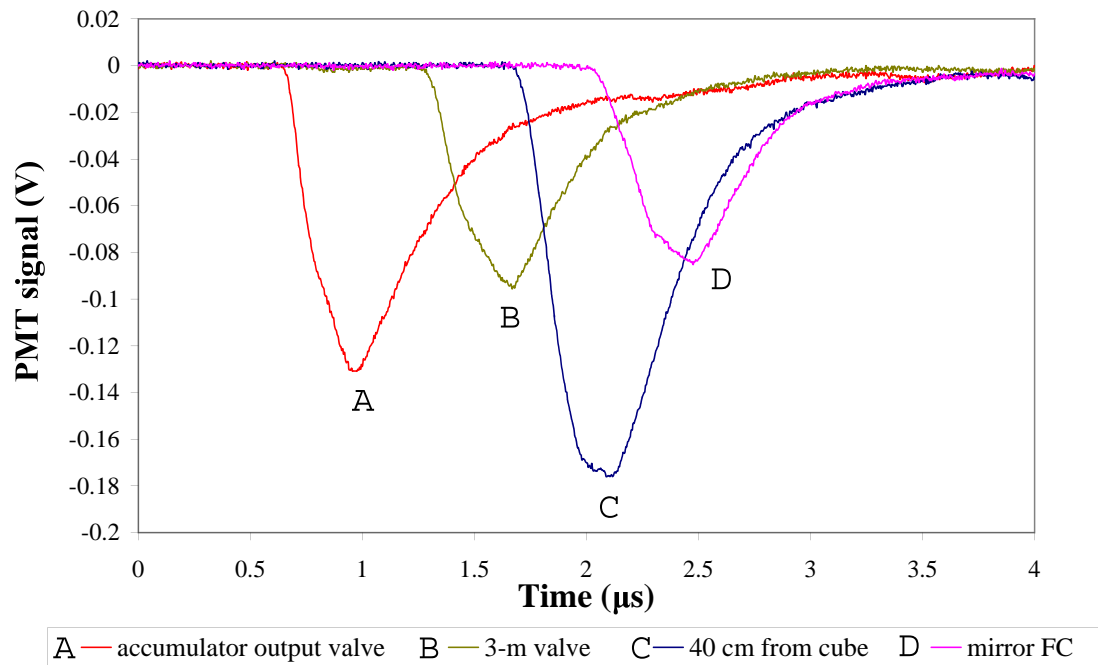


Figure 4.23: Signal from the NaI detector and PMT viewed on a digital oscilloscope. The output valve is positioned at the end of the accumulator, before the transfer guide (A). The 3-m annihilation point is obtained by closing a gate valve located 10-cm from the 3-meter FC along the transfer guide (B). The next annihilation point (C) is obtained by applying a field with a horseshoe magnet laid directly onto the guiding solenoidal field, 40 cm from the end of the last solenoidal magnet. The final annihilation point occurs when the positrons hit the mirror FC, positioned along the vertical leg of the transfer guide (D). In all cases, the positrons are travelling with 61 eV of kinetic energy.

Chapter 5

Catching Positrons in the ATRAP

Penning Trap

The positrons ejected from the accumulator travel through the positron guide and enter the ATRAP Penning trap through the 1-mm tube separating the electrode stack vacuum chamber from the positron guide vacuum chamber. The positrons that make it through the 1-mm tube are then free to travel through the electrode stack unabated. Since the positrons are pulsed from the accumulator, they are bunched together in a cloud and can be captured inside the electrode stack in a similar method to that used to capture the antiprotons. The captured positrons and antiprotons can then be used to create antihydrogen (as described in Section 1.6).

5.1 Cloud Characteristics

To capture the positrons in the ATRAP Penning trap, the characteristics of the pulsed cloud of positrons must be understood. In order to catch the cloud of positrons in the most

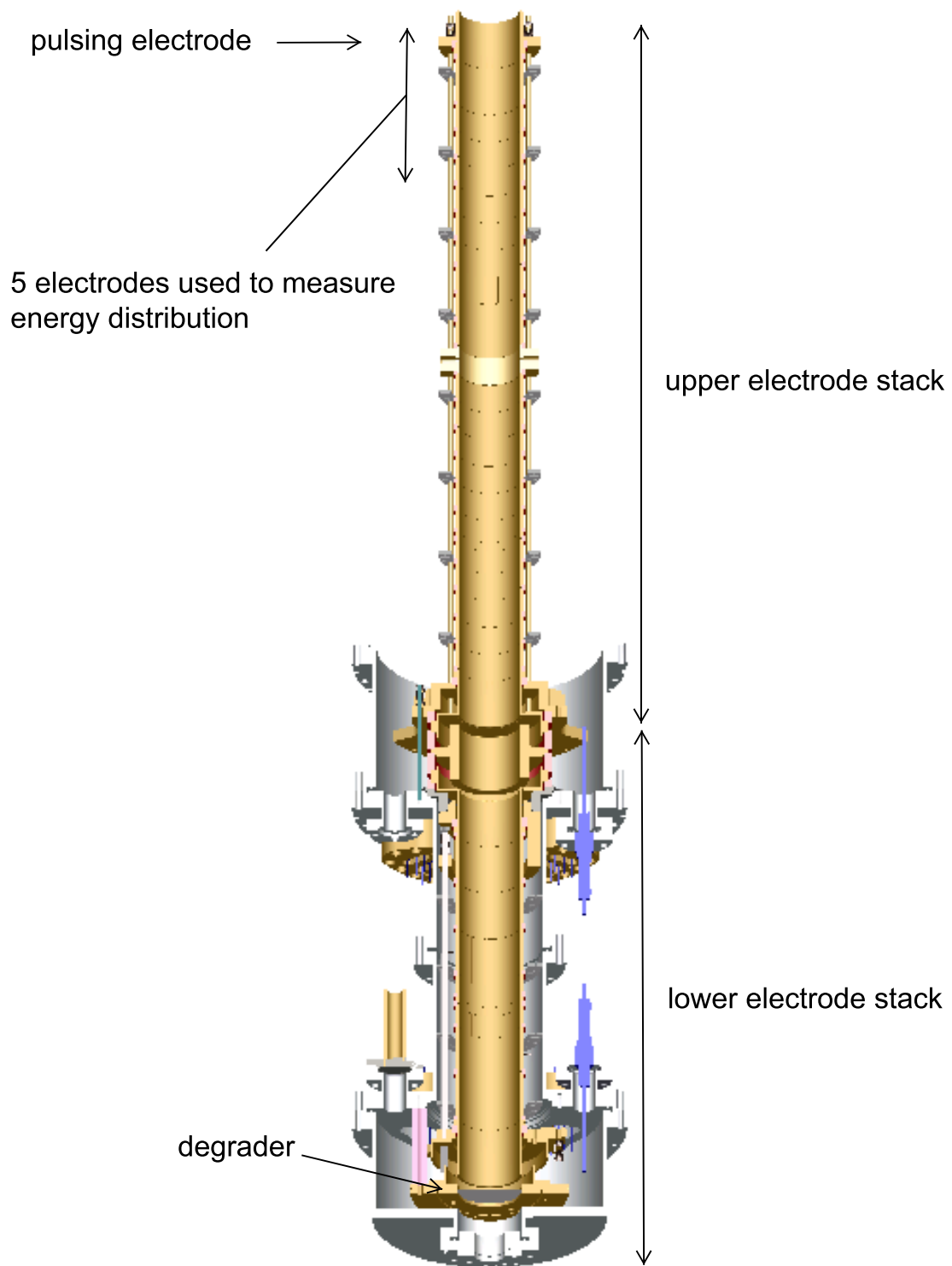


Figure 5.1: Sections of the ATRAP Penning trap

reliable and efficient manner possible, the energy distribution, temporal distribution and cloud shape must be known.

5.1.1 Energy Distribution

The energy profile once the positrons have reached the ATRAP 1-tesla superconducting solenoid is determined using the ATRAP electrode stack. The positrons that make it through the 1-mm tube will continue on through the electrode stack (if grounded), until they reach the degrader, positioned on axis, as shown in Figure 5.1. As described in Section 4.9.1, the degrader can be used as a Faraday cup (since it can be attached to a charge amplifier) to measure the number of positrons hitting its surface.

A blocking potential is applied to the first 5 adjacent electrodes in the ATRAP electrode stack shown in Figure 5.1. The number of positrons that make it past the blocking potential is measured. The on-axis blocking potential is shown in Figure 5.2 for settings of 55V, 60V and 65V. The resulting energy distribution is shown in Figure 5.3. As measured inside the ATRAP Penning trap, the positrons have an average energy of 63 eV and an energy spread of 8 eV (FWHM).

Prior to transferring the positrons from the accumulator, they are held in the final well (depicted in Figure 3.2) for a short time (approximately 1 second) where they cool due to collisions with the buffer gas. They are not left in the final well for longer since the positrons will also annihilate with the buffer gas. The positrons will not all cool into the bottom of the well, so the final energy spread (shown in Figure 5.3) can partially be attributed to the initial pulsing conditions.

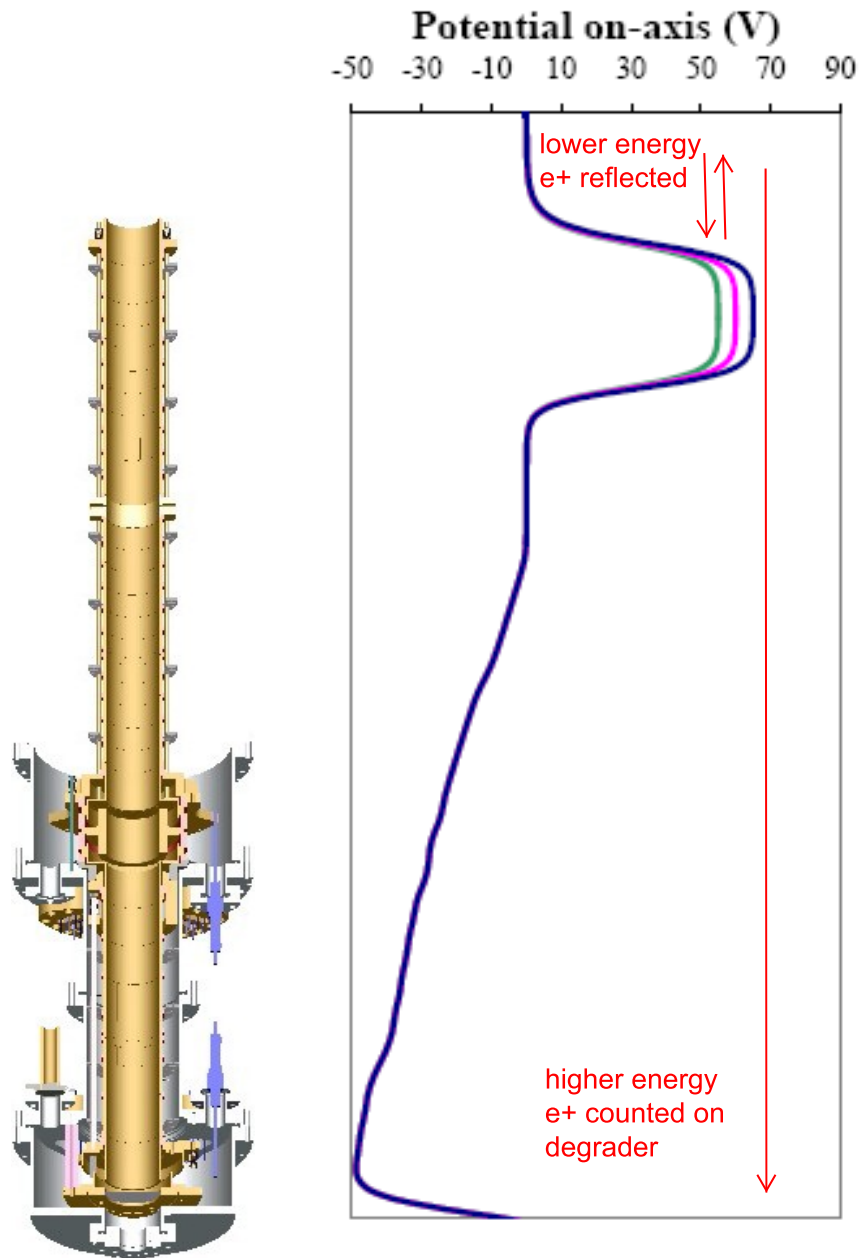


Figure 5.2: The on-axis potential of the ATRAP electrode stack to measure the energy distribution. The number of positrons is measured using the degrader. The potentials shown are for settings of 55V, 60V and 65V.

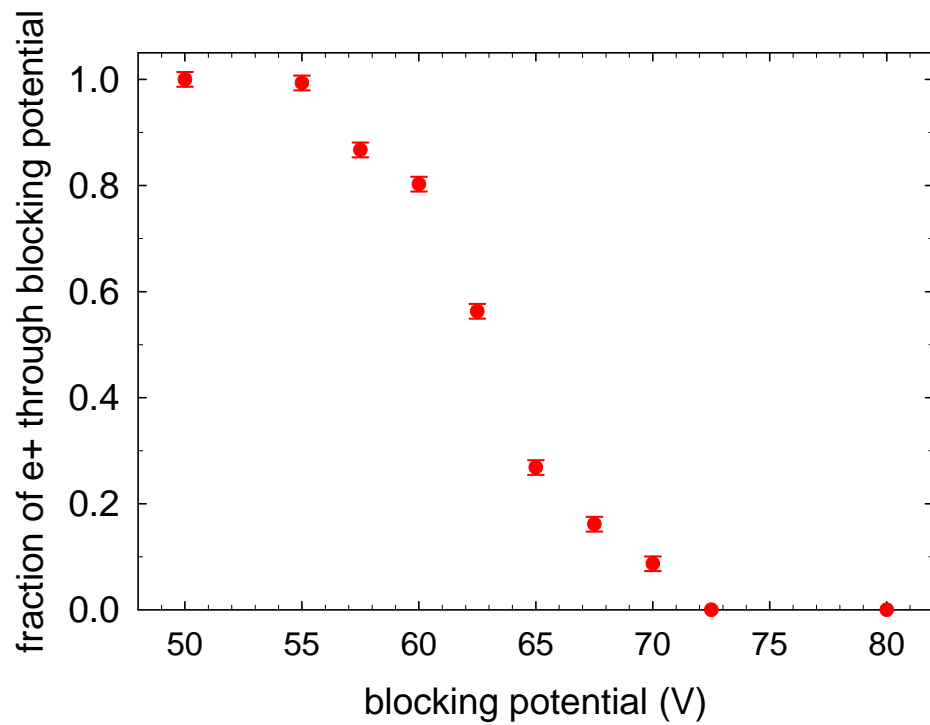


Figure 5.3: The energy distribution measured inside the ATRAP Penning trap. The blocking potential is applied by setting 5 adjacent electrodes to the voltage shown to ensure that the electric field within the centre of the trap is equal to the applied voltage. The number of positrons is measured using the degrader, positioned on axis as the bottom of the electrode stack, as a Faraday cup.

5.1.2 Temporal Distribution

The temporal spread is also measured using the degrader as a Faraday cup. A positive potential is applied to an electrode in the ATRAP Penning trap that completely blocks the positrons from hitting the degrader. As seen in Figure 5.3, any potential higher than 72.5 V will completely block the incoming positrons. The same electrode is attached to a DEI pulser, capable of producing a pulse at 1 kV (in the negative direction) with a fall time of 7 ns. A pulse, equal in magnitude and opposite in direction to the +72.5 V potential applied to the electrode, is applied by the DEI pulser for 100 ns and the number of positrons hitting the degrader is recorded. When the positrons are ejected from the accumulator, a trigger signal is sent to a pulse generator triggering the DEI pulser for the ATRAP electrodes. Figure 5.4 shows the potentials applied to measure the temporal spread. Figure 5.4b shows the potential at the point where the positrons are pulsed from the accumulator. Figure 5.4c shows the potential applied once the DEI pulser is triggered. The time between when the positrons are released from the accumulator and when the DEI is pulsed down, as shown in Figure 5.4c, is the delay time for the pulse. Figure 5.4d shows the potential applied 100 ns after the DEI pulser is triggered. The delay time between when the trigger-signal arrives and when the DEI pulser is triggered is varied so that different time windows are sampled and the entire temporal picture can be viewed. Figure 5.5 shows the number of positrons counted on the degrader for different 100-ns bins. The result is a measure of the temporal spread of the positron cloud transferred from the accumulator and measured inside the ATRAP Penning trap.

Another method of acquiring information concerning the temporal spread of the cloud of positrons is to use scintillating fiber detectors, originally designed to detect antiproton annihilations inside the ATRAP electrode stack. The fiber detectors are very useful since

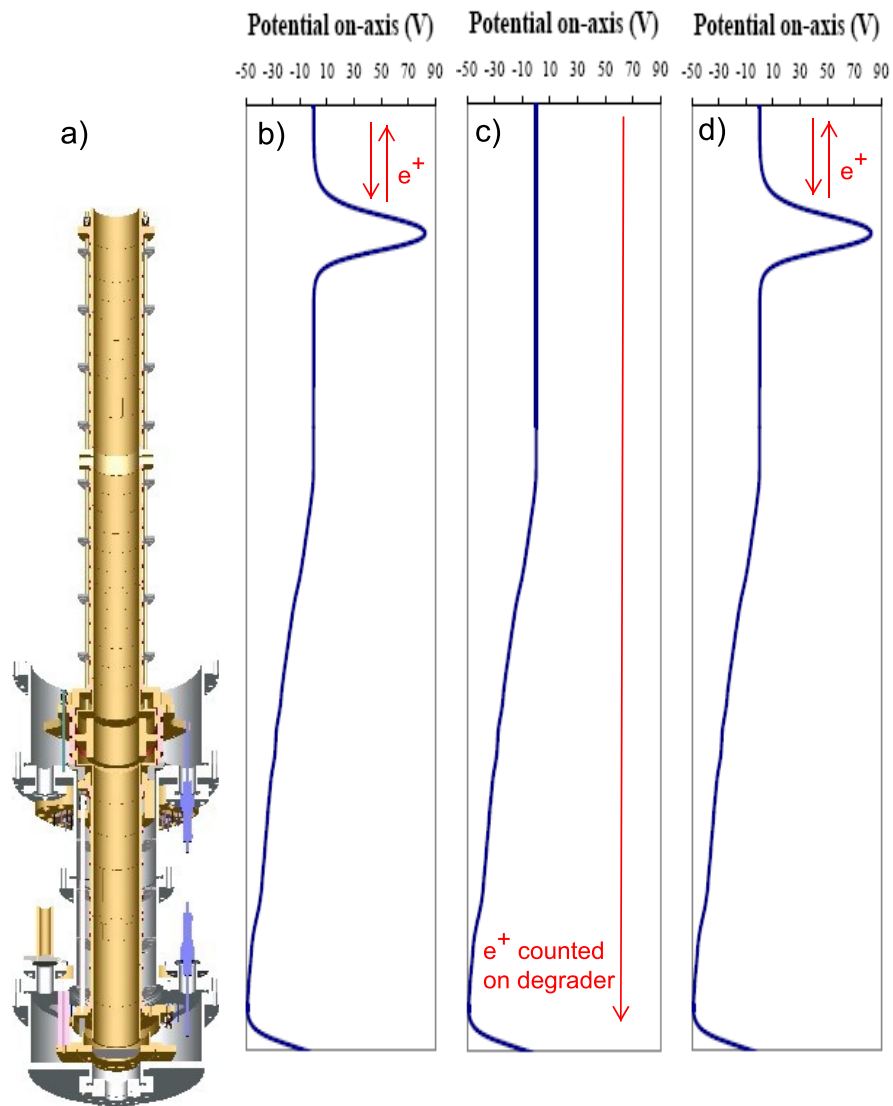


Figure 5.4: a) The ATRAP electrode stack. b) On-axis potential applied when positrons are initially pulsed from accumulator. c) On-axis potential applied when DEI pulser is triggered. d) On-axis potential applied 100 ns following DEI pulser trigger.

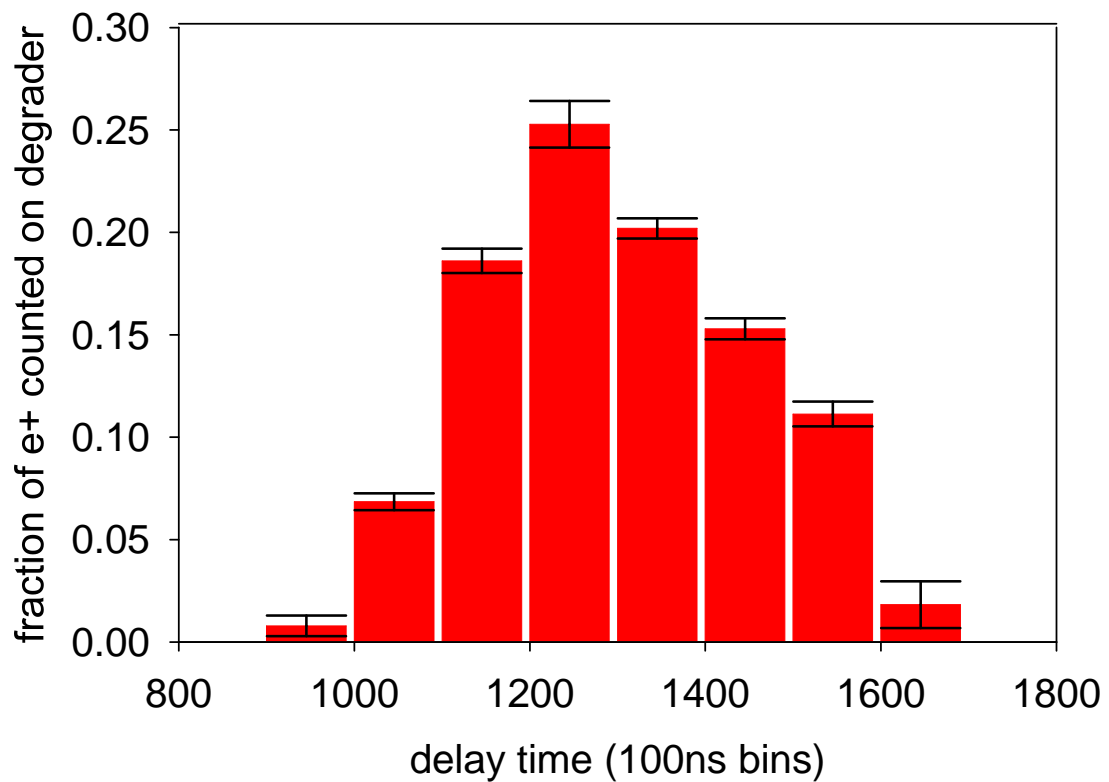


Figure 5.5: Temporal spread measured using the degrader as a Faraday cup. A front door voltage is applied to an electrode and is pulsed down for 100 ns to let the positrons through during a specified time window. The delay time is in reference to the signal sent from the accumulator indicating that the positrons are being transferred.

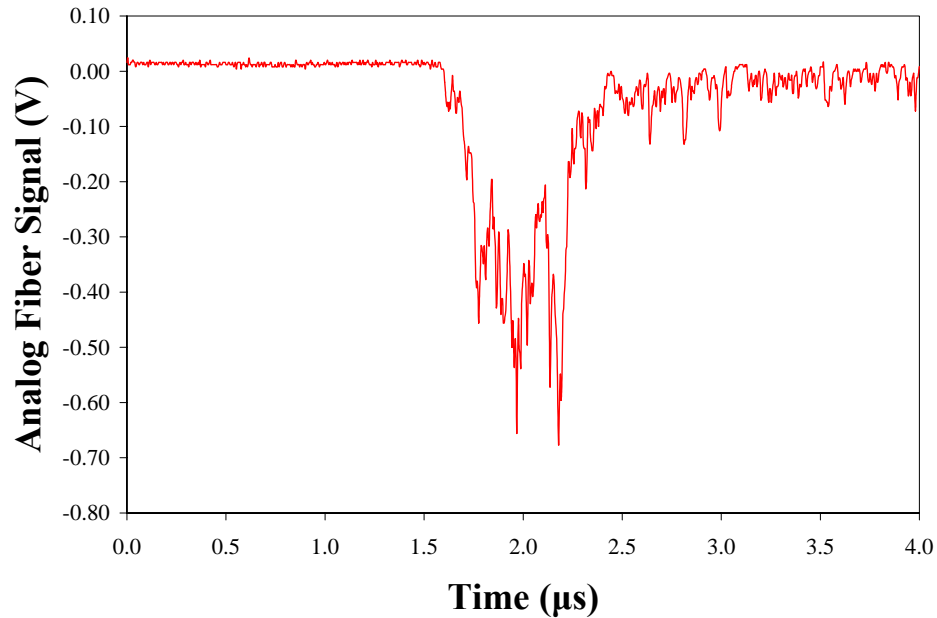


Figure 5.6: The fiber detectors used to count antiprotons are also sensitive to positron annihilation gammas. This signal shows the annihilation signal from a cloud of approximately 8 million positrons annihilating on the degrader. This signal is the raw analog signal from one quarter of the fiber channels, before they are input into the counting electronics.

they cover most of the solid angle around the degrader, where the positrons annihilate. These fibers are however quite insensitive to positron annihilations, with a positron counting efficiency of only 0.5%. Since the number of positrons hitting the degrader is as large as 10 million, the poor efficiency is not a problem. When a cloud of positrons annihilates on the degrader, the fiber detectors show the analog signal shown in Figure 5.6.

The temporal spread is not unexpected because, as the positrons travel along the positron guide, they do not all travel along the same path. The cloud has a diameter of 6.2 mm in a 0.02-tesla field (the average guiding field along the transfer system). The extent of the cloud will travel along slightly different field lines, thus different path lengths, producing different travel times. Different travel times will translate into different segments

of the cloud arriving to the degrader at different times, thus temporally spreading out the cloud.

A more dominant effect arises due to the energy spread in the cloud of positrons, as can be seen in Figure 5.3. The faster positrons will take a shorter amount of time to travel the distance of the positron guide than will the slower positrons, again spreading out the cloud. Since the positrons do not travel in a homogeneous field the entire way along the positron guide, they also slow down and speed up due to the magnetic mirroring effect.

5.1.3 Cloud Shape

The vertical profile of the positron cloud is determined at the exit of the accumulator, as described in Section 2.11.1. The radial profile can also be determined (in two dimensions rather than only one) inside the 1-tesla superconducting magnetic field. The 1-mm tube and associated 4-segment Faraday cup shown in Figure 4.20 are mounted on an xy stage. The stage shown in Figure 5.7 moves relative the rest of the ATRAP apparatus so that the 1-mm tube can be translated relative to the axis of the electrode stack. By moving the 1-mm tube, a radial profile is obtained by measuring the number of positrons that make it through the tube. At each tube position, the number of positrons making it through the 1-mm tube is measured on the degrader. A contour plot of the position measurements is shown in Figure 5.8.

The contour plot shows that, inside the 1-tesla magnetic field, the cloud extends approximately 1.5 mm in one direction and 1 mm in the other direction. At this size, the entire cloud cannot travel through the 1-mm tube. In fact, the large cloud size is quite clearly seen in the segmented Faraday-cup signals positioned above the 1-mm tube. Even when the cloud is steered through the centre of the 1-mm tube, and the signal on the de-

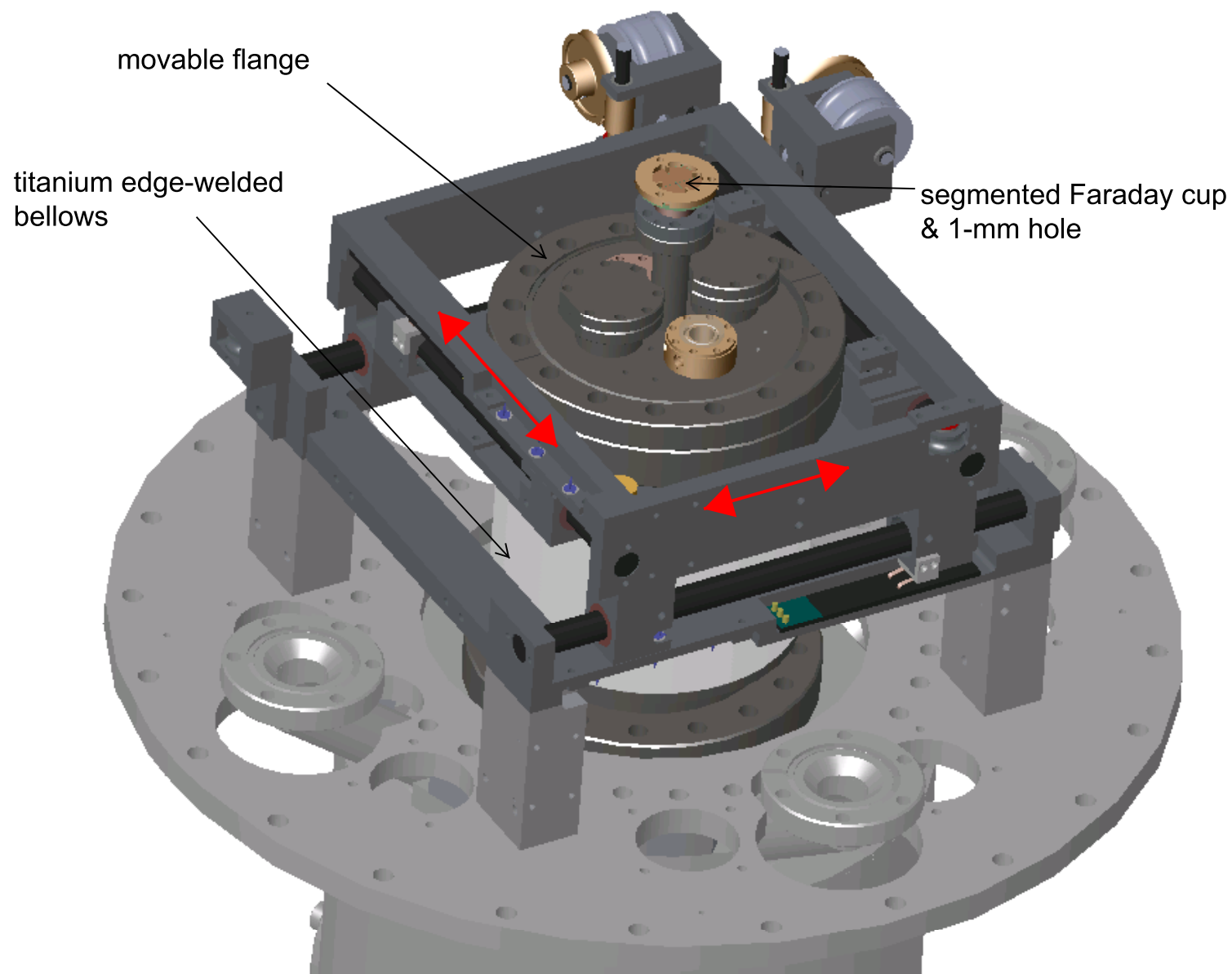


Figure 5.7: XY stage that enables the 1-mm tube to be moved relative to the electrode stack. The red arrows indicate the two directions in which the stage can move.

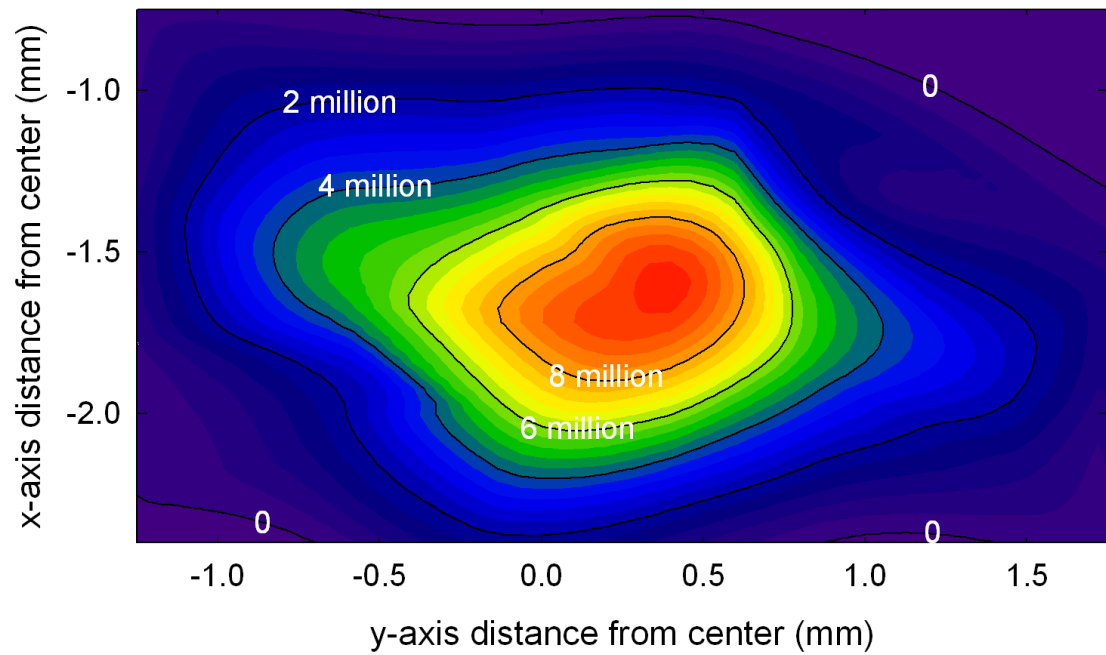


Figure 5.8: The radial profile of the positron cloud measured using the degrader Faraday cup and moving the 1-mm tube on the x-y stage.

grader is therefore maximized, there is still a significant signal on the segmented Faraday cups positioned round the 1-mm tube shown in Figure 4.20.

The height of the cloud is measured at 6.2 mm in a 0.02-tesla field (see Section 2.11.1). Due to magnetic compression, the height measurement represents a diameter of 0.88 mm in a 1-T field, which is consistent with the measurement of the diameter shown in Figure 5.8. The cloud shape does not greatly change along the positron guide and there is no significant radial expansion occurring during the transfer (other than the expected expansion due to changing magnetic fields).

5.2 Catching Positrons in the ATRAP Electrode Stack

Once the positrons travel through the 1-mm tube at the top of Figure 4.19, they can be captured within the electrode stack. The ATRAP electrode stack is split into two regions, to simultaneously capture antiprotons and positrons. The upper 0.3 m of the electrode stack shown in Figure 5.1 is used to capture positrons while the lower stack is used to capture antiprotons. The last electrode in the upper stack is biased positively to reflect the positrons back out up the electrode stack. Therefore, the positrons can travel twice the distance of the upper electrode stack (a distance of 0.6 m) before they leave the electrode stack.

To capture the positrons, a DEI pulser is attached to the first electrode of the ATRAP electrode stack in the same way as described in Section 5.1.2 where it is used to measure the temporal distribution. The pulsed electrode acts as a door to the positrons. When the trigger-signal from the accumulator is acquired (signaling the pulsing of the positrons out of the accumulator), the negative pulse from the DEI pulser pulses down the first electrode to let the positrons enter the catching region. Using the timing information from Figure

5.4, the duration of the pulse is set to 1600 ns, just after all of the positrons have entered the electrode stack.

To efficiently capture positrons within the ATRAP electrode stack, the positrons are slowed down during their time in the stack. At an average kinetic energy of 63 eV (in Figure 5.3), the speed of a positron is 4.8×10^6 m/s. At this speed, a positron travels a distance of 0.6 m (the return path through the 0.3 m used for capturing positrons) in 126 ns. 126 ns represents only approximately one quarter of the temporal width of the positron cloud as shown in Figure 5.5. For positrons travelling at 63 eV, the catching window is too small to capture the entire cloud of positrons pulsed from the accumulator. By removing kinetic energy from the positrons, the effective temporal window for which the positrons can be captured is greatly increased.

To reduce the kinetic energy of the positrons, a potential is applied to the ATRAP electrode stack, as shown in Figure 5.9. The positrons must first climb the potential barrier, thus losing kinetic energy. As long as the potential is not high enough to reflect the cloud of positrons, it provides an efficient method of lengthening the time window in which the positrons can be captured. As shown in Figure 5.3, at 55 V, none of the positrons are reflected, meaning that all of the positrons have more axial kinetic energy than 55 eV. By applying a potential of 55 V, the positrons have an average speed of 1.8×10^6 m/s inside the electrode stack and a catching window of 337 ns, nearly the temporal extent of the cloud shown in Figure 5.5.

Once the positrons have been slowed down and captured, they are travelling between the first and last electrode of the upper stack. To be useful for antihydrogen experiments, the positrons must be contained within a single-electrode well. To get into a single-electrode well, the positrons must first cool to the bottom of the long well, and then

further cool into the single electrode well, labelled the ‘positron well’ in Figure 5.9.

The cooling method is well understood [37]. The kinetic energy in a Penning trap is divided between the axial and cyclotron motions. Since the magnetic field of the ATRAP Penning trap is large (1 tesla), cooling can occur via synchrotron radiation of the cyclotron motion. Even after the positron is slowed down by the potential ramp, it still has 8 eV of kinetic energy in the axial direction. For a single particle in an ideal Penning trap, there is no coupling between the axial, cyclotron and magnetron motions; each motion can be considered separately. For a single particle, the axial motion cannot be damped using the technique of synchrotron radiation.

When a large number of particles are trapped in a Penning trap, collisions occur between the trapped particles. These collisions couple the axial and cyclotron motions and as the cyclotron energy is decreased by synchrotron radiation the axial motion is damped as well.

As seen in Figure 5.9b & c, a single electrode potential well is applied to the catching region. After the initial capture, as the positrons travel between the back barrier and the front door, they lose energy due to synchrotron radiation and collisions that allow for the exchange of axial and transverse momentum and eventually cool into the bottom of the single well. From the single well, they can be moved into other regions of the electrode stack to combine with antiprotons to create antihydrogen.

5.3 Counting Positrons in the ATRAP Penning Trap

Once the positrons have cooled into a single-electrode well, they can be adiabatically moved one electrode at a time to any electrode in the electrode stack by changing the potentials applied to neighbouring electrodes. The sequence of potentials used to transfer

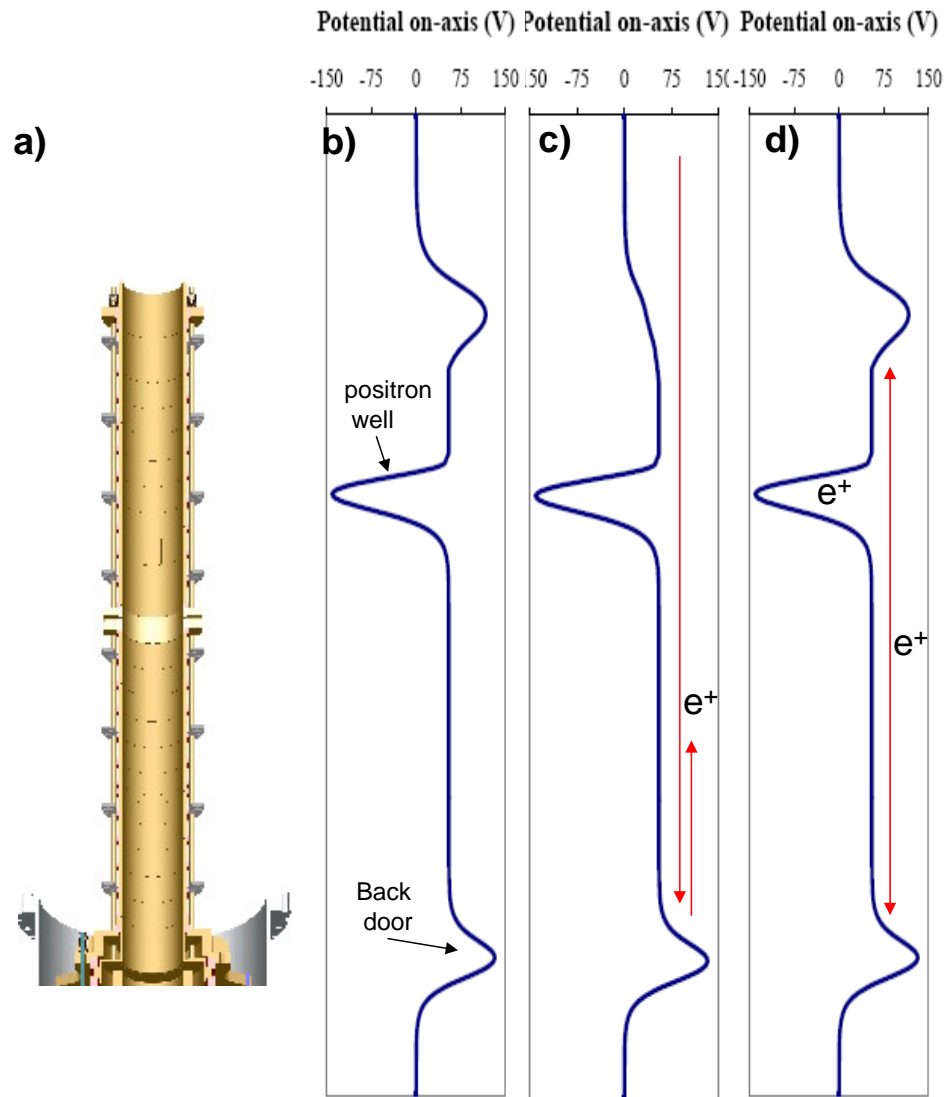


Figure 5.9: a) Diagram of the ATRAP electrode stack. b) On-axis potential applied to the ATRAP electrodes before trigger signal from the accumulator is sent. A single electrode well is applied in the middle of the stack in which the positrons will eventually cool. c) On-axis potentials applied to accept positrons into the stack. The fist electrode is pulsed down with a DEI pulser. d) On-axis potentials applied when the front door is closed and positrons are captured within the electrode stack.

the positrons adiabatically along three electrodes in the ATRAP electrode stack is shown in Figure 5.10. Another method of moving the particles is to pulse them out of the trap. The pulsing technique is also used to pulse the trapped positrons onto the degrader where they are counted.

The potential for pulsing is setup by adding a back wall to the single electrode well, to force the positrons in the direction of the degrader, and not towards the top of the electrode stack. The back wall is produced using the electrode directly above the trapping electrode, and produces a slightly non-symmetric potential, as shown in Figure 5.11. The electrode in which the positrons are held is also attached to an Avtec saturated switch (the same type of switch used to pulse to positrons from the accumulator) . The switch acts as a pulser, since the rise time is only 10 ns. The well where the positrons are held is initially set to a voltage of -100 V, significantly deeper than the 10 V the filtered pulser can apply. The pulse is applied for 200 ns, in which the positrons that are within the top 10 V of the well are pulsed towards the degrader. The potential of the electrode where the positrons are being held is then raised by 10 V and the process is repeated. Subsequent pulses enables the energy distribution within the single electrode to be determined. The distribution changes with different numbers of positrons in the potential well. A sample energy distribution is shown in Figure 5.12, for 138-million positrons cooled and subsequently counted with the ATRAP Penning trap.

5.4 Electron Cooling of Positrons

As described earlier, for the positrons to be used for making antihydrogen, they must be cooled within a single-electrode potential well. From a single-electrode well, they can be adiabatically moved along the electrode stack and positioned to create antihydrogen.

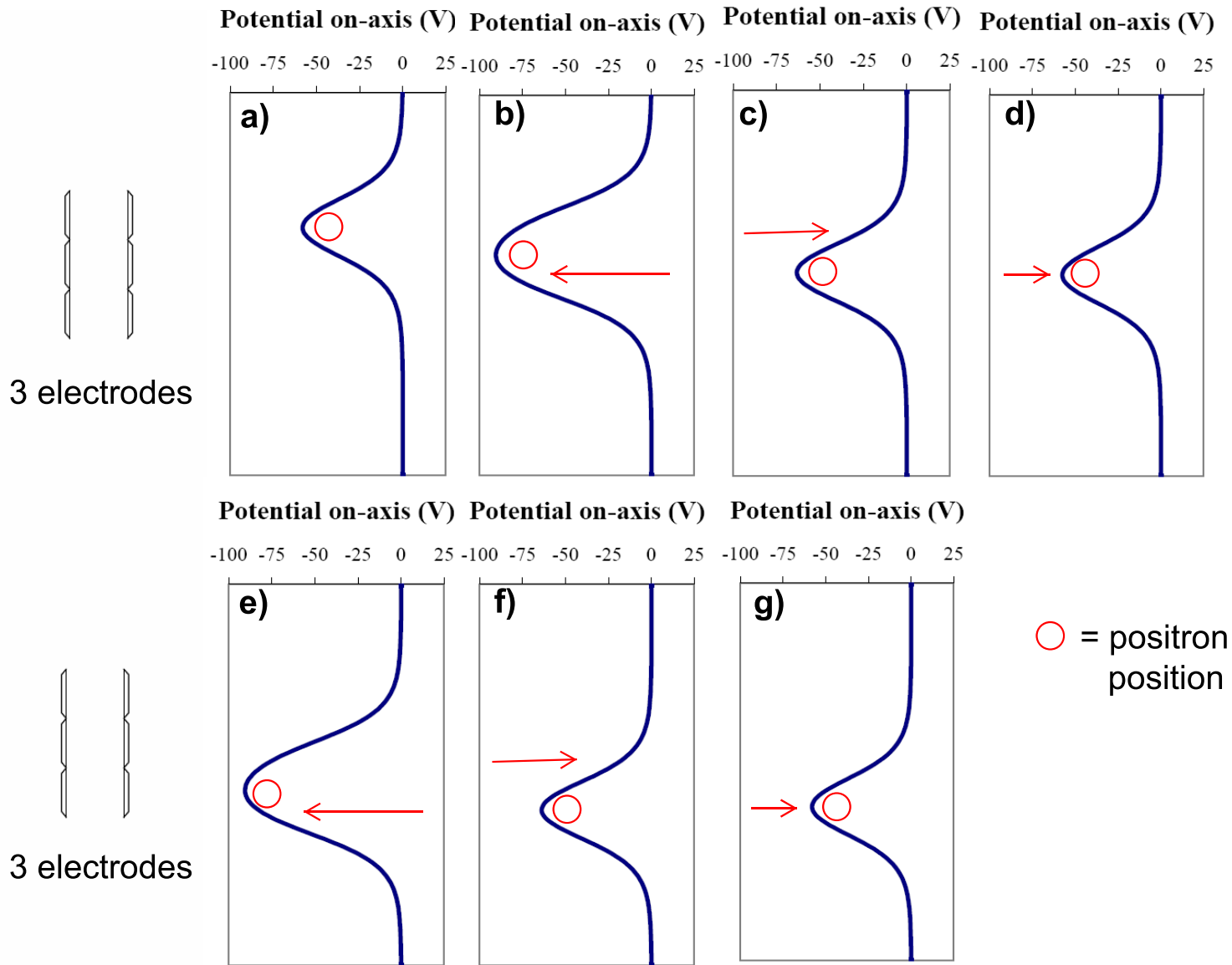


Figure 5.10: Adiabatic transfer of positrons between three electrodes in the ATRAP Penning trap

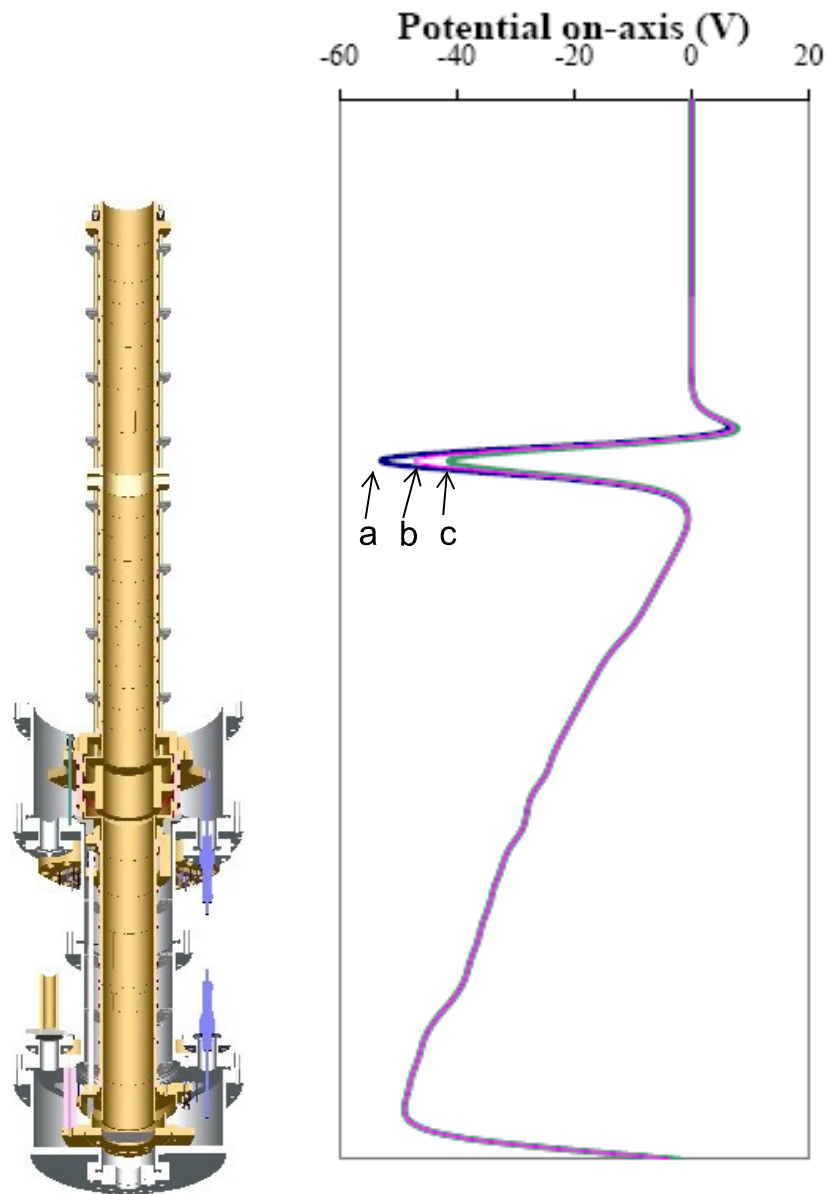


Figure 5.11: On-axis potential applied to pulse positrons onto degrader. a) At an applied voltage of -100V. b) At an applied voltage of -90V. c) At an applied voltage of -80V.

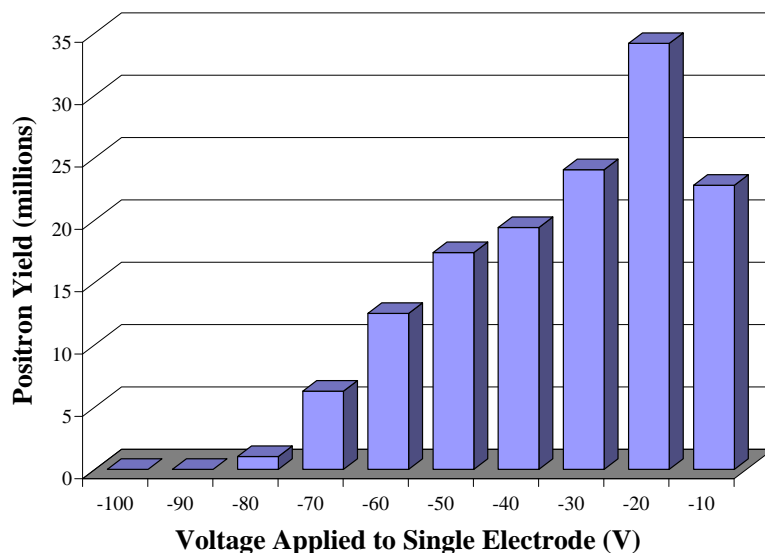


Figure 5.12: Energy distribution of 138-million positrons collected and cooled in ATRAP Penning trap.

To get them into the single-electrode well, they must cool into the bottom of the potential well used for positron loading shown in Figure 5.9. For a typical positron transfer, 5 million positrons are trapped in the ATRAP electrode stack and the cloud is spread over the 30-cm trapping region, and thus the positron density is low, and collisions are infrequent. With a low particle density, a long time is required to transfer the axial energy into cyclotron energy and thus cool the axial energy of the positrons.

Using a method similar to that of electron cooling antiprotons [38], large numbers of electrons are used to cool the positrons. Since the electrons and positrons have opposite charges, the electrons are held in a nested Penning trap, as shown in Figure 5.13, to simultaneously hold electrons and create a potential well in which the positrons can be cooled. Once captured between x and y in Figure 5.13a, the positrons encounter the large cloud of electrons at z on each pass, providing a greatly increased collision frequency and

a substantially faster cooling time.

5.4.1 Electron Loading

To increase the collision frequency, very large numbers of electron are required. Large numbers of electrons are loaded into the ATRAP Penning trap using photoelectrons from short pulses of 248-nm laser light [39]. 10-ns pulses of 248-nm light are provided by a KrF excimer laser and are directed (with a mirror positioned on the same linear stage as the mirror Faraday cup shown in Figure 4.18) down a 1.5-m path, along the axis of the 1-tesla superconducting solenoid, towards the electrode stack. The light travels through the 1-mm tube and hits the degrader.

Once the light hits the degrader, 10-ns pulses of photoelectrons are emitted and are captured within the ATRAP Penning trap. The electron pulses are synchronized to the laser pulses. Since the electron pulses are short and the timing well known, a method similar to that of trapping the positrons is used to trap the electrons. Figure 5.14 shows the potential structure used to capture the pulses of photoelectrons. Once the light hits the degrader, the pulse-electrode is lowered by 12V (shown in Figure 5.14c) to allow low-energy electrons to enter the region between the barriers shown in Figure 5.14b. The voltage on an electrode is then suddenly pulsed on, which completes the door of a potential well in which the electrons are enclosed shown in Figure 5.14d. Once the electrons are captured, they cool to the bottom of the potential well and the process is repeated to capture subsequent pulses of electrons. Using the pulsing scheme described enables up to a 4-eV slice of the photoelectron distribution to be captured.

The electrons are loaded with very little axial kinetic energy and have only a few electron volts of energy once they are liberated from the degrader surface. The electrons are

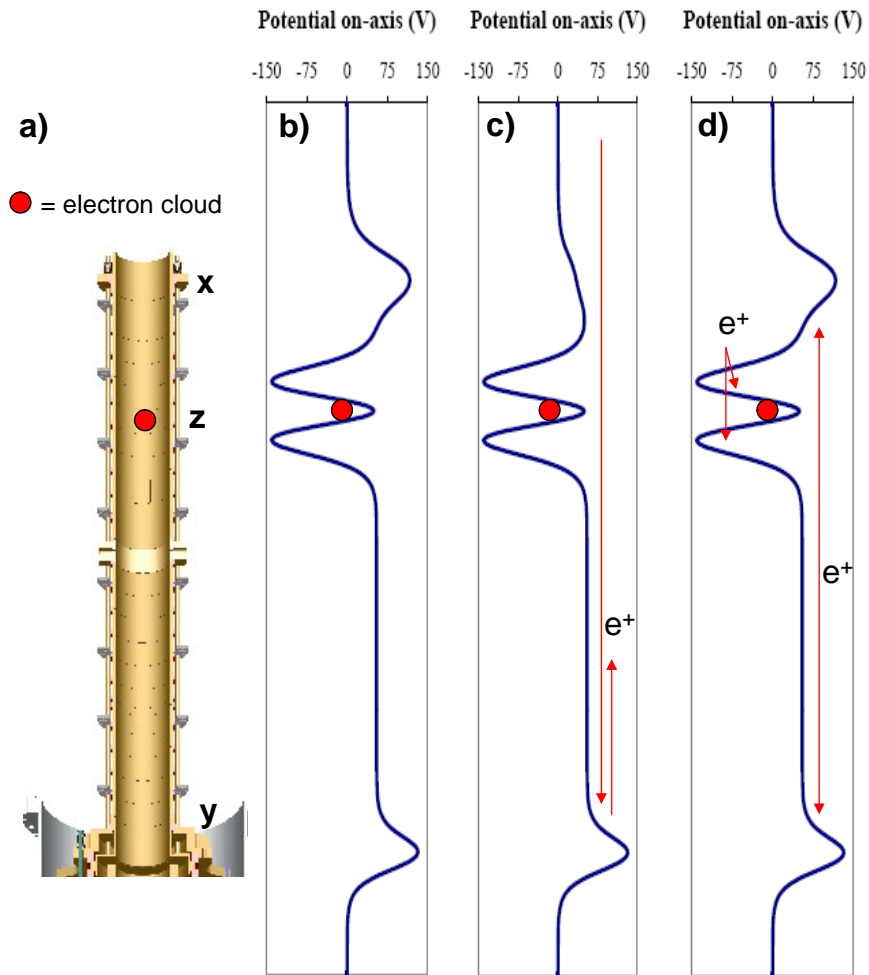


Figure 5.13: a) Diagram of the ATRAP electrode stack. b) On-axis potential applied to the ATRAP electrodes before trigger signal from the accumulator is sent. The electrons are held in a positive well while two negative single-electrode wells are applied where the positrons to cool into. c) On-axis potentials applied to accept positrons into the stack. The first electrode is pulsed down with a DEI pulser. d) On-axis potentials applied when the front door is closed and positrons are captured within the electrode stack.

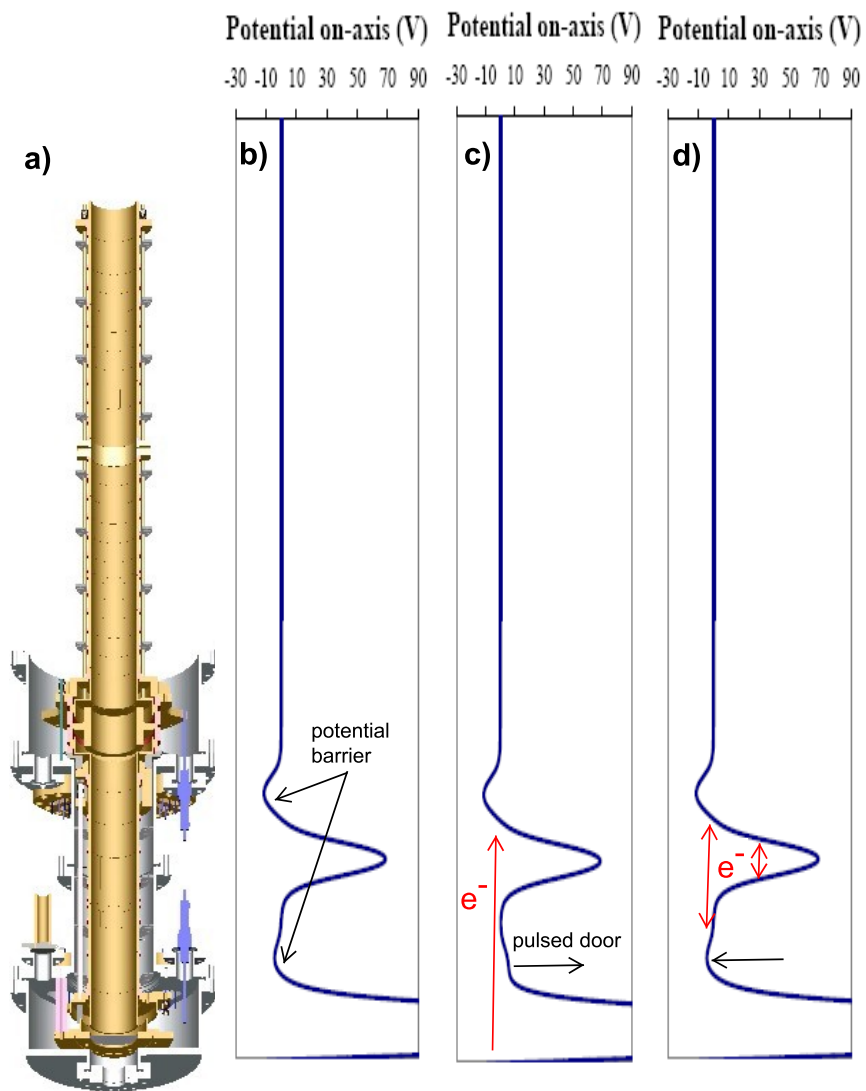


Figure 5.14: a) Diagram of the ATRAP electrode stack. b) On-axis potential applied to the ATRAP electrodes to capture photoelectrons off of the degrader. c) On-axis potentials applied when the laser light hits the degrader. The pulsed door drops to allow the low-energy photoelectrons to enter the capture electrode. d) On-axis potential applied 2.3- μ s after the the pulse door is pulsed down. The low-energy electrons are captured in the potential well where they cool.

trapped in a small region and thus have a large density, allowing frequent collisions which couple the axial motion to the radiating cyclotron motion, thus cooling the electrons to the bottom of the well. The frequency at which the laser pulses are repeated is approximately 1 Hz. With good alignment of the mirror, it takes approximately 70 laser pulses to load 150 million electrons.

5.4.2 Enhancement Using Electron Cooling

The advantage to using electron cooling is that the cooling time (defined as the time that is required for the positrons to cool to energies below the offset voltage of 55 eV so that they are confined within the one-electrode well labelled ‘positron well’ in Figure 5.9) is dramatically reduced. The cooling time is measured by lowering the back door at different times after the positrons are loaded. If the positrons are not cooled into the single-electrode well, they have enough kinetic energy to leave the trapped region and travel to the degrader, where they annihilate. The resulting gammas can be seen on the fiber detectors that are surrounding the Penning trap. Figure 5.15 shows the difference in cooling time with and without cooling electrons. When cooling electrons are used, a cloud of 150-million electrons is loaded using the method described in the previous section and is positioned into the Penning trap in the configuration shown in Figure 5.13. The numbers shown on the graph are determined by counting the positrons that are left in the single-electrode well after the back door has been dropped. As can be seen from Figure 5.15, the cooling time is reduced by two orders of magnitude when using 150 million electrons to increase the collision frequency. Figure 5.16 shows how positron loading is dependent on the number of cooling electrons that are used. For 50-second cooling times, the required number of electrons is greater than 50 million, and 150 million

is the standard number that we used.

5.5 Stacking Positrons

To get the largest possible clouds of positrons in the ATRAP Penning trap, we must be able to stack subsequent pulses of positrons. Stacking is only possible once the positrons have cooled into the single-electrode well because the front door must be pulsed down to accept the next pulse of positrons as shown in Figures 5.9 & 5.13. Stacking is possible with and without the use of electrons but the waiting time is greatly increased if no cooling electrons are used. Looking at the loading rate of the accumulator alone (Figure 2.17), the positron loading is only linear for the first 75 seconds, and completely levels off after 150 seconds. To maximize the number of positrons that are caught in the ATRAP Penning trap, the accumulation step should not last longer than 75 seconds, the time in which there is a linear loading rate. A very short accumulation time is not efficient since the pulse step shown in Figure 3.2 to prepare the positrons to be transferred out of the accumulator takes 5 seconds, in which positron loading must be stopped. Another consideration concerning the amount of time used to accumulate and transfer the positrons is the fact that the AD antiproton cycle is 100 seconds. Since repeated bunches of antiprotons are caught every 100 seconds, the sequence for positron capture must not conflict with the sequence for antiproton capture. All these conditions taken into account, the most efficient repetition rate for accumulation was found to be 50 seconds (which includes 45 seconds of accumulation and 5 seconds for set-up and transferring the positrons). A repetition rate of 50 seconds enables two positron transfers for every antiproton shot (defined as one AD cycle).

Because the most efficient transfer frequency is once every 50 seconds, electron cool-

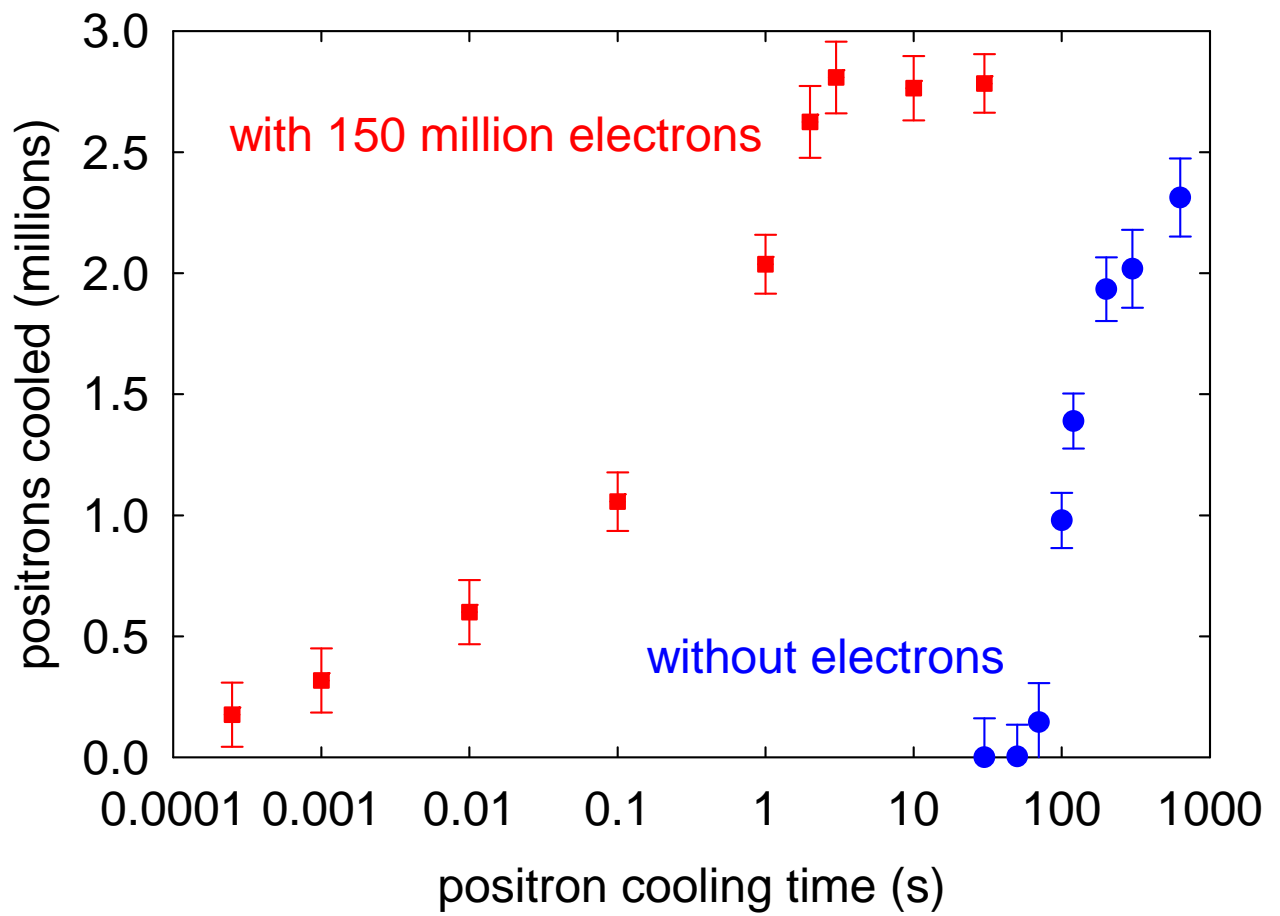


Figure 5.15: Time required to cool positrons into a single electrode well with and without electrons.

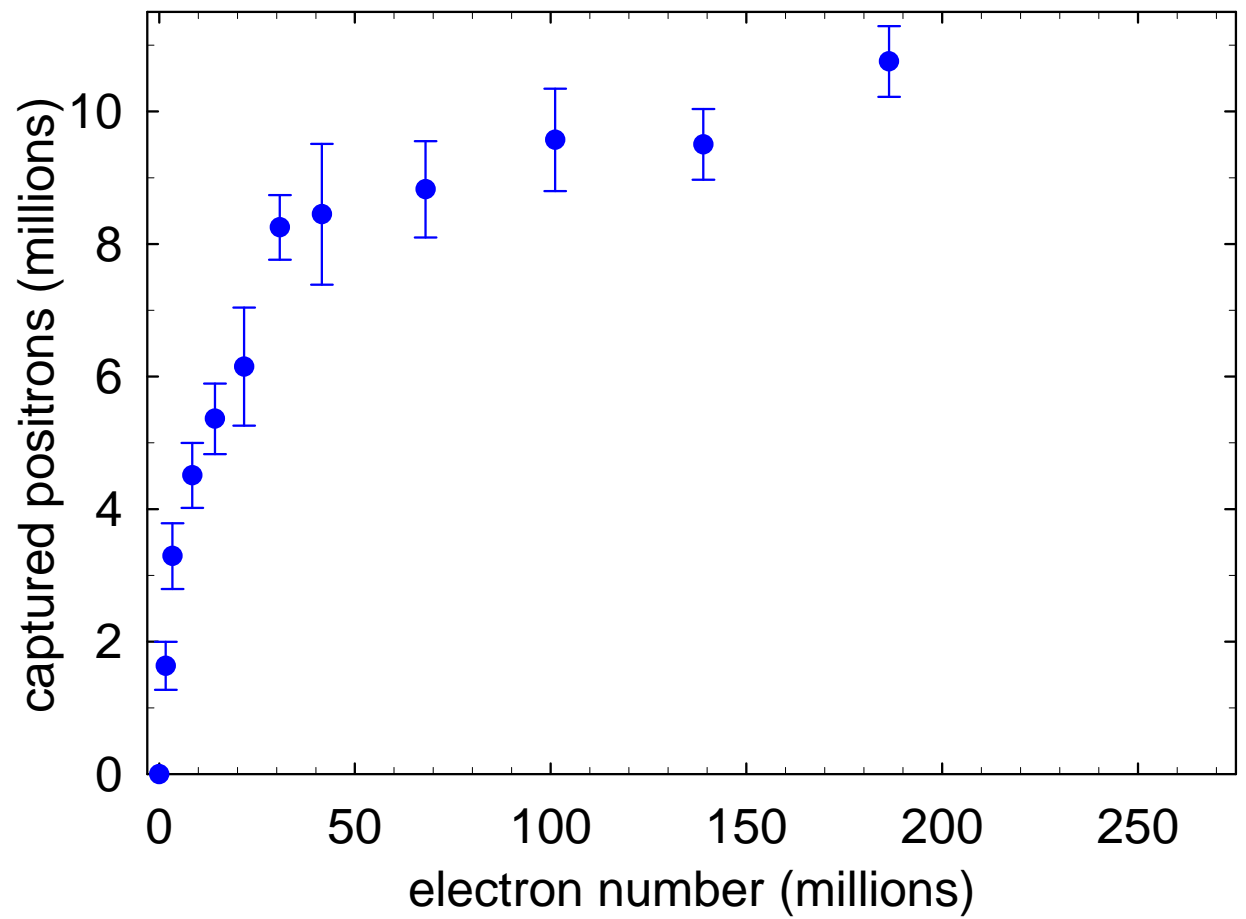


Figure 5.16: Electron number dependence on the efficiency of positron catching. The positrons are allowed to cool for 50 seconds.

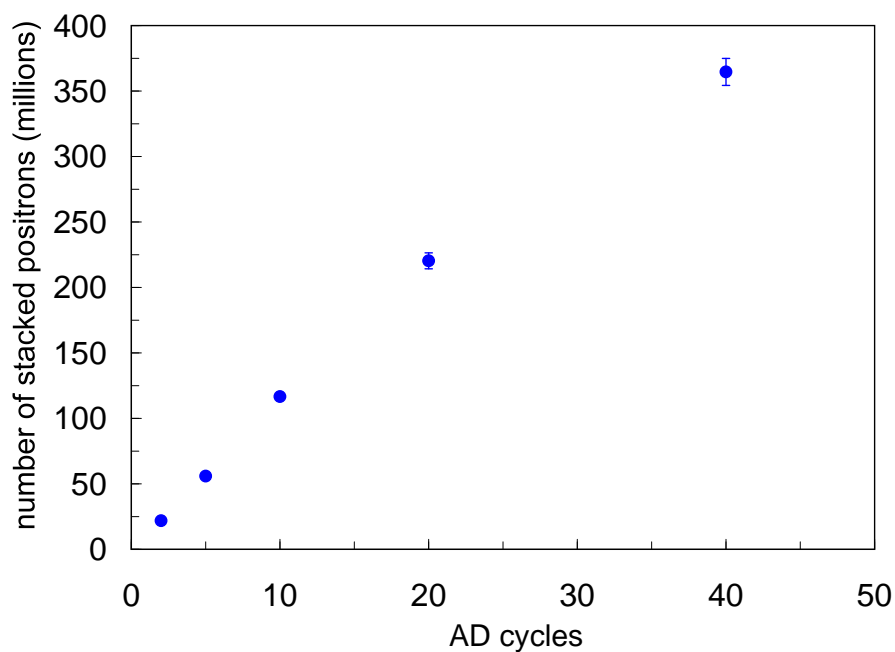


Figure 5.17: Stacking positrons into the ATRAP Penning trap. 150-million electrons are used to cool the positrons into the single-electrode well. The pulse frequency is once every 50-seconds, meaning that two pulses of positrons are caught during each AD cycle.

ing must be employed in order to achieve stacking. Figure 5.17 shows the efficiency of stacking positrons inside the ATRAP Penning trap. The stacking is linear up to 20-AD cycles at 11-million positrons per AD cycle. The maximum number of positrons that were accumulated, cooled and counted in the ATRAP Penning trap was 350 million.

Chapter 6

Summary of Results

Positrons can now be loaded in a robust, efficient and repeatable manner for antihydrogen production. The number of positrons transferred to each region of the accumulator/positron guide are shown in Figure 6.1 for a 50-second loading window. At a ^{22}Na source strength of 39.9 mCi and a moderator efficiency of 0.36(4)%, the accumulation efficiency was 17%. A 100% efficiency of transfer along the positron guide was achieved as measured on the mirror Faraday cup. Magnetic mirroring is the likely reason for the loss in signal between the mirror Faraday cup and the segmented Faraday cup located inside the 1-tesla superconducting solenoid.

The 1-mm tube opening is one of the main areas of positron loss throughout the entire transfer path. In future work, a larger tube will be implemented to increase the throughput of positrons, since it is found that there was no significant loss (due to poor vacuum) with the 1-mm tube.

With the old technique of positron loading, it would take over 3 hours to load the same number of positrons that have been loaded in 50 seconds. Positrons can be loaded at the same time as antiprotons and large numbers for each experimental run can be achieved.

Position	Number of Positrons (for 50s)
Moderated (after jog)	150-million
Accumulated	26-million
Mirror Faraday cup	26-million
Segmented Faraday cup	> 17-million
Hitting Degradar	10-million
Caught and Cooled in ATRAP	5.5-million

Table 6.1: Efficiencies along the transfer system and into the ATRAP Penning trap. The accumulation time is 50-seconds (including pulse sequence). All other parameters are set to maximize the signal at each point.

With a peak rate of over 1×10^7 (e^+ /hr)/mCi, the buffer-gas accumulator has greatly enhanced the production of antihydrogen for the ATRAP collaboration.

ATRAP has been working towards confining ground-state antihydrogen, with a goal of using the confined antihydrogen for precise spectroscopy. In 2006, a completely new apparatus was built to incorporate a magnetic neutral atom trap (Ioffe trap) that will eventually be used to capture antihydrogen. The first step towards the ultimate spectroscopy goal is to determine whether charged particles (antiprotons and positrons) can be confined in a charged particle trap (Penning trap) in the presence of the quadrupole magnetic field of a Ioffe trap. ATRAP showed [40] not only that the constituent charged particles can be held for long enough to create antihydrogen, but that the rate of detected antihydrogen is increased by the application of the Ioffe field.

Bibliography

- [1] G. Baur, G. Boero, A. Brauksiepe, A. Buzzo, W. Eyrich, R. Geyer, D. Grzonka, J. Hauffe, K. Kilian, M. LoVetere, M. Macri, M. Moosburger, R. Nellen, W. Oelert, S. Passaggio, A. Pozzo, K. Rühlrich, K. Sachs, G. Schepers, T. Sefzick, R.S. Simon, R. Stratmann, F. Stinzing, and M. Wolke. Production of antihydrogen. *Physics Letters B*, 368(3):251–258, 1996.
- [2] S. Maury. The antiproton decelerator: Ad. *Hyperfine Interactions*, 109:43–52, 1997.
- [3] G. Gabrielse, N. S. Bowden, P. Oxley, A. Speck, C. H. Storry, J. N. Tan, M. Wessels, D. Grzonka, W. Oelert, G. Schepers, T. Sefzick, J. Walz, H. Pittner, T. W. Hänsch, and E. A. Hessels. Driven production of cold antihydrogen and the first measured distribution of antihydrogen states. *Phys. Rev. Lett.*, 89:233401, Nov 2002.
- [4] M. Amoretti, C. Amsler, G. Bonomi, A. Bouchta, P. Bowe, C. Carraro, C. L. Cesar, M. Charlton, M. J. T. Collier, M. Doser, V. Filippini, K. S. Fine, A. Fontana, M. C. Fujiwara, R. Funakoshi, P. Genova, J. S. Hangst, R. S. Hayano, M. H. Holzscheiter, L. V. Jorgensen, V. Lagomarsino, R. Landua, D. Lindelof, E. Lodi Rizzini, M. Macri, N. Madsen, G. Manuzio, M. Marchesotti, P. Montagna, H. Pruys, C. Regenfus, P. Riedler, J. Rochet, A. Rotondi, G. Rouleau, G. Testera, A. Variola, T. L. Wat-

- son, and D. P. van der Werf. Production and detection of cold antihydrogen atoms. *Nature*, 419:456–459, 2002.
- [5] P. A. M. Dirac. The quantum theory of the electron. *Proceedings of the Royal Society of London. Series A*, 117(778):610–624, 1928.
- [6] Carl D. Anderson. The positive electron. *Phys. Rev.*, 43:491–494, Mar 1933.
- [7] Blackett and Occhialini. Some photographs of the tracks of penetrating radiation. *Proc. R. Soc. Lond. A*, 139:699–726, 1933.
- [8] Owen Chamberlain, Emilio Segrè, Clyde Wiegand, and Thomas Ypsilantis. Observation of antiprotons. *Phys. Rev.*, 100:947–950, Nov 1955.
- [9] C. H. Storry, A. Speck, D. Le Sage, N. Guise, G. Gabrielse, D. Grzonka, W. Oelert, G. Schepers, T. Sefzick, H. Pittner, M. Herrmann, J. Walz, T. W. Hänsch, D. Comeau, and E. A. Hessels. First laser-controlled antihydrogen production. *Phys. Rev. Lett.*, 93:263401, Dec 2004.
- [10] G. Gabrielse, X. Fei, L. A. Orozco, S. L. Rolston, R. L. Tjoelker, T. A. Trainor, J. Haas, H. Kalinowsky, and W. Kells. Barkas effect with use of antiprotons and protons. *Phys. Rev. A*, 40:481–484, Jul 1989.
- [11] G. Gabrielse, X. Fei, K. Helmerson, S. L. Rolston, R. Tjoelker, T. A. Trainor, H. Kalinowsky, J. Haas, and W. Kells. First capture of antiprotons in a penning trap: A kiloelectronvolt source. *Phys. Rev. Lett.*, 57:2504–2507, Nov 1986.
- [12] G. Gabrielse, X. Fei, L. A. Orozco, R. L. Tjoelker, J. Haas, H. Kalinowsky, T. A. Trainor, and W. Kells. Cooling and slowing of trapped antiprotons below 100 meV. *Phys. Rev. Lett.*, 63:1360–1363, Sep 1989.

- [13] G. Gabrielse, X. Fei, L. A. Orozco, R. L. Tjoelker, J. Haas, H. Kalinowsky, T. A. Trainor, and W. Kells. Thousandfold improvement in the measured antiproton mass. *Phys. Rev. Lett.*, 65:1317–1320, Sep 1990.
- [14] L.S. Brown and G. Gabrielse. Geonium theory: Physics of an electron or ion in a penning trap. *Rev. Mod. Phys.*, 58:233–311, 1986.
- [15] M. Kretschmar. Particle motion in a penning trap. *Eur. J. Phys.*, 12:240–246, 1991.
- [16] G. Gabrielse, L. Haarsma, and S.L. Rolston. Open-endcap penning traps for high precision experiments. *International Journal of Mass Spectrometry and Ion Processes*, 88(2–3):319–332, 1989.
- [17] G. Gabrielse, N. S. Bowden, P. Oxley, A. Speck, C. H. Storry, J. N. Tan, M. Wessels, D. Grzonka, W. Oelert, G. Schepers, T. Seifzick, J. Walz, H. Pittner, T. W. Hänsch, and E. A. Hessels. Background-free observation of cold antihydrogen with field-ionization analysis of its states. *Phys. Rev. Lett.*, 89:213401, Oct 2002.
- [18] G. Gabrielse, S.L. Rolston, L. Haarsma, and W. Kells. Antihydrogen production using trapped plasmas. *Physics Letters A*, 129(1):38–42, 1988.
- [19] E. A. Hessels, D. M. Homan, and M. J. Cavagnero. Two-stage rydberg charge exchange: An efficient method for production of antihydrogen. *Phys. Rev. A*, 57:1668–1671, Mar 1998.
- [20] J. Estrada, T. Roach, J. N. Tan, P. Yesley, and G. Gabrielse. Field ionization of strongly magnetized rydberg positronium: A new physical mechanism for positron accumulation. *Phys. Rev. Lett.*, 84:859–862, Jan 2000.

- [21] T. J. Murphy and C. M. Surko. Positron trapping in an electrostatic well by inelastic collisions with nitrogen molecules. *Phys. Rev. A*, 46:5696–5705, Nov 1992.
- [22] R.G. Greaves, M.D. Tinkle, and C.M Surko. Creation and uses of positron plasmas. *Phys. Plasmas*, 1:1439–1446, May 1994.
- [23] C.M. Surko, R.G. Greaves, and M. Charlton. Stored positrons for antihydrogen production. *Hyperfine Interactions*, 109:181–188, 1997. 10.1023/A:1012657517779.
- [24] R. G. Greaves and C. M. Surko. Solid neon moderator for positron-trapping experiments. *Canadian Journal of Physics*, 74(7-8):445–448, 1996.
- [25] V.A. Kuzminikh, I.A. Tsekhanovski, and S.A. Vorobiev. Backscattering of positrons from thick targets. *Nucl. Instr. and Meth.*, 118(1):269–271, Jun 1974.
- [26] *iThemba LABS documentation*.
- [27] P.G. Coleman, L. Albrecht, K.O. Jensen, and A.B. Walker. Positron backscattering from elemental solids. *Journal of Physics: Condensed Matter*, 4(50):10311–10322, 1992.
- [28] G.R. Massoumi, P.J. Schultz, W.N. Lennard, and J. Ociepa. Positron emission yields for encapsulated ^{22}Na sources. *Nuclear Instruments and Methods in Physics Research Section B: Beam Interactions with Materials and Atoms*, 30(4):592–597, 1988.
- [29] E. M. Gullikson and A. P. Mills. Solid neon moderator for producing slow positrons. *Appl. Phys. Lett.*, 49:1121–1123, Aug 1986.

- [30] E. M. Gullikson and A. P. Mills. Positron dynamics in rare-gas solids. *Phys. Rev. Lett.*, 57:376–379, Jul 1986.
- [31] R. Khatri, M. Charlton, P. Sferlazzo, K. G. Lynn, A. P. Mills, and L. O. Roellig. Improvement of rare-gas solid moderators by using conical geometry. *Appl. Phys. Lett.*, 57:2374–2376, Nov 1990.
- [32] D.B. Cassidy, S.H.M. Deng, R.G. Greaves, and A.P. Mills. Accumulator for the production of intense positron pulses. *Review of Scientific Instruments*, 77(7):073106, 2006.
- [33] J. Allison, K. Amako, J. Apostolakis, H. Araujo, P.A. Dubois, M. Asai, G. Barrand, R. Capra, S. Chauvie, R. Chytraccek, G.A.P. Cirrone, G. Cooperman, G. Cosmo, G. Cuttone, G.G. Daquino, M. Donszelmann, M. Dressel, G. Folger, F. Foppiano, J. Generowicz, V. Grichine, S. Guatelli, P. Gumplinger, A. Heikkinen, I. Hrivnacova, A. Howard, S. Incerti, V. Ivanchenko, T. Johnson, F. Jones, T. Koi, R. Kokoulin, M. Kossov, H. Kurashige, V. Lara, S. Larsson, F. Lei, O. Link, F. Longo, M. Maire, A. Mantero, B. Mascialino, I. McLaren, P.M. Lorenzo, K. Minamimoto, K. Murakami, P. Nieminen, L. Pandola, S. Parlati, L. Peralta, J. Perl, A. Pfeiffer, M.G. Pia, A. Ribon, P. Rodrigues, G. Russo, S. Sadilov, G. Santin, T. Sasaki, D. Smith, N. Starkov, S. Tanaka, E. Tcherniaev, B. Tome, A. Trindade, P. Truscott, L. Urban, M. Verderi, A. Walkden, J.P. Wellisch, D.C. Williams, D. Wright, and H. Yoshida. Geant4 developments and applications. *Nuclear Science, IEEE Transactions on*, 53(1):270–278, Feb 2006.
- [34] J. H. Malmberg and C. F. Driscoll. Long-time containment of a pure electron plasma. *Phys. Rev. Lett.*, 44:654–657, Mar 1980.

- [35] E. M. Hollmann, F. Anderegg, and C. F. Driscoll. Measurement of cross-magnetic-field heat transport due to long-range collisions. *Physics of Plasmas*, 7:1767–1773, 2000.
- [36] Andrew Speck. *Two Techniques to Produce Cold Antihydrogen*. PhD thesis, Harvard University, 2005.
- [37] S.L. Rolston and G. Gabrielse. Cooling antiprotons in an ion trap. *Hyperfine Interactions*, 44:233–245, 1989.
- [38] G. Gabrielse, J. Estrada, J.N. Tan, P. Yesley, N.S. Bowden, P. Oxley, T. Roach, C.H. Storry, M. Wessels, J. Tan, D. Grzonka, W. Oelert, G. Schepers, T. Sefzick, W.H. Breunlich, M. Cargnelli, H. Fuhrmann, R. King, R. Ursin, J. Zmeskal, H. Kalinowsky, C. Wesdorp, J. Walz, K.S.E. Eikema, and T.W. Hänsch. First positron cooling of antiprotons. *Physics Letters B*, 507(1):1–6, 2001.
- [39] B. Levitt, G. Gabrielse, P. Larochele, D. Le Sage, W.S. Kolthammer, R. McConnell, J. Wrubel, A. Speck, D. Grzonka, W. Oelert, T. Sefzick, Z. Zhang, D. Comeau, M.C. George, E.A. Hessels, C.H. Storry, M. Weel, and J. Walz. Single-component plasma of photoelectrons. *Physics Letters B*, 656(1):25–29, 2007.
- [40] G. Gabrielse, P. Larochele, D. Le Sage, B. Levitt, W. S. Kolthammer, I. Kuljanishvili, R. McConnell, J. Wrubel, F. M. Esser, H. Glückler, D. Grzonka, G. Hansen, S. Martin, W. Oelert, J. Schillings, M. Schmitt, T. Sefzick, H. Soltner, Z. Zhang, D. Comeau, M. C. George, E. A. Hessels, C. H. Storry, M. Weel, A. Speck, F. Nililius, J. Walz, and T. W. Hänsch. Antiproton confinement in a Penning-Ioffe trap for antihydrogen. *Phys. Rev. Lett.*, 98:113002, Mar 2007.